EUROPEAN ORGANISATION FOR NUCLEAR RESEARCH (CERN)

Submitted to: JHEP

CERN-EP-2021-105
19th July 2021

Measurement of the production cross section of pairs of isolated photons in *pp* collisions at 13 TeV with the ATLAS detector

The ATLAS Collaboration

A measurement of prompt photon-pair production in proton–proton collisions at $\sqrt{s} = 13$ TeV is presented. The data were recorded by the ATLAS detector at the LHC with an integrated luminosity of 139 fb^{-1}. Events with two photons in the well-instrumented region of the detector are selected. The photons are required to be isolated and have a transverse momentum of $p_{\mathrm{T},\gamma_{1(2)}} > 40$ (30) GeV for the leading (sub-leading) photon. The differential cross sections as functions of several observables for the diphoton system are measured and compared with theoretical predictions from state-of-the-art Monte Carlo and fixed-order calculations. The QCD predictions from next-to-next-to-leading-order calculations and multi-leg merged calculations are able to describe the measured integrated and differential cross sections within uncertainties, whereas lower-order calculations show significant deviations, demonstrating that higher-order perturbative QCD corrections are crucial for this process. The resummed predictions with parton showers additionally provide an excellent description of the low transverse-momentum regime of the diphoton system.

Contents

1 Introduction

The production of a prompt photon pair in proton–proton collisions is one of the cornerstone processes of the LHC physics programme. Most prominently, photon pairs are of vital importance in searching for or studying the properties of particles that decay into photon pairs, such as the Higgs boson or other neutral particles. The main background to resonant diphoton production originates from the continuum production of such pairs, which is the topic of this publication. Despite the electromagnetic nature of this process, diphoton production in hadron colliders involves intricate strong-interaction dynamics. Theoretical predictions are therefore highly non-trivial and measurements are necessary to scrutinise and validate such predictions.

Non-resonant photons can be produced by various mechanisms in *pp* collisions at the LHC. In theoretical calculations, prompt photons, i.e. those not produced in hadron decays, are typically subdivided into

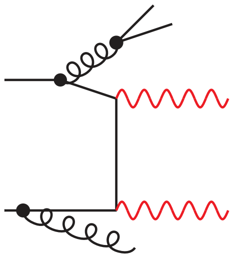

(a) Direct photons

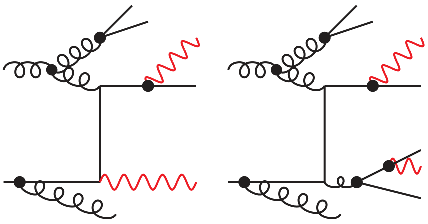

(b) Single- and double-fragmentation photons

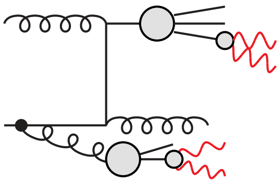

(c) Non-prompt photons

Figure 1: Schematics of theoretical photon pair production mechanisms. The black dots represent resummed bremsstrahlung, e.g. from a fragmentation function or parton shower, while the grey circles represent hadronisation and hadron decay processes. The presence of jets is not required in the following and only included for illustration purposes.

two different production mechanisms: the *direct* production mode, represented by a $q\bar{q} \to \gamma\gamma$ t-channel diagram at leading order; and the single- and double-*fragmentation* component with a hard γ+jet or dijet configuration and sub-leading photon emissions in a resummed approach. A schematic representation exemplifies these photon production mechanisms in Figures 1(a) and 1(b), respectively. Hadron decays such as $\pi^0 \to \gamma\gamma$, cf. Figure 1(c), are the most abundant source of photons in pp collisions, but are considered as background in this publication. To suppress this non-prompt contribution, photons are required to be isolated from hadronic activity in their vicinity.

In this publication, prompt diphoton production is measured in $\sqrt{s} = 13$ TeV pp collisions at the LHC using the full Run-2 dataset. Previous diphoton cross-section measurements were performed in $p\bar{p}$ collisions at $\sqrt{s} = 1.96$ TeV by CDF [1] and D0 [2], in pp collisions at $\sqrt{s} = 7$ TeV by CMS [3, 4] and ATLAS [5, 6], and at $\sqrt{s} = 8$ TeV by ATLAS [7]. Other prompt-photon measurements have studied single photon production in CMS [8] and in ATLAS [9–13] at $\sqrt{s} = 13$ TeV.

The main challenge and source of uncertainty on the experimental side is the estimation of the background from non-prompt photons in jet events; in this analysis, a data-driven technique is used to estimate this background. The background-subtracted yield is then corrected for detector effects using an iterative unfolding procedure. Differential cross-section measurements are presented in a fiducial region as functions of several kinematic observables of the photon pair. State-of-the-art theoretical predictions from fixed-order calculations and from Monte Carlo (MC) event generators are compared with the data.

2 ATLAS detector

The ATLAS experiment [14] at the LHC is a multipurpose particle detector with a forward–backward symmetric cylindrical geometry and a near 4π coverage in solid angle.[1] It consists of an inner tracking detector surrounded by a thin superconducting solenoid providing a 2 T axial magnetic field, electromagnetic and hadronic calorimeters, and a muon spectrometer.

The inner tracking detector covers the pseudorapidity range $|\eta| < 2.5$. It consists of silicon pixel, silicon microstrip, and transition radiation tracking detectors.

The calorimeter system covers the pseudorapidity range $|\eta| < 4.9$. Within the region $|\eta| < 3.2$, electromagnetic (EM) calorimetry is provided by a lead/liquid-argon (LAr) sampling calorimeter with accordion geometry. It is divided into a barrel section covering $|\eta| < 1.475$ and two endcap sections covering $1.375 < |\eta| < 3.2$. For $|\eta| < 2.5$, it is divided into three layers in depth, which are finely segmented in η and ϕ. An additional thin LAr presampler layer covering $|\eta| < 1.8$ is used to correct for energy loss in material upstream of the calorimeters. Hadronic calorimetry is provided by a steel/scintillator-tile calorimeter, segmented into three barrel structures within $|\eta| < 1.7$, and two copper/LAr hadronic endcap calorimeters. The solid angle coverage is completed with forward copper/LAr and tungsten/LAr calorimeter modules optimised for electromagnetic and hadronic measurements respectively.

The muon spectrometer surrounds the calorimeters and is based on three large air-core toroidal superconducting magnets with eight coils each. The field integral of the toroids ranges between 2.0 and 6.0 T m across most of the detector. The muon spectrometer includes a system of precision tracking chambers and fast detectors for triggering.

A two-level trigger system is used to select events. The first-level trigger is implemented in hardware and uses a subset of the detector information to keep the rate of accepted events below 100 kHz. This is followed by a software-based trigger that reduces the accepted event rate to 1 kHz on average depending on the data-taking conditions [15].

An extensive software suite [16] is used for the reconstruction and analysis of real and simulated data, for detector operations, and in the trigger and data acquisition systems of the experiment.

3 Data and simulated event samples

3.1 Data samples

The data used in this measurement were recorded by the ATLAS detector in pp collisions at $\sqrt{s} = 13$ TeV during the LHC Run-2 data taking period. Events were selected using a diphoton trigger requiring the presence of two clusters of energy depositions in the EM calorimeter with transverse momentum (p_{T}) above 35 GeV and 25 GeV for the p_{T}-ordered leading and sub-leading clusters, respectively. Only events taken during stable beam conditions and satisfying detector and data-quality requirements [17] are considered. These requirements ensure that the calorimeters and inner tracking detectors are operating normally.

[1] ATLAS uses a right-handed coordinate system with its origin at the nominal interaction point (IP) in the centre of the detector and the z-axis along the beam pipe. The x-axis points from the IP to the centre of the LHC ring, and the y-axis points upwards. Cylindrical coordinates (r, ϕ) are used in the transverse plane, ϕ being the azimuthal angle around the z-axis. The pseudorapidity is defined in terms of the polar angle θ as $\eta = -\ln\tan(\theta/2)$. Angular distance is measured in units of $\Delta R \equiv \sqrt{(\Delta\eta)^2 + (\Delta\phi)^2}$.

The total integrated luminosity of the collected sample after trigger and data-quality requirements amounts to 139 fb^{-1}. Multiple pp interactions (pile-up) can occur in the same bunch crossing, with 34 simultaneous interactions produced on average. The efficiency of the diphoton triggers relative to the offline selection presented in the next section ranges between 96% and 100% [18] as a function of the transverse momentum of the sub-leading photon.

3.2 Simulated event samples for signal and background processes

MC simulation samples are used for the subtraction of subdominant background as well as for cross-checks of the subtraction of the dominant background, for the unfolding of detector effects, and as theoretical predictions in the final comparison with the measured data.

In all samples, pile-up effects from both the same bunch crossing and previous/subsequent crossings were simulated by overlaying additional generated minimum-bias events on the hard-scatter event prior to reconstruction. The MC samples were reweighted to match the distribution of the number of pile-up interactions in data events. All samples were processed through the ATLAS detector simulation [19] based on Geant4 [20] and through the same reconstruction algorithms as used for data.

Diphoton signal samples. Simulated samples of prompt diphoton production were generated with two different programs, Sherpa [21] and Pythia 8 [22]. The nominal samples used in the analysis were simulated with the Sherpa 2.2 generator. Their effective luminosity is approximately twice that of data. In this set-up, matrix elements for the $pp \to \gamma\gamma + 0, 1j$ process[2] at next-to-leading-order (NLO) accuracy in the strong coupling constant α_s and $pp \to \gamma\gamma + 2, 3j$ at leading-order (LO) accuracy are matched and merged with the Sherpa parton shower based on Catani–Seymour dipoles [23, 24] using the MEPS@NLO prescription [25, 26]. The virtual QCD correction for matrix elements at NLO accuracy is provided by the OpenLoops library [27, 28]. Samples were generated using the NNPDF3.0 next-to-next-to-leading-order (NNLO) set [29] of parton distribution functions (PDF), along with the dedicated set of tuned parton-shower parameters developed by the Sherpa authors. Both the direct and fragmentation components of isolated photon production are included by setting the merging scale dynamically in the scheme of Ref. [30], and a photon isolation requirement based on a smooth cone [31] is used with $n = 2$, $\delta_0 = 0.1$ and $\varepsilon = 0.1$. In addition, the loop-induced $gg \to \gamma\gamma$ box process is included in these samples at LO accuracy.

An alternative signal sample was generated with Pythia 8. Direct production was simulated using LO matrix elements for $pp \to \gamma\gamma$ and showered in Pythia 8.186 [22] using the NNPDF2.3 LO [32] PDF set with the A14 set of tuned parameters [33]. The same framework was used to generate the single-fragmentation component based on LO matrix elements for $pp \to \gamma j$ with one additional photon produced in the parton shower, and the double-fragmentation component based on LO matrix elements for $pp \to jj$ with both additional photons produced in the parton shower. No photon isolation requirement is applied in these samples at the generator level.

Electron background sources. Since electrons can fake photons, background processes with prompt electron production from Drell–Yan processes, $Z/\gamma^*(\to ee)$ and $W(\to e\nu)$, are considered and estimated from MC simulation. The samples used to estimate these backgrounds were generated using Powheg Box v2 [34, 35] interfaced to the Pythia 8.186 [22] parton shower model with the AZNLO set of tuned parameters [36].

[2] Here and in the following, j denotes a 'jet', which at matrix-element level corresponds to a quark or gluon.

The effect of QED final-state radiation was simulated with Photos++ 3.52 [37]. The W/Z samples are normalised to NNLO cross sections calculated with FEWZ [38]. Even though the impact is negligible, poor modelling of the $p_{\mathrm{T}}(Z)$ spectrum in the $Z(\rightarrow ee)$ sample is corrected for using data/MC correction factors from the measurement in Ref. [39].

γj simulation. While the non-prompt background is determined in a data-driven approach, Sherpa 2.2 [21] simulations of the $pp \rightarrow \gamma$+jets process are used for cross-checks. The set-up is the same as for the diphoton signal samples described above, including matrix elements for $pp \rightarrow \gamma + 1,2j$ at NLO and $pp \rightarrow \gamma + 3,4j$ at LO accuracy in α_{s}.

4 Event selection and definition of observables

The photon and event selections are explained in Section 4.1, the particle-level selection to which the data are unfolded is described in Section 4.2 and the definition of the observables is included in Section 4.3.

4.1 Photon reconstruction and event selection

Photon candidates are reconstructed from clusters of energy depositions in the electromagnetic calorimeter [40]; the clusters are formed using a dynamical topological cell-clustering algorithm [41]. Clusters matched to a track consistent with originating from an electron produced in the beam interaction region are considered electron candidates, otherwise they are considered photon candidates. Photons which convert to electron–positron pairs in the inner detector are distinguished from unconverted photons by matching reconstructed conversion vertices or tracks consistent with originating from photon conversion to the clusters. The photon energy is calibrated in several steps as described in Refs. [40, 42, 43]. The energy resolution is optimised using a multivariate regression algorithm based on properties of the shower development in the EM calorimeter and trained on simulated events. The absolute energy scale is adjusted using $Z \rightarrow ee$ events, and validated using radiative Z boson decays. The energy scale uncertainty depends on the p_{T} and η of the photon, and varies between 0.25%–1% for photons with transverse momentum in the range 30–100 GeV dominating this analysis.

For this study, at least two photon candidates are required per event, with transverse momentum $p_{\mathrm{T},\gamma}$ above 40 GeV and 30 GeV for the $p_{\mathrm{T},\gamma}$-ordered leading and sub-leading photons, respectively. These $p_{\mathrm{T},\gamma}$ thresholds are each 5 GeV above the corresponding trigger thresholds, at the plateau of the trigger efficiency versus $p_{\mathrm{T},\gamma}$ [18]. The photon pseudorapidity is required to be $|\eta_\gamma| < 2.37$, excluding the transition region between the barrel and endcaps ($1.37 < |\eta_\gamma| < 1.52$). In this acceptance region, the high granularity of the EM calorimeter allows efficient identification of photons.

The momenta of the photon candidates are corrected for the position of their associated reconstructed primary interaction vertex. The associated vertex is chosen among all reconstructed vertices, which are each required to have at least two inner detector tracks with $p_{\mathrm{T}} > 0.5$ GeV. The measured trajectories of the two photons, along with the reconstructed vertex information in the event, are used as inputs to a neural-network algorithm trained on simulated events to select the most probable primary vertex [44] for the photon pair. The photon trajectories are reconstructed using the shower-depth (longitudinal) segmentation of the EM calorimeter; for converted photons, the position of the conversion vertex is also used if the conversion tracks have hits in the silicon detectors.

The identification of photons is based on multiple variables that quantify the longitudinal and lateral shape of the electromagnetic shower produced by the photon. Requirements on these shower variables are used to identify photons. A detailed description of all variables and selections for the *tight* photon identification used in this analysis is given in Ref. [40]. The identification variables f_{side} (energy fraction outside of core cells) and w_{s3} (lateral shower width) are used to define control regions for the background estimation presented in Section 5.1. These variables use information from the finely segmented first layer of the electromagnetic calorimeter, and are sensitive to differences between candidates from prompt photons and background candidates, e.g. from the two collimated photons of a neutral hadron decay.

To further reject background candidates from hadron decays, which are in general surrounded by hadronic activity, the photons are required to be isolated. The isolation measurement is based on calorimeter information [40]. The initial isolation variable is defined as the scalar sum of the transverse momenta computed from topological clusters of calorimeter cells [41] in a cone of $\Delta R = 0.2$ around the photon candidate direction. The contribution of the photon to the transverse isolation energy is subtracted, based on the energy depositions in a rectangular window of $\Delta\eta \times \Delta\phi = 0.125 \times 0.175$ around the photon candidate and the energy expected to leak out of this window. Effects of pile-up and from the underlying event (UE) are corrected for in calculating the isolation variable $E_{\mathrm{T},\gamma_{1(2)}}^{\text{iso},0.2}$ used for the analysis. The pile-up and UE correction is estimated on an event-by-event basis, using the ambient transverse momentum density [45]. This density is determined as the median transverse momentum density of jets reconstructed with the k_t-algorithm [46] with a radius parameter $R = 0.5$; it is computed separately in two pseudorapidity regions, $|\eta| < 1.5$ and $1.5 < |\eta| < 3$, and used accordingly depending on the photon pseudorapidity. The photon candidates are required to have $E_{\mathrm{T},\gamma_{1(2)}}^{\text{iso},0.2} < 0.05 \cdot p_{\mathrm{T},\gamma_{1(2)}}$. This isolation requirement is optimised to minimise the overall uncertainties, achieving high signal purities while retaining good signal efficiency. More stringent requirements and use of a larger isolation area would increase the purity at the cost of higher uncertainties from pile-up modelling in the simulation.

The angular separation of the photons is required to be $\Delta R_{\gamma\gamma} > 0.4$, thus avoiding overlap between their isolation cones, and minimising the correlation between the transverse isolation energy of the two photons. The isolation criterion is also used for the background estimation (cf. Section 5), and such a correlation between the isolation criteria of the two photons would have an impact on the background estimation results.

The event selection described above is summarised in Table 1, where the particle-level event selection is also presented, which is described in more detail in the next section. With these requirements 4 708 978 events are selected in the data.

Table 1: Overview of the event selection at the detector level and at the particle level, i.e. definition of the fiducial phase space.

Selection	Detector level	Particle level
Photon kinematics	$p_{\mathrm{T},\gamma_{1(2)}} > 40\,(30)$ GeV,	$|\eta_\gamma| < 2.37$ excluding $1.37 < |\eta_\gamma| < 1.52$
Photon identification	tight	stable, not from hadron decay
Photon isolation	$E_{\mathrm{T},\gamma}^{\text{iso},0.2} < 0.05 \cdot p_{\mathrm{T},\gamma}$	$E_{\mathrm{T},\gamma}^{\text{iso},0.2} < 0.09 \cdot p_{\mathrm{T},\gamma}$
Diphoton topology	$N_\gamma \geq 2, \quad \Delta R_{\gamma\gamma} > 0.4$	

4.2 Particle-level event selection

The particle-level selection, to which the data are unfolded (cf. Section 6), closely follows the detector-level event requirements, and is also shown in Table 1. Some aspects are clarified in detail in the remainder of this section.

The particle-level event selection in MC samples takes the leading two photons into account, and vetoes the event if one of them is not prompt or fails the fiducial cuts.

The transverse isolation energy at particle level is determined as the scalar sum of the transverse momenta of all stable particles,[3] excluding particles from pile-up, muons, neutrinos and the photon itself. Furthermore, to ensure that the side effects of the detector-level UE subtraction are matched at the particle level,[4] a final-state-based subtraction using the same method as described in Section 4.1 is applied. The value of the isolation requirement at the particle level (0.09) is chosen to be different from the one at the detector level (0.05). This difference accounts for the non-compensating nature of the ATLAS calorimeter. The particle-level value is optimised to minimise the number of events where photons pass a detector-level isolation requirement but fail the particle-level one, or vice versa.

4.3 Observables

Cross sections are measured differentially as functions of several observables defined for the diphoton system:

- Transverse momentum p_{T,γ_1} (p_{T,γ_2}) of the leading (sub-leading) photon.
- Invariant mass $m_{\gamma\gamma}$ and transverse momentum $p_{\mathrm{T},\gamma\gamma}$ of the photon pair.
- The absolute value of the cosine of the scattering angle with respect to the z-axis in the Collins–Soper frame [47]:

$$|\cos\theta^*|^{(\mathrm{CS})} = \left| \frac{\sinh(\Delta\eta_{\gamma\gamma})}{\sqrt{1+(p_{\mathrm{T},\gamma\gamma}/m_{\gamma\gamma})^2}} \cdot \frac{2p_{\mathrm{T},\gamma_1}p_{\mathrm{T},\gamma_2}}{m_{\gamma\gamma}^2} \right| = \left| \frac{p^+_{\gamma_1}p^-_{\gamma_2} - p^-_{\gamma_1}p^+_{\gamma_2}}{m_{\gamma\gamma}\cdot\sqrt{m_{\gamma\gamma}^2 + p_{\mathrm{T},\gamma\gamma}^2}} \right|,$$

  with $\Delta\eta_{\gamma\gamma} = \eta_{\gamma_1} - \eta_{\gamma_2}$ and $p^\pm_\gamma = E_\gamma \pm p_{z,\gamma}$, where E_γ is the energy of the photon and $p_{z,\gamma}$ is the z-component of the momentum of the photon. The definition in the Collins–Soper frame simplifies an interpretation of the scattering angle in the presence of initial-state radiation.

- An angular variable sensitive to $p_{\mathrm{T},\gamma\gamma}$ defined as:

$$\phi^*_\eta = \tan\frac{\pi-\Delta\phi_{\gamma\gamma}}{2}\sin\theta^*_\eta = \tan\frac{\pi-\Delta\phi_{\gamma\gamma}}{2}\sqrt{1-\left(\tanh\frac{\Delta\eta_{\gamma\gamma}}{2}\right)^2}.$$

  Angular variables are typically measured with better resolution than the photon energy. Therefore, a particular reference frame that allows ϕ^*_η to be expressed in terms of angular variables only, denoted by the subscript η and described in Ref. [48], is used in order to optimise the resolution. In

[3] Stable particles are defined as those with a decay length $c\tau > 10$ mm.

[4] While there is no pile-up at particle level, there are still other effects, e.g. multiple parton interactions, that can cause such a subtraction procedure to have an influence.

particular, ϕ^*_η is an ideal probe of QCD effects because it probes similar dynamics to $p_{\mathrm{T},\gamma\gamma}$, but with a significantly better resolution in the low-$p_{\mathrm{T},\gamma\gamma}$ region. A similar argument holds for $a_{\mathrm{T},\gamma\gamma}$ below.

- Acoplanarity $\pi - \Delta\phi_{\gamma\gamma}$, where $\Delta\phi_{\gamma\gamma}$ is the azimuthal angular separation of the two photons.
- Transverse component of $p_{\mathrm{T},\gamma\gamma}$ with respect to the thrust axis:[5]

$$a_{\mathrm{T},\gamma\gamma} = 2 \cdot \frac{\left|p_{x,\gamma_1} p_{y,\gamma_2} - p_{y,\gamma_1} p_{x,\gamma_2}\right|}{\left|\vec{p}_{\mathrm{T},\gamma_1} - \vec{p}_{\mathrm{T},\gamma_2}\right|},$$

where $p_{x(y),\gamma_{1(2)}}$ are the $x(y)$-component of the leading (sub-leading) photon momenta, and $\vec{p}_{\mathrm{T},\gamma_1} - \vec{p}_{\mathrm{T},\gamma_2}$ is the vectorial difference of the transverse momenta of the two photons.

5 Background estimation

Reconstructed photon pairs can appear in the detector from a variety of sources beyond prompt production processes. These are summarised in this section along with details about how they are estimated and subtracted from the selected events to give the actual $\gamma\gamma$ signal yield.

Most of the background arises from jets misidentified as photons; these are mainly jets containing a neutral hadron which carries most of the jet energy and decays into a collimated pair of photons with overlapping showers in the calorimeter. This background consists of γj, $j\gamma$, or jj events with one or two jets misidentified as photons, respectively; the notation $j\gamma$ (γj) here and in the following refers to the component where the leading (sub-leading) photon candidate stems from a misidentified jet, while in jj events both photon candidates do. The data-driven determination is described in detail in Section 5.1.

A few percent of the sample corresponds to the *electron background (ee)*, with one or two electrons[6] being misidentified as photons. The electromagnetic showers created by electrons in the calorimeter are very similar to the ones from photons, and therefore electrons can be misidentified as photons. The main process contributing to this background is Drell–Yan production. It is estimated using the MC simulation described in Section 3.2. It makes its largest contribution to the background in the analysis region at $m_{\gamma\gamma} \sim m_Z$.

Finally, less than a percent of the sample is associated with *pile-up background* (PU), i.e. pairs of γj events from different pp collisions in the same bunch crossing. It is determined with a data-driven approach discussed in Section 5.2.

The selected diphoton data sample also contains signal events in which the two photon candidates come from the decay of a Higgs boson. Their contribution to the signal region is predicted to be 0.2% of the integrated signal and increases to a few percent in the relevant $m_{\gamma\gamma}$ bin. This contribution is not subtracted from the data as background, since it is a small genuine part of prompt-photon pair production.

[5] The thrust axis is defined as $\hat{t} = (\vec{p}_{\mathrm{T},\gamma_1} - \vec{p}_{\mathrm{T},\gamma_2})/|\vec{p}_{\mathrm{T},\gamma_1} - \vec{p}_{\mathrm{T},\gamma_2}|$.

[6] An ‘electron’ here and in the following always refers to an electron or a positron.

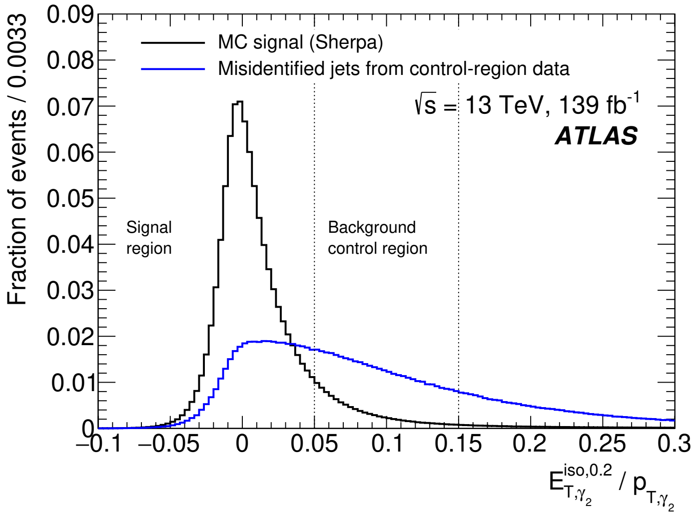

Figure 2: Relative photon isolation distribution for the sub-leading photon candidate as extracted from the SHERPA diphoton sample (black histogram), and from misidentified jets, estimated from data events with sub-leading photon candidates failing the tight identification requirement (blue histogram). A small prompt-photon contribution to the non-tight control region is subtracted from the blue histogram, according to the SHERPA sample predictions.

5.1 Jet background

The background from jets misidentified as prompt photons is estimated using a data-driven method, extrapolating the amount from multiple control regions enriched in background to the *signal region*, i.e. the region defined by the nominal event selection. This extrapolation is done performing a Poisson likelihood fit. The method is an extension of the 'two-dimensional sideband' technique used in the single-photon analyses [9, 10, 12, 49–55] to the two-photon case. It is similar to the method used in previous diphoton analyses [5, 6]. The fit is performed separately in each bin of each observable.

To define the background control regions, two almost independent jet–photon discriminant criteria are used: the lateral shape of the shower at the first layer of the electromagnetic calorimeter and the photon isolation. Specifically, if a photon candidate fails the tight identification selection, by failing the requirements on either f_{side}, w_{s3}, or both shower shape variables (defined in Section 4.1), but satisfies the rest of the identification criteria, the event enters into one of the control regions. If a photon fails the nominal isolation requirement, but falls into $0.05 \cdot p_{\text{T},\gamma_{1(2)}} < E_{\text{T},\gamma_{1(2)}}^{\text{iso},0.2} < 0.15 \cdot p_{\text{T},\gamma_{1(2)}}$, the event enters in a control region. The isolation signal and control regions are indicated in Figure 2, which shows the $E_{\text{T},\gamma_2}^{\text{iso},0.2}/p_{\text{T},\gamma_2}$ relative isolation distribution for prompt photons and for misidentified jets.

In addition to the signal region, where both photons satisfy both the isolation and identification criteria, 15 background control regions are defined representing all possible combinations where at least one photon fails to meet at least one of the criteria, as illustrated in Figure 3. These regions are labelled by the index $i = 1 \ldots 16$, with $i = 1$ being the signal region.

The fit model is built of probability functions $f_{p,i}$, corresponding to the probability of an event from process $p \in \{\gamma\gamma, \gamma j, j\gamma, jj, ee, \text{PU}\}$ to fall in the diphoton region i. They are constructed as a product of the four probabilities: the probabilities for each of the two photon candidates to fulfil both the isolation and

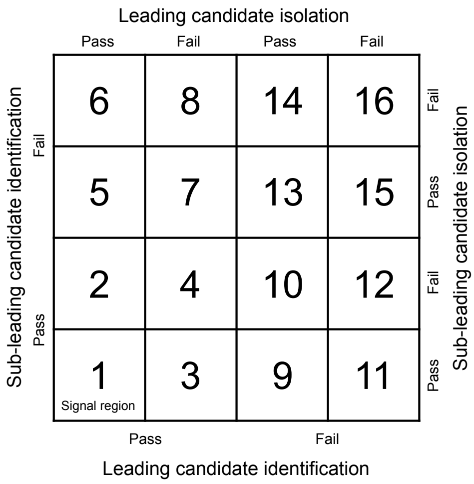

Figure 3: Definition of background control regions, and their corresponding label index.

identification requirements of the given region, according to

$$
\begin{aligned}
f_{p,i} &= f_{p,i}(\varepsilon^{\mathrm{iso}}_{p,1}, \varepsilon^{\mathrm{iso}}_{p,2}, R^{\mathrm{iso}}_{p}, \varepsilon^{\mathrm{id}}_{p,1}, \varepsilon^{\mathrm{id}}_{p,2}, R^{\mathrm{id}}_{p}, R^{\mathrm{iso-id}}_{p,1}, R^{\mathrm{iso-id}}_{p,2}) \\
&= \left\{ \begin{array}{lllll}
\varepsilon^{\mathrm{iso}}_{p,1} & \varepsilon^{\mathrm{iso}}_{p,2} & \varepsilon^{\mathrm{id}}_{p,1} & \varepsilon^{\mathrm{id}}_{p,2} & \text{for } i=1 \\
\varepsilon^{\mathrm{iso}}_{p,1} & (1-\varepsilon^{\mathrm{iso}}_{p,2}) & \varepsilon^{\mathrm{id}}_{p,1} & \varepsilon^{\mathrm{id}}_{p,2} & \text{for } i=2 \\
(1-\varepsilon^{\mathrm{iso}}_{p,1}) & \varepsilon^{\mathrm{iso}}_{p,2}R^{\mathrm{iso}}_{p} & \varepsilon^{\mathrm{id}}_{p,1} & \varepsilon^{\mathrm{id}}_{p,2} & \text{for } i=3 \\
(1-\varepsilon^{\mathrm{iso}}_{p,1}) & (1-\varepsilon^{\mathrm{iso}}_{p,2}R^{\mathrm{iso}}_{p}) & \varepsilon^{\mathrm{id}}_{p,1} & \varepsilon^{\mathrm{id}}_{p,2} & \text{for } i=4 \\
 & & & & \\
\varepsilon^{\mathrm{iso}}_{p,1} & \varepsilon^{\mathrm{iso}}_{p,2}R^{\mathrm{iso-id}}_{p,2} & \varepsilon^{\mathrm{id}}_{p,1} & (1-\varepsilon^{\mathrm{id}}_{p,2}) & \text{for } i=5 \\
\varepsilon^{\mathrm{iso}}_{p,1} & (1-\varepsilon^{\mathrm{iso}}_{p,2}R^{\mathrm{iso-id}}_{p,2}) & \varepsilon^{\mathrm{id}}_{p,1} & (1-\varepsilon^{\mathrm{id}}_{p,2}) & \text{for } i=6 \\
(1-\varepsilon^{\mathrm{iso}}_{p,1}) & \varepsilon^{\mathrm{iso}}_{p,2}R^{\mathrm{iso}}_{p}R^{\mathrm{iso-id}}_{p,2} & \varepsilon^{\mathrm{id}}_{p,1} & (1-\varepsilon^{\mathrm{id}}_{p,2}) & \text{for } i=7 \\
(1-\varepsilon^{\mathrm{iso}}_{p,1}) & (1-\varepsilon^{\mathrm{iso}}_{p,2}R^{\mathrm{iso}}_{p}R^{\mathrm{iso-id}}_{p,2}) & \varepsilon^{\mathrm{id}}_{p,1} & (1-\varepsilon^{\mathrm{id}}_{p,2}) & \text{for } i=8 \\
 & & & & \\
\varepsilon^{\mathrm{iso}}_{p,1}R^{\mathrm{iso-id}}_{p,1} & \varepsilon^{\mathrm{iso}}_{p,2} & (1-\varepsilon^{\mathrm{id}}_{p,1}) & \varepsilon^{\mathrm{id}}_{p,2}R^{\mathrm{id}}_{p} & \text{for } i=9 \\
\varepsilon^{\mathrm{iso}}_{p,1}R^{\mathrm{iso-id}}_{p,1} & (1-\varepsilon^{\mathrm{iso}}_{p,2}) & (1-\varepsilon^{\mathrm{id}}_{p,1}) & \varepsilon^{\mathrm{id}}_{p,2}R^{\mathrm{id}}_{p} & \text{for } i=10 \\
(1-\varepsilon^{\mathrm{iso}}_{p,1}R^{\mathrm{iso-id}}_{p,1}) & \varepsilon^{\mathrm{iso}}_{p,2}R^{\mathrm{iso}}_{p} & (1-\varepsilon^{\mathrm{id}}_{p,1}) & \varepsilon^{\mathrm{id}}_{p,2}R^{\mathrm{id}}_{p} & \text{for } i=11 \\
(1-\varepsilon^{\mathrm{iso}}_{p,1}R^{\mathrm{iso-id}}_{p,1}) & (1-\varepsilon^{\mathrm{iso}}_{p,2}R^{\mathrm{iso}}_{p}) & (1-\varepsilon^{\mathrm{id}}_{p,1}) & \varepsilon^{\mathrm{id}}_{p,2}R^{\mathrm{id}}_{p} & \text{for } i=12 \\
 & & & & \\
\varepsilon^{\mathrm{iso}}_{p,1}R^{\mathrm{iso-id}}_{p,1} & \varepsilon^{\mathrm{iso}}_{p,2}R^{\mathrm{iso-id}}_{p,2} & (1-\varepsilon^{\mathrm{id}}_{p,1}) & (1-\varepsilon^{\mathrm{id}}_{p,2}R^{\mathrm{id}}_{p}) & \text{for } i=13 \\
\varepsilon^{\mathrm{iso}}_{p,1}R^{\mathrm{iso-id}}_{p,1} & (1-\varepsilon^{\mathrm{iso}}_{p,2}R^{\mathrm{iso-id}}_{p,2}) & (1-\varepsilon^{\mathrm{id}}_{p,1}) & (1-\varepsilon^{\mathrm{id}}_{p,2}R^{\mathrm{id}}_{p}) & \text{for } i=14 \\
(1-\varepsilon^{\mathrm{iso}}_{p,1}R^{\mathrm{iso-id}}_{p,1}) & \varepsilon^{\mathrm{iso}}_{p,2}R^{\mathrm{iso}}_{p}R^{\mathrm{iso-id}}_{p,2} & (1-\varepsilon^{\mathrm{id}}_{p,1}) & (1-\varepsilon^{\mathrm{id}}_{p,2}R^{\mathrm{id}}_{p}) & \text{for } i=15 \\
(1-\varepsilon^{\mathrm{iso}}_{p,1}R^{\mathrm{iso-id}}_{p,1}) & (1-\varepsilon^{\mathrm{iso}}_{p,2}R^{\mathrm{iso}}_{p}R^{\mathrm{iso-id}}_{p,2}) & (1-\varepsilon^{\mathrm{id}}_{p,1}) & (1-\varepsilon^{\mathrm{id}}_{p,2}R^{\mathrm{id}}_{p}) & \text{for } i=16.
\end{array} \right.
\end{aligned}
\tag{1}
$$

Here, $\varepsilon^{\mathrm{iso}}_{p,n}$ ($\varepsilon^{\mathrm{id}}_{p,n}$) is the efficiency of the leading ($n = 1$) or sub-leading ($n = 2$) photon candidate to fulfil the signal region isolation (identification) requirement, relative to the looser requirements that include the control regions. The correlation correction factors R account either for correlations between the isolation and identification of one photon candidate, $R^{\text{iso-id}}_{p,n}$, or for correlations between the isolation (identification) of both candidates, R^{iso}_{p} (R^{id}_{p}). A value $R = 1$ corresponds to no correlation between the relevant variables, while values below or above unity indicate a certain degree of positive or negative correlation, respectively.

The expected number of events n_i^{exp} in each region i can then be written as:

$$n_i^{\text{exp}} = \frac{n_{\gamma\gamma}}{\varepsilon^{\text{id}}_{\gamma\gamma,1}\,\varepsilon^{\text{iso}}_{\gamma\gamma,1}\,\varepsilon^{\text{id}}_{\gamma\gamma,2}\,\varepsilon^{\text{iso}}_{\gamma\gamma,2}}\, f_{\gamma\gamma,i} + N_{\gamma j} f_{\gamma j,i} + N_{j\gamma} f_{j\gamma,i} + N_{jj} f_{jj,i} + N_{ee} f_{ee,i} + N_{\text{PU}} f_{\text{PU},i}.$$

Here, $N_{\gamma\gamma}$, $N_{\gamma j}$, $N_{j\gamma}$, N_{jj}, N_{ee} and N_{PU} are the total number of events integrated in all 16 regions, attributed to the signal or background processes, respectively. The parameter of interest, i.e. the number of $\gamma\gamma$ events in the signal region, is given by $n_{\gamma\gamma} \equiv N_{\gamma\gamma} \cdot \varepsilon^{\text{id}}_{\gamma\gamma,1}\,\varepsilon^{\text{iso}}_{\gamma\gamma,1}\,\varepsilon^{\text{id}}_{\gamma\gamma,2}\,\varepsilon^{\text{iso}}_{\gamma\gamma,2}$.

Most of the parameters associated with misidentified jets are estimated from the data, by allowing them to float in the fit, because their MC predictions are not accurate, which motivates this sophisticated approach. The correlation correction factors R are fixed in the fit after being estimated either from MC simulation or from data in validation regions, except for R^{id}_{jj} and R^{iso}_{jj}, which are allowed to float in the fit. In total, a set of 13 nuisance parameters are allowed to float in the fit in addition to $n_{\gamma\gamma}$:

$$\theta = \{N_{\gamma j},\, \varepsilon^{\text{id}}_{\gamma j,2},\, \varepsilon^{\text{iso}}_{\gamma j,2},\, N_{j\gamma},\, \varepsilon^{\text{id}}_{j\gamma,1},\, \varepsilon^{\text{iso}}_{j\gamma,1},\, N_{jj},\, \varepsilon^{\text{id}}_{jj,1},\, \varepsilon^{\text{iso}}_{jj,1},\, \varepsilon^{\text{id}}_{jj,2},\, \varepsilon^{\text{iso}}_{jj,2},\, R^{\text{id}}_{jj},\, R^{\text{iso}}_{jj}\}.$$

The Poisson likelihood function is given by

$$\mathcal{L}(n_{\gamma\gamma}, \theta \,|\, \vec{n}^{\text{obs}}) = \prod_i \frac{\left[n_i^{\text{exp}}(n_{\gamma\gamma}, \theta)\right]^{n_i^{\text{obs}}}}{n_i^{\text{obs}}!} \mathrm{e}^{-n_i^{\text{exp}}(n_{\gamma\gamma}, \theta)},$$

where n_i^{obs} is the number of diphoton candidates observed in each region i.

The efficiency parameters ε corresponding to prompt photons are determined from MC simulation and fixed in the fit. Details about the predetermined input parameters are given in Section 5.1.1. The parameters of the electron and pile-up background probability functions, $f_{ee,i}$ and $f_{\text{PU},i}$, as well as N_{ee} and N_{PU}, are also predetermined and fixed in the fit; the normalisation of the pile-up background N_{PU} is estimated in a data-driven way, as described in Section 5.2, while the values for the other parameters are extracted from MC simulation.

As an example, the distribution of the inclusive data sample in the 16 regions is shown in Figure 4, together with the result of the fit to this inclusive sample; the fractional composition of the data in the signal region resulting from this fit is given in Table 2. For the nominal measurement, as mentioned above, the fit is performed separately in each bin of each observable, and the equivalent sample decomposition in the signal region is displayed differentially in Figure 5. The purity of the $\gamma\gamma$ signal process ranges from 35% at low invariant mass to 80% at high $p_{\text{T},\gamma}$.

This background and signal estimation method is tested using MC simulation. A pseudo-dataset is prepared including $\gamma\gamma$ signal and jet background events, with proportions similar to the ones observed in the data. The results obtained with the fit to the pseudo-dataset are compatible with the fractional composition of the MC events included in the sample.

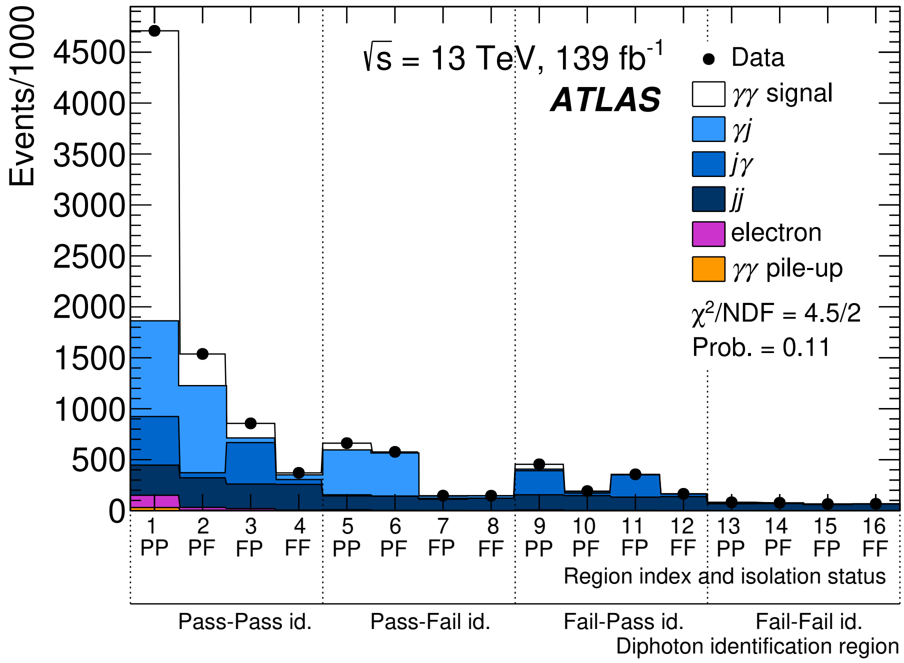

Figure 4: Event yields of the inclusive data sample in the 16 diphoton regions. Both the observed counts and the fit result, including the estimated contributions from the signal and each background component, are shown. The quoted χ^2 value is computed taking into account the systematic uncertainties of the fit model, and their correlation between bins. Labels 'PP/PF/FP/FF' are used to denote the isolation status ('P' = pass, 'F' = fail) of the leading and sub-leading photon candidates. Similarly, the labels 'Pass-Pass id.', 'Pass-Fail id.', etc., denote the identification status of the two photon candidates.

Table 2: Estimated composition of the signal region diphoton candidate samples, resulting from the inclusive sample fit. The uncertainties are fully dominated by the systematic uncertainties, which are discussed in Section 7.

Process	Event fraction [%]
$\gamma\gamma$ signal	60.4 ± 3.0
γj	20.0 ± 1.3
$j\gamma$	10.1 ± 1.1
jj	6.3 ± 1.2
Electron	2.6 ± 0.1
$\gamma\gamma$ pile-up	0.6 ± 0.4

5.1.1 Fit model input parameters

This section describes the parameters of the fit model that are predetermined and fixed in the fit, and how their values and systematic uncertainties are determined. The propagation of the systematic uncertainties to the estimated $n_{\gamma\gamma}$ is done by rerunning the fit using systematic variations of the input parameters, keeping the uncertainty from each source fully correlated between the bins of the observables.

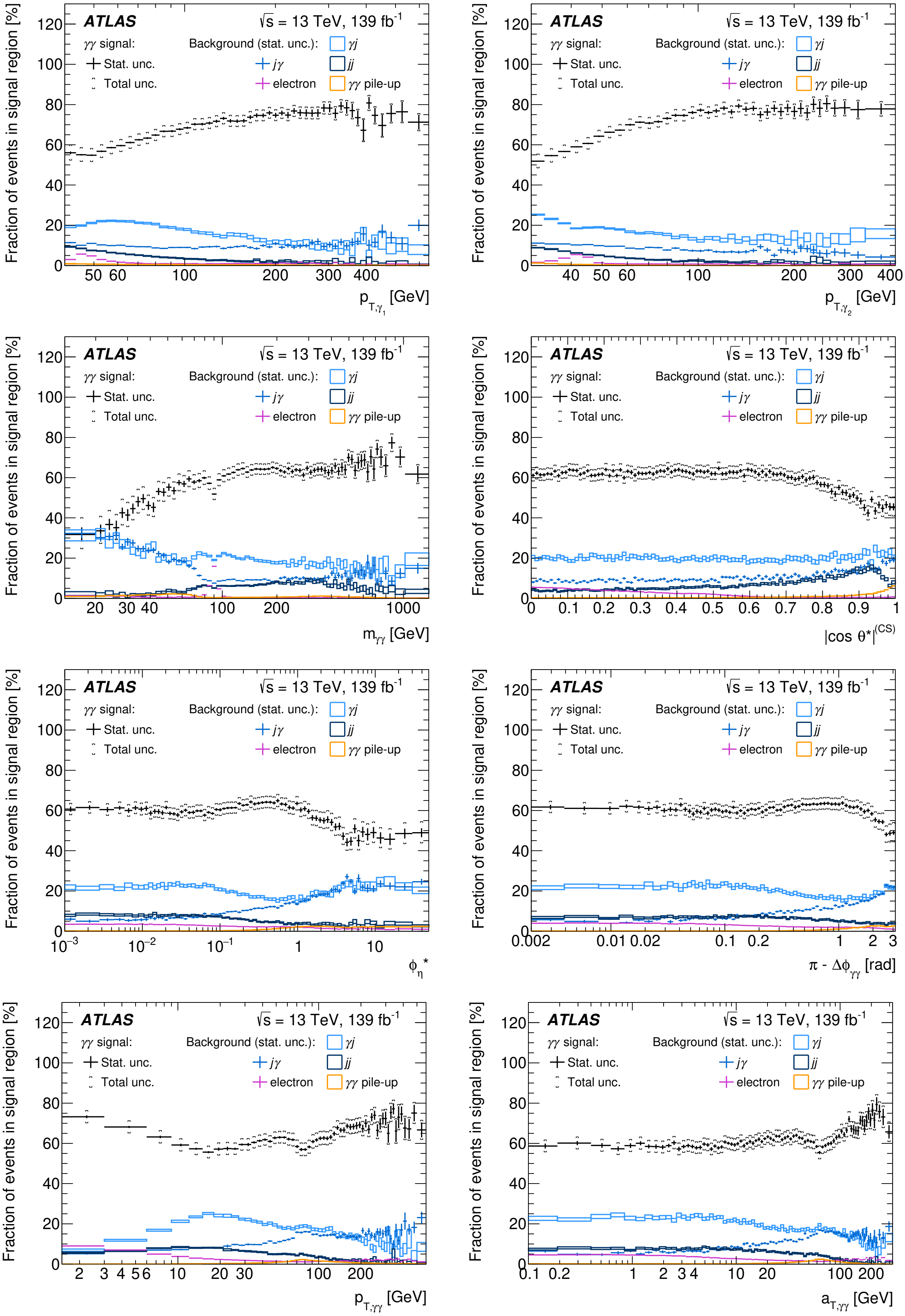

Figure 5: Sample decomposition as a function of each observable. For the $\gamma\gamma$ signal fraction, the total uncertainty is shown, while for the background fractions only the data and Monte Carlo statistical uncertainty component is shown.

Signal parameters: $\boldsymbol{\varepsilon^{\mathrm{id}}_{\gamma\gamma,1}}$, $\boldsymbol{\varepsilon^{\mathrm{id}}_{\gamma\gamma,2}}$, $\boldsymbol{R^{\mathrm{id}}_{\gamma\gamma}}$, $\boldsymbol{\varepsilon^{\mathrm{iso}}_{\gamma\gamma,1}}$, $\boldsymbol{\varepsilon^{\mathrm{iso}}_{\gamma\gamma,2}}$, $\boldsymbol{R^{\mathrm{iso}}_{\gamma\gamma}}$, $\boldsymbol{R^{\mathrm{iso-id}}_{\gamma\gamma,1}}$ and $\boldsymbol{R^{\mathrm{iso-id}}_{\gamma\gamma,2}}$

The values of the eight $\gamma\gamma$ signal parameters are extracted from the Sherpa MC signal sample, corrected to match the isolation and identification variable distributions in data [40]. These parameters are extracted as a function of each observable for which the differential cross section is measured. Uncertainties in these parameter values due to the detector simulation and theory modelling, in particular for the isolation distribution, are taken into account as described in Section 7.2.

Prompt-photon isolation and identification efficiencies in $\boldsymbol{\gamma j}$ and $\boldsymbol{j\gamma}$ events: $\boldsymbol{\varepsilon^{\mathrm{iso}}_{\gamma j,1}}$, $\boldsymbol{\varepsilon^{\mathrm{iso}}_{j\gamma,2}}$, $\boldsymbol{\varepsilon^{\mathrm{id}}_{\gamma j,1}}$, $\boldsymbol{\varepsilon^{\mathrm{id}}_{j\gamma,2}}$

For the γj and $j\gamma$ background components, isolation and identification efficiencies for the prompt photons are derived from the $\gamma\gamma$ signal MC sample. The underlying assumption is cross-checked by comparing these efficiencies with the ones derived from the γj Sherpa MC sample. The efficiencies are compatible within statistical uncertainties. In addition, a change of 2% in those efficiencies is tested, which is roughly the size of the statistical uncertainty of the comparison ratio, and the impact on the estimated signal yield result is found to be negligible.

Isolation–identification correlation for misidentified jets: $\boldsymbol{R^{\mathrm{iso-id}}_{\gamma j,2}}$, $\boldsymbol{R^{\mathrm{iso-id}}_{j\gamma,1}}$, $\boldsymbol{R^{\mathrm{iso-id}}_{jj,1}}$ and $\boldsymbol{R^{\mathrm{iso-id}}_{jj,2}}$

The correlation between isolation and identification for jets misidentified as photons is studied with γj events as a function of p_{T,γ_2}. A twofold approach is used to estimate it. First, a γj MC simulation sample is used, yielding $R^{\mathrm{iso-id,MC}}_{\gamma j,2} = 0.990 \pm 0.025$ (stat) without a significant trend as a function of p_{T,γ_2} given the limited MC sample size. In addition to the MC study, a γj-rich validation region in data is constructed by requiring the sub-leading photon to fail a track isolation requirement. The track isolation variable $p^{\mathrm{iso},0.2}_{\mathrm{T},\gamma_2}$ is computed as the sum of the transverse momenta of charged-particle tracks coming from the primary vertex, in a cone of $\Delta R = 0.2$ around the photon candidate direction. In the validation region, the sub-leading photon candidates are required to have $p^{\mathrm{iso},0.2}_{\mathrm{T},\gamma_2} > 0.02 \cdot p_{\mathrm{T},\gamma_2} + 1.5\,\mathrm{GeV}$. The contamination from $\gamma\gamma$ events in that validation region is subtracted using the signal MC simulation. With the higher statistical power of the data, an enhancement of the positive correlation as a function of p_{T,γ_2} is observed, i.e. values of $R^{\mathrm{iso-id}}_{\gamma j,2}$ further from one, below one. This dependency is extrapolated to the signal region using the MC simulation. An average of the MC and data results is used for the central values of this correction factor versus p_{T,γ_2}; the values vary in a range of $0.93 < R^{\mathrm{iso-id}} < 0.99$ as shown in Figure 6. The MC simulation is susceptible to mismodelling of the correlation, while the data estimation relies on the MC-based subtraction of $\gamma\gamma$ events in the validation region, and on the low correlation between the calorimetric and track isolation. Half of the difference between the MC and data results is assigned as a systematic uncertainty, and combined in quadrature with the MC statistical uncertainty. For each bin of the observables and each of the four $R^{\mathrm{iso-id}}$ parameters for misidentified jets, an average is calculated taking into account the corresponding photon candidate $p_{\mathrm{T},\gamma}$ distribution, estimated from data events in the control regions dominated by each background process.

In addition to p_{T,γ_2}, the dependency of $R^{\mathrm{iso-id}}_{\gamma j,2}$ on the photon candidate pseudorapidity is also studied; however, its impact is found to be negligible.

Correlation between isolation in $\boldsymbol{\gamma j}$ and $\boldsymbol{j\gamma}$ events: $\boldsymbol{R^{\mathrm{iso}}_{\gamma j}}$ and $\boldsymbol{R^{\mathrm{iso}}_{j\gamma}}$

The correction factor R^{iso}_{p} parameterises the correlation between the isolation variables of the two photon candidates. For the signal probability function, this parameter is extracted from MC simulation as $R^{\mathrm{iso}}_{\gamma\gamma}$. A similar extraction for misidentified jets from γj MC samples alone is not possible because of the limited statistical precision available. A slight correlation is expected, as found for the signal process, where $0.95 < R^{\mathrm{iso}}_{\gamma\gamma} < 1$. It is also extracted from jj background events, as R^{iso}_{jj} is left to float in the fit and yields values in the range $0.9 < R^{\mathrm{iso}}_{jj} < 1$. For the γj and $j\gamma$ backgrounds, $R^{\mathrm{iso}}_{\gamma j} = R^{\mathrm{iso}}_{j\gamma} = 0.95 \pm 0.05$ is chosen in all regions of phase space, thus the uncertainties

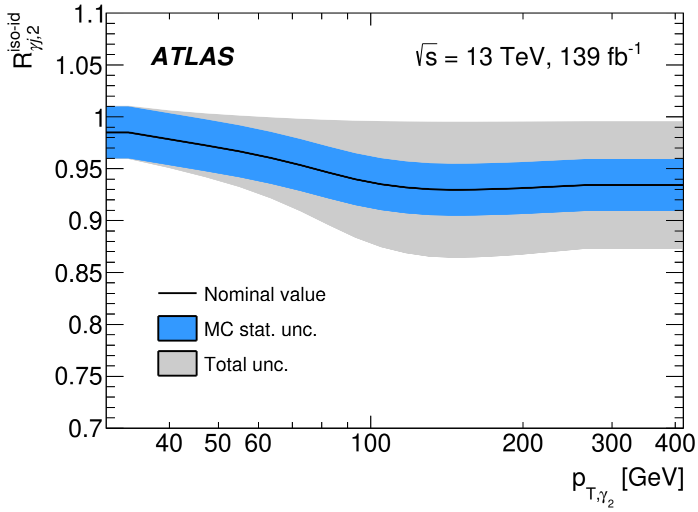

Figure 6: Correction factor $R^{\text{iso-id}}_{\gamma j,2}$ for the isolation–identification correlation, for jets misidentified as photons. The nominal value is indicated in black, and is the average of the values obtained from a data validation region and a γj MC sample. The blue band corresponds to the simulation statistical uncertainty, and the grey band shows the total uncertainty, taking into account half of the difference between the MC and data results.

cover the extreme cases. This uncertainty is treated as fully correlated between all the bins of the observables, in the same way as all the uncertainties discussed in this section.

In order to have the common correction factor $R^{\text{iso}}_{\gamma j} = R^{\text{iso}}_{j\gamma}$ consistently affecting the isolation efficiency of the photon candidate associated with the misidentified jet in both processes, γj and $j\gamma$, the probability function for the $j\gamma$ background $f_{j\gamma,i}$ is slightly modified relative to the Eq. (1) function. In Eq. (1), the R^{iso}_{p} parameter corrects the isolation efficiency of the sub-leading photon candidate $\varepsilon^{\text{iso}}_{p,2}$ in the regions where the leading candidate fails the nominal isolation requirement, i.e. in the regions 3, 4, 7, 8, 11, 12, 15 and 16. In the $j\gamma$ case, the function is modified, and $R^{\text{iso}}_{j\gamma}$ corrects the leading candidate efficiency $\varepsilon^{\text{iso}}_{j\gamma,1}$ in the regions where the sub-leading candidate fails the nominal isolation criterion, i.e. in the regions 2, 4, 6, 8, 10, 12, 14 and 16. For example, for regions 3 and 4:

$$f_{j\gamma,i} = \begin{cases} (1-\varepsilon^{\text{iso}}_{j\gamma,1}) \quad \varepsilon^{\text{iso}}_{j\gamma,2} \quad \varepsilon^{\text{id}}_{j\gamma,1}\ \varepsilon^{\text{id}}_{j\gamma,2} & \text{for } i = 3 \\ (1-\varepsilon^{\text{iso}}_{j\gamma,1}R^{\text{iso}}_{j\gamma})\ (1-\varepsilon^{\text{iso}}_{j\gamma,2})\ \varepsilon^{\text{id}}_{j\gamma,1}\ \varepsilon^{\text{id}}_{j\gamma,2} & \text{for } i = 4. \end{cases}$$

Identification correlation in γj events: $R^{\text{id}}_{\gamma j}$ and $R^{\text{id}}_{j\gamma}$

The correlation between the identification of the two objects is in general very low. This is cross-checked with MC simulation for the $\gamma\gamma$ signal process. For the jj process, the correlation is extracted from the data, by allowing R^{id}_{jj} to float in the fit. In both cases, R^{id} is close to one within 2%. Performing the fit with the $R^{\text{id}}_{\gamma j}$ and $R^{\text{id}}_{j\gamma}$ values changed by 2% produces negligible variations of the final result. The assumption $R^{\text{id}}_{\gamma j} = R^{\text{id}}_{j\gamma} = 1$ is thus kept without an additional uncertainty.

5.2 Pile-up of multiple single-photon events

Pairs of γj events from different pp collisions in the same bunch crossing can form a diphoton final state in the detector. The normalisation of this background is estimated using a fit to the data. The shape of the background in the diphoton observables is based on MC simulations. Details of the procedure are given below.

In diphoton events, in general, there is not enough information to efficiently identify and reject the pile-up background. However, around 0.5% of the events do have sufficiently precise information for both photons to effectively determine whether they are produced at the same primary interaction vertex or not. This subsample of events is used to estimate the pile-up background normalisation. It consists of events with both photons converted to electron–positron pairs within the detector material, with both conversions fully reconstructed, i.e. each including the reconstruction of the two charged-particle tracks, and with both photons in the central pseudorapidity region, $|\eta| < 1.37$.[7] In addition, the conversion tracks are required to have hits in the silicon detectors of the inner tracking system. For each photon, the trajectory is reconstructed using the shower-depth segmentation of the calorimeter, and the position of the conversion vertex. The intersection of the extrapolated trajectory with the beam axis provides a precise estimate of the longitudinal position z_γ of the vertex at which the photon is produced. This information is used in a two-component fit to $\Delta z = |z_{\gamma_1} - z_{\gamma_2}|$, as can be seen in Figure 7.

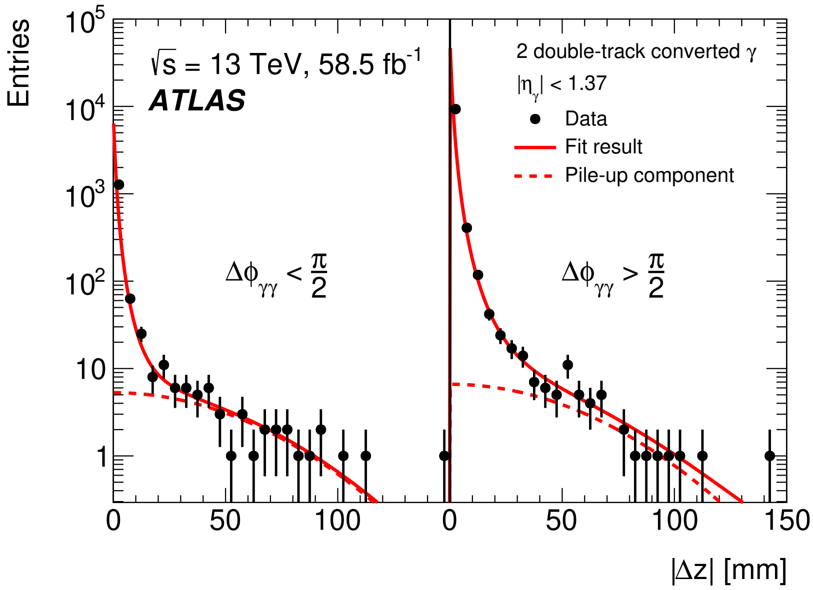

Figure 7: The two-component fit to determine the global normalisation of pile-up events is shown. Data events in which each of the two photon candidates is associated with two inner detector tracks are used for the fit. The dashed lines represent the pile-up-like component of the total model marked with a solid line. The left side of the plot shows the events with azimuthal angular separation of the photon candidates $\Delta\phi_{\gamma\gamma} < \pi/2$, and the right side of the plot shows the events with $\Delta\phi_{\gamma\gamma} > \pi/2$. The fit is performed in the two regions simultaneously.

The first component of the model, representing the distribution of pile-up events in Δz, is considered to be a convolution of the two individual Gaussian z_γ distributions that have a width of $\sigma_z = 34.15 \pm 0.16$ mm, resulting in a Gaussian with a width of $\sigma_{\Delta z} = \sqrt{2} \times \sigma_z$. The σ_z value is estimated by fitting a Gaussian function to the z_γ distribution. Since σ_z changes between data-taking periods, depending on the beam conditions, only data collected in 2018 are used for this pile-up background study; during this period σ_z was relatively stable, with a root-mean-square of the σ_z variations of 2.8 mm. The integrated luminosity of

[7] The fraction of converted photons is fairly constant as a function of photon E_T and η and well modelled in MC simulation. The conversion events can thus be used directly for an extrapolation to the full dataset.

the 2018 dataset is 58.5 fb^{-1}. Afterwards, the estimated amount of pile-up background is extrapolated to the full Run-2 dataset, taking into account the integrated luminosity and the average number of interactions per bunch crossing $\langle\mu\rangle$ of the two datasets, $\langle\mu\rangle_{2018} = 36.1$ and $\langle\mu\rangle_{\mathrm{Run\,2}} = 33.7$. The amount of pile-up background is proportional to $\langle\mu\rangle$.

The second component of the fit model, representing the non-pile-up contribution, is taken as a power-law function. For most of the photon candidates, the z_γ resolution is around 0.2 mm; however, some candidates have significantly larger z_γ resolution, which induces a long tail in the Δz distribution. This tail is well modelled by the power-law function.

To extract the fraction of events due to pile-up, the power-law parameters and the normalisation of each component are fitted simultaneously to the measured Δz distribution. The fit is performed in two regions simultaneously, $\Delta\phi_{\gamma\gamma} < \pi/2$ and $\Delta\phi_{\gamma\gamma} > \pi/2$. For non-pile-up diphoton candidates, there are 10 times more events with $\Delta\phi_{\gamma\gamma} > \pi/2$ than with $\Delta\phi_{\gamma\gamma} < \pi/2$; this proportion is allowed to float in the fit. On the other hand, for the pile-up background, the events are almost equally distributed between the two regions; only the $\Delta R_{\gamma\gamma} > 0.4$ selection requirement unbalances the $\Delta\phi_{\gamma\gamma}$ distribution, slightly reducing the fraction of pile-up events with $\Delta\phi_{\gamma\gamma} < \pi/2$. In this case, this fraction is fixed in the fit, according to the MC simulation prediction. The difference between the proportions of pile-up and non-pile-up events in the two $\Delta\phi_{\gamma\gamma}$ regions helps to constrain the fit parameters. The fit yields an uncertainty of $\delta_{\mathrm{fit}}^{\mathrm{PU}} = \pm 15\%$ for the pile-up background fraction.

The event yield resulting from this fit still contains contributions from misidentified jets, which are subtracted in the main background fit also for pile-up events. To avoid a double subtraction, the nominal background fit is performed for the events with $\Delta z > 48$ mm to determine the fraction of prompt $\gamma\gamma$ events within the pile-up contribution. The large uncertainty of $\delta_{\gamma\gamma}^{\mathrm{PU}} = \pm 50\%$ in this fraction is of statistical nature due to the low number of input events, and is added in quadrature with the $\delta_{\mathrm{fit}}^{\mathrm{PU}}$ to form the total uncertainty in the pile-up background propagated to the final results, as described in Section 7.

With the normalisation of the pile-up background fixed, the shape of this background in the fiducial phase space and as a function of each observable is derived using a sample of pseudo-events. Events in this sample are constructed by overlaying two separate reconstructed events from a γj MC simulation. This shape is combined with the normalisation determined as above and fed into the background estimation fit as a predetermined component. Given the large relative uncertainty of the normalisation and the small contribution from this background, the uncertainties of the MC sample are negligible.

In the inclusive sample, the pile-up background is found to be $(0.6 \pm 0.4)\%$. Differentially, the largest contribution from this background is around 6% at $|\cos\theta^*|^{(\mathrm{CS})}$ close to one, cf. Figure 5.

6 Correction to particle level

Effects such as the finite resolution of the detector and the event selection efficiency have to be corrected for, in order to be able to compare results from different experiments and to allow comparisons with theory predictions without detector simulation. The particle-level selection to which the data are unfolded is presented in Table 1. The unfolding procedure is applied to the background-subtracted distribution at the detector level in three steps.

First, the measured distribution is corrected for the fraction of MC events reconstructed and selected at detector level that do not pass the particle-level selection. The contribution of these *unmatched*

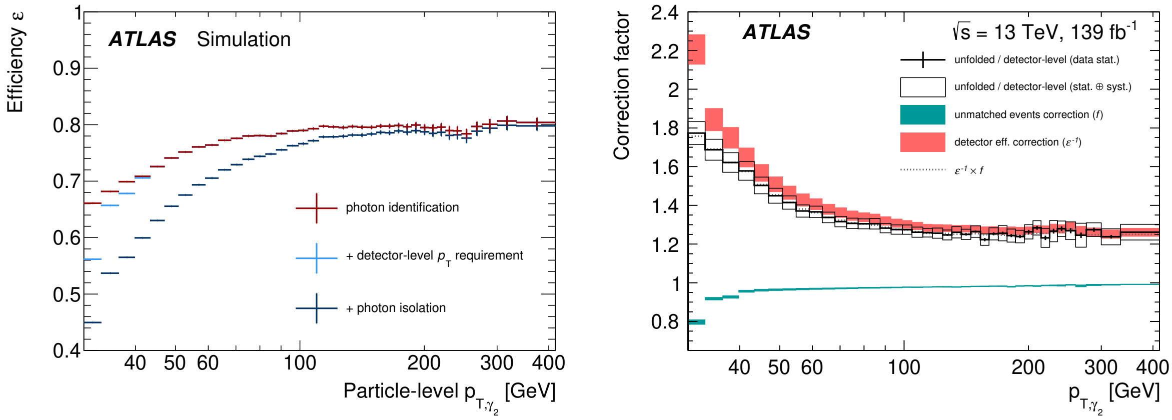

(a) (b)

Figure 8: (a) Efficiency of consecutive sets of detector-level selections for diphoton events passing the particle-level selection as a function of the particle-level p_{T,γ_2}. (b) Impact of the unfolding on the detector-level yields after background subtraction as a function of p_{T,γ_2}. The correction for the fraction of unmatched events not passing the particle-level cuts is depicted in green. The correction for the detector efficiency is shown in red. The black line is the ratio of the detector-level yields to the result after the three corrections (i.e. for unmatched events, the iterative migration unfolding and the correction for detector inefficiencies) are applied. The impact of the iterative unfolding can be seen by comparison with the grey dotted line, which is the product of the efficiency and unmatched events correction.

reconstructed events is estimated using the signal MC samples. The main source of unmatched photons is failure to satisfy the transverse momentum and isolation requirements. The particle-level selection is chosen to be close to the detector-level selection to reduce the influence of this correction.

The second step is to correct for detector resolution effects which cause migrations from one particle-level bin to multiple detector-level bins. For this step, an iterative unfolding method [56] based on Bayes' theorem is used. Response matrices parameterise these migrations and are constructed from simulated events passing both the detector-level and particle-level selections. A first iteration of the migration correction uses the particle-level prediction from Sherpa as the prior input. The prior then gets updated with the obtained result, and the procedure is repeated; three iterations are done in this analysis. The chosen number of iterations is high enough to minimise the dependence on the prior, but low enough to not be sensitive to statistical fluctuations.

In the last step, the unfolded results are corrected for detector inefficiencies. This accounts for the fraction of particle-level selected events in the signal region which do not pass the signal selections at detector level. Their contribution is also estimated using the signal MC samples. The largest corrections stem from the photon identification and isolation selection, as shown in Figure 8(a) as a function of p_{T,γ_2}.

Figure 8(b) illustrates individual steps of the unfolding correction, as well as the total correction, for the p_{T,γ_2} observable. The efficiency and unmatched-photon corrections partially cancel each other out due to the symmetric shape of the detector response, e.g. for the photon transverse momentum criteria.

Table 3: Breakdown of the relative uncertainties in the integrated fiducial cross-section measurement. The uncertainties are grouped into different categories and the first row of each category shows the sum in quadrature of its components.

Source	Relative uncertainty [%]
Background estimation	4.3
$R_j^{\mathrm{iso-id}}$	4.2
$\gamma\gamma$ pile-up background	0.6
$R_{\gamma \mathrm{j}}^{\mathrm{iso}}$	0.5
Electron background	0.2
Photon isolation	4.1
Pile-up reweighting	3.5
Data-driven correction	1.9
Theory modelling of isolation	0.6
Photon reconstruction and identification	3.0
Photon identification	2.9
Photon reconstruction	0.4
Other	3.5
Data-period stability	2.9
Luminosity	1.7
Trigger efficiency	0.7
Theory modelling of p_{T,γ_1}	0.2
MC statistical uncertainty	0.1
Unfolding method	<0.1
Photon energy	0.5
Total systematic uncertainty	7.5
Data statistical uncertainty	0.3

7 Uncertainties

Several uncertainties affect the measurement. They are evaluated independently and then added in quadrature as uncorrelated components into a total uncertainty, with its breakdown shown in Table 3 for the integrated fiducial cross section. Figure 9 shows the breakdown of the systematic uncertainties in the differential cross section.

The individual sources of uncertainties and the methods to propagate them to the final result are described in more detail in the following sections.

7.1 Background estimation

Jets misidentified as photons. The correlation between isolation and identification for jets misidentified as photons, $R_j^{\mathrm{iso-id}}$, is determined both from MC simulations and from a data-driven approach, as described in Section 5.1.1. While the average of the two methods is used for the central value, half of the difference is assigned as an uncertainty to cover both approaches and is combined in quadrature with the statistical uncertainty of the MC result. This is by far the dominant contribution to the total uncertainty for the background, which amounts to 4.2% in general and rises to 17% in the low-$m_{\gamma\gamma}$

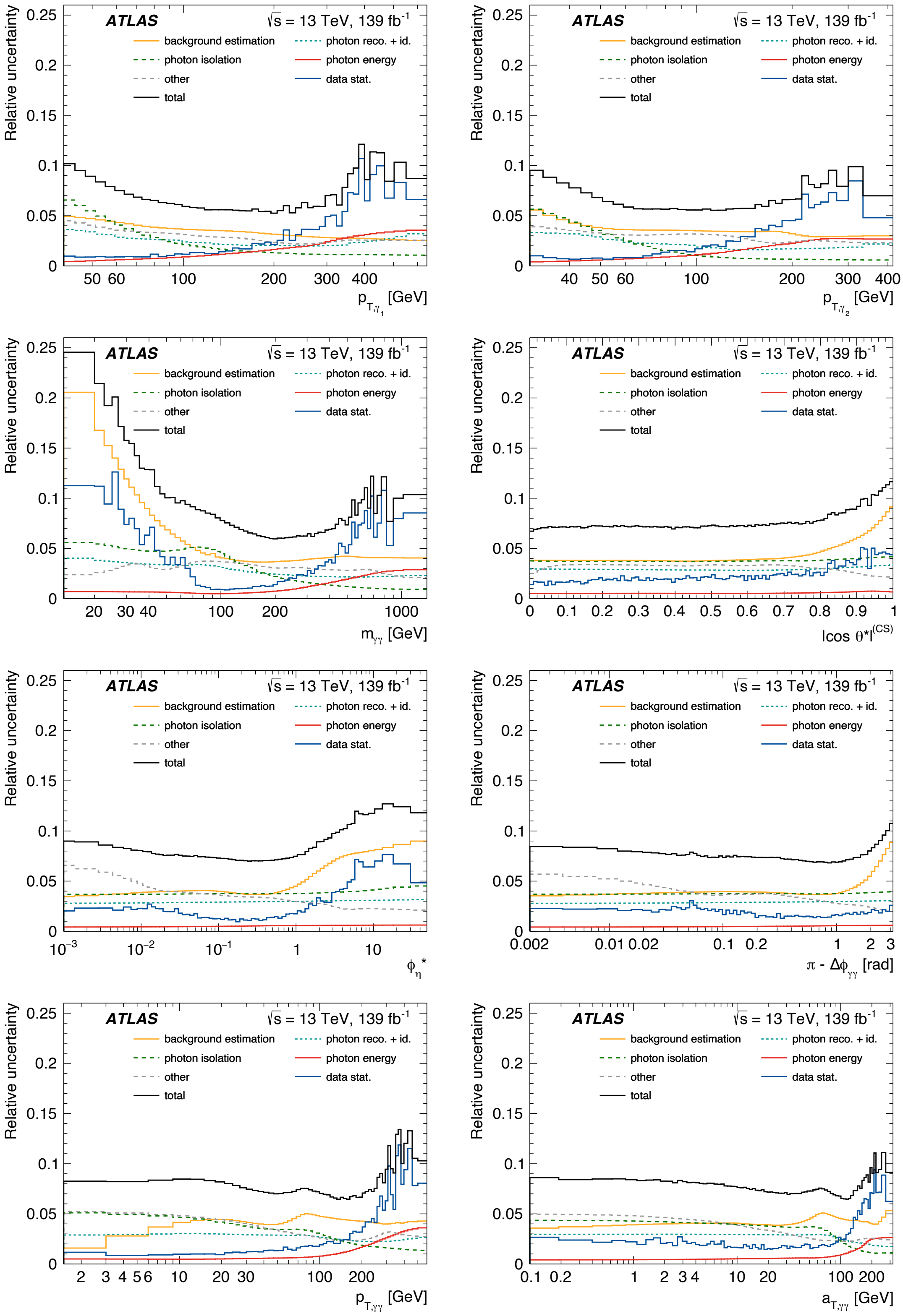

Figure 9: The relative uncertainties in the unfolded result associated with different sources are summarised. The uncertainty components and the total uncertainty are shown as a function of each of the observables.

region.
The correlation between the photon and jet isolation in γj and $j\gamma$ events is varied around its central value by ±5%, as determined from cross-checks in the $\gamma\gamma$ MC sample and in the control regions dominated by jj events in data. This uncertainty is at the sub-percent level almost everywhere, except at low $m_{\gamma\gamma}$, where it rises to 6%.
Uncertainties in the identification and isolation efficiencies of the prompt photons also affect the background estimation. They are discussed in the Section 7.2.

Electrons misidentified as photons. Three components are taken into account as uncertainties for the electron-related background sources. The physics modelling of the $Z \to ee$ MC sample is varied by a 5% normalisation uncertainty, and a p_{T}^{Z}-dependent shape uncertainty covers the difference between MC simulation and data [39]. The uncertainty related to the modelling of $e \to \gamma$ fake rates is estimated from a dedicated measurement using $Z \to ee$ events. All of these uncertainties have a completely negligible contribution almost everywhere, rising to 2% only in the $m_{\gamma\gamma} \sim m_Z$ bin.

Pile-up background. The uncertainty in the normalisation of the pile-up background stems from a combination of two uncertainties arising from the fits, namely the fit to extract the total pile-up yield, and the $\gamma\gamma$ extraction in the pile-up sample. The main impact of this background contribution is located at $|\cos\theta^*|^{(\mathrm{CS})} \to 1$ (see Figure 5) and its uncertainty rises to 6% in this region, whereas it is small in all other regions of phase space.

The uncertainties described above are propagated to the final cross-section results by using different background-subtracted signal yields as input to the unfolding procedure, with all bins varied in a correlated way, and response matrices unaffected.

7.2 Photon selection

The detector simulation and reconstruction of photons within the MC samples play significant roles in the background estimation and unfolding. This results in uncertainties from various sources.

Photon isolation. The modelling of the photon isolation variable in simulated events is corrected using a data-driven technique when deriving the nominal results [40]. An uncertainty due to a potential isolation mismodelling is estimated by disabling these data-driven corrections. The corrections modify the position of the peak of the isolation variable.
Additionally, the width of the isolation transverse energy distribution is affected significantly by the modelling of pile-up in the simulation. In the MC samples, the noise induced by the pile-up in the calorimeters is found to be overestimated, increasing the width of the distribution of the used calorimetric isolation. This simulation feature is observed in the electron isolation distribution in $Z \to ee$ events. Therefore, to extract the efficiency of the photon isolation requirement, the simulation pile-up profile is reweighted, scaling down the number of pile-up interactions by 17%, based on the observations from the $Z \to ee$ studies. Systematic uncertainties are estimated by further reducing and increasing the amount of pile-up similarly by 17%. The uncertainty in the modelling of pile-up dominates the isolation uncertainty and constitutes one of the leading sources of uncertainty in the analysis, with a typical size of 4%.
The isolation distribution is also affected by a theory modelling uncertainty; the estimation of this uncertainty is discussed in Section 7.3.

Photon trigger, reconstruction and identification efficiency. The uncertainties in the modelling of the detector efficiency of the photon trigger, reconstruction and identification are addressed using scale factors that depend on the transverse momentum $p_{\mathrm{T},\gamma}$ and pseudorapidity η of the photon. The trigger and identification scale factors and their uncertainties are derived to match the detector efficiency in simulation to data as described in Refs. [18, 40]. The trigger efficiency uncertainty is around 0.7% while the uncertainty in the measured diphoton cross section related to the photon identification efficiency ranges between 2% and 4%. The photon reconstruction efficiency is studied with $Z \to \mu\mu\gamma$ events by looking for events in which the reconstructed cluster is misclassified as an electron. The fraction of photons misreconstructed as electrons is around 4%. To match the data, the simulated reconstruction efficiency of the diphoton systems is corrected on average by -1.8%, with an uncertainty of 0.4%. The reconstruction efficiency corrections are derived and applied independently for data taken in the years 2015+2016 and 2017+2018.

Photon energy. Uncertainties in the photon energy scale and resolution are taken into account by modifying the MC simulation used to determine response matrices, efficiencies and unmatched-photon rates [43]. This is done separately for independent sources of the uncertainty, e.g. from the overall energy scale determined in $Z \to ee$ decays, the non-linearity of the energy measurement at the calorimeter cell level, the relative calibration of the different calorimeter layers, the amount of material in front of the calorimeter, and the simulation modelling of the photon conversion reconstruction, lateral shower shape, and energy resolution. They are propagated separately to account for correlations and their η dependence, and are combined in quadrature afterwards. This uncertainty is at the sub-percent level in most regions of the analysis, rising to 3% only at high transverse momentum and $m_{\gamma\gamma}$.

For the photon isolation and identification variations described above, modified MC simulations are used coherently in the background fit and unfolding, to propagate the uncertainty for each source to the final result and maintain the correlations. The photon energy and photon trigger efficiency uncertainty affect only the unfolding.

7.3 Other uncertainties

Signal theory modelling. The theory modelling in the signal MC samples can affect the correction to the particle level as well as the signal model parameters in the background fit. The resulting uncertainty is estimated by reweighting the nominal SHERPA sample in two different ways and repeating the whole analysis chain. The first reweighting is based on the photon isolation distribution taken from a PYTHIA 8 sample at particle level. The uncertainty in the final results is relatively constant at the 1% level but rises to 4% in the low-$m_{\gamma\gamma}$ region. Additionally, a reweighting of the leading photon's transverse momentum distribution is performed such that the detector-level distribution matches the background-subtracted result. The effect of this variation is below 1%. The differences between the nominal and each of the two reweighted results are treated as independent uncertainties and applied coherently in the background fit and the unfolding.

Unfolding method uncertainties. The results of the unfolding procedure can depend on the choice of prior and the number of iterations. To estimate an uncertainty, the MC simulation is reweighted such that it matches the data at the detector level, and this emulated data is then unfolded using the nominal sample. The non-closure with respect to the reweighted particle-level simulation then yields an additional uncertainty orthogonal to the one from signal theory modelling and is negligible everywhere.

Table 4: Overview of the theory predictions and their relevant features. The label 'QCD res.' ('NP effects') stands for QCD resummation (non-perturbative effects).

	Fixed-order accuracy						Fragmentation		QCD	NP
	$\gamma\gamma$	$+1j$	$+2j$	$+3j$	$+\geq 4j$	$gg \to \gamma\gamma$	single	double	res.	effects
Diphox	NLO	LO	-	-	-	LO	NLO		–	–
Nnlojet	NNLO	NLO	LO	-	-	LO	–	–	–	–
Sherpa	NLO		LO		PS	LO	ME+PS		PS	✓

Data period stability A test is performed comparing the results obtained by splitting the data into 2015+2016, 2017 and 2018 periods, and the MC sample in their corresponding representative subsamples. The whole analysis is redone for these three individual datasets. An additional uncertainty is assigned as a function of the different observables to cover the non-closure among the different years. It is typically around 3%.

MC statistics. The influence of the limited size of the MC samples on the final result is evaluated using pseudo-experiments. Each experiment is generated by assigning a random weight according to a Poisson distribution with an expectation value of one to every MC event. The MC statistical uncertainty is estimated from the standard deviation of the results of the pseudo-experiments and is negligible everywhere.

Data statistics. The statistical uncertainty of the data sample is propagated from the signal extraction to the particle level using pseudo-experiments. It is the dominant uncertainty at high p_{T} and high $m_{\gamma\gamma}$, but sub-leading in general.

Luminosity. The uncertainty in the combined 2015–2018 integrated luminosity is 1.7% [57], obtained using the LUCID-2 detector [58] for the primary luminosity measurements. This uncertainty is sub-leading in comparison with the other uncertainties.

8 Theory predictions

The unfolded data are compared with several state-of-the-art theory predictions, which are summarised in Table 4 and detailed in this section.

Fixed-order NNLO with Nnlojet. The Nnlojet framework [59] is used to obtain fixed-order predictions for diphoton production up to NNLO QCD accuracy. It is based on the antenna subtraction method [60, 61] and the NNLO prediction includes the loop-induced $gg \to \gamma\gamma$ contribution at leading-order accuracy. The nominal factorisation and renormalisation scales are chosen as $\mu_{\mathrm{f,r}} = m_{\gamma\gamma}$ and varied independently to estimate the perturbative uncertainties in a 7-point variation to $\mu_{\mathrm{f}} = c_{\mathrm{f}} \cdot m_{\gamma\gamma}$ and $\mu_{\mathrm{r}} = c_{\mathrm{r}} \cdot m_{\gamma\gamma}$, where $c_{\mathrm{f,r}} = 0.5, 1, 2$ with $0.5 \leq c_{\mathrm{f}}/c_{\mathrm{r}} \leq 2$. For the nominal predictions, the NNPDF3.0 NNLO PDF set [29] is used. NNLO predictions for the fragmentation component are not yet available. Thus, the prediction is calculated only from the direct component using an implementation of the hybrid scheme for photon isolation [30, 62, 63]:

- a very loose smooth cone isolation [31] with $n = 2$, $\delta_0 = 0.1$, $\varepsilon = 0.1$, and

- the experimental cone isolation with the fiducial photon isolation given in Table 1 but without the UE subtraction.

The smooth-cone isolation requirement is necessary to remove collinear photon–quark configurations from the calculation, which would be singular and would have to be factorised into a fragmentation function for a full calculation. The hybrid scheme helps to minimise the bias from not taking such configurations into account.

Fixed-order NLO with Diphox. Fixed-order NLO predictions including the direct and single- and double-fragmentation contributions are made with Diphox [64] using CT10 NLO PDFs [65]. The nominal factorisation, renormalisation, and fragmentation scales are chosen as $\mu_\mathrm{r} = \mu_\mathrm{f} = \mu_\mathrm{frag} = m_{\gamma\gamma}$. The loop-induced $gg \to \gamma\gamma$ process is included in the direct component at leading order. Since the fragmentation contributions are included, the Diphox predictions are valid for a cone-based photon isolation consistent with the one used in the measurement, $E_{\mathrm{T},\gamma_{1(2)}}^{\mathrm{iso},0.2} < 0.09 \cdot p_{\mathrm{T},\gamma_{1(2)}}$. To estimate the perturbative uncertainties of the Diphox predictions, three sets of input parameters are varied. Factorisation and renormalisation scales undergo 7-point variations as defined above. This is the dominant uncertainty for this prediction. The fragmentation scale is raised and lowered by a factor of 2, yielding an uncertainty which is always significantly smaller than that from the factorisation and renormalisation scale variations. Finally, variations between predictions based on the nominal PDF set and those based on MSTW2008 [66] and NNPDF2.3 [32] are also significantly smaller than those from the scale variation in all phase-space regions.

The fixed-order predictions do not include non-perturbative effects. The impact of the non-perturbative effects is found to be negligible, except in soft or collinear regions of the phase space, where they grow to $O(10\%)$; in such regions, fixed-order predictions are not valid without resummation. Thus, no correction is applied to the fixed-order predictions.

Sherpa In addition to these fixed-order calculations, the unfolded data are also compared with fully hadronised particle-level predictions from the Sherpa signal calculations described in Section 3.2. This sample is used extensively throughout the analysis chain, e.g. in the background fit and the correction for detector effects.

Systematic theory uncertainties for the following comparisons are obtained from three sets of variations performed using event reweighting [67]. Factorisation and renormalisation scales are varied independently in a 7-point variation as defined above to estimate the perturbative uncertainties. A second set of uncertainties is obtained by coherently varying the strong coupling used in the simulation and in the PDF fit, $\alpha_\mathrm{s}(m_Z)$ in the range 0.117–0.119. A third uncertainty set is constructed from all replicas within the NNPDF3.0 NNLO set. These uncertainties are completely dominated by the scale uncertainties and are summed in quadrature to obtain a final uncertainty envelope for the Sherpa predictions.

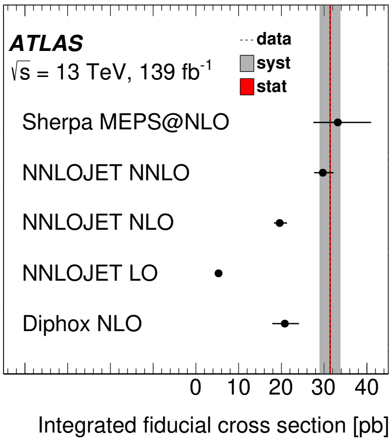

Figure 10: Integrated fiducial cross-section comparison between ATLAS data and theory predictions.

9 Results

9.1 Integrated cross section in the fiducial phase space

The measurement of the differential cross section as a function of p_{T,γ_2} is used to compute the integrated fiducial cross section,

$$\sigma_{\gamma\gamma} = 31.4 \pm 0.1\,(\text{stat.}) \pm 2.4\,(\text{syst.})\ \text{pb}.$$

The integration is also performed over the other differential cross-section measurements yielding compatible results. The fiducial phase space is defined in Table 1.

A comparison of the measured cross section with the theoretical predictions (see Figure 10 and Table 5) shows the importance of higher-order QCD contributions even for such an inclusive diphoton measurement. The predictions from Sherpa MEPS@NLO, which has NLO multi-leg matrix elements supplemented by a parton shower, and that from the fixed-order NNLO prediction as implemented in Nnlojet are the only predictions compatible with the data within the uncertainties. The predictions limited to LO or NLO QCD, as implemented in Nnlojet (N)LO and Diphox NLO, fail to agree with the data and also do not provide a reliable estimate of the perturbative uncertainties, as will be discussed further below.

Table 5: Integrated fiducial cross section from ATLAS data compared with theory predictions with their systematic uncertainties from QCD scale variations.

Fiducial cross section [pb]	$\sigma_{\gamma\gamma}$	$\pm$ unc.
Sherpa MEPS@NLO	33.2	$^{+7.7}_{-5.6}$
Nnlojet NNLO	29.7	$^{+2.4}_{-2.0}$
NLO	19.6	$^{+1.6}_{-1.3}$
LO	5.3	$^{+0.5}_{-0.5}$
Diphox NLO	20.8	$^{+3.2}_{-2.9}$
Data	31.4	2.4

9.2 Differential cross sections

The measured differential cross sections as functions of the different observables are shown in Figures 11 and 12. Comparisons between the data and Diphox NLO, Nnlojet NNLO and Sherpa MEPS@NLO predictions are also included for all observables. Nnlojet and Sherpa provide the best agreement with the data in the regions expected to be modelled well by perturbative QCD. Since Diphox and Nnlojet are fixed-order predictions, they are not expected to be valid in regions where the effects of multiple collinear or soft QCD emissions are relevant, while Sherpa provides remarkably good agreement with the data in these regions also. The systematic uncertainties of the fixed-order calculations estimated from scale variations fail to provide a reliable estimate of the true uncertainties, as indicated by the failure of the uncertainty bands to overlap with each other. This is a typical feature of the diphoton process, where significant contributions and their uncertainties only appear at higher orders, namely the single- and double-fragmentation contributions shown in Figure 1(b). For example, the largest part of the fixed-order uncertainty bands stems from renormalisation scale variations in the real-emission topologies, which are by definition spuriously absent at LO. The multi-leg merged prediction from Sherpa includes real-emission topologies for higher multiplicities than in the other predictions and also exhibits correspondingly large uncertainties.

For the transverse momentum spectrum of the leading photon, p_{T,γ_1}, Nnlojet and Sherpa predictions are compatible with the data over the full measured range. Diphox adequately describes the shape of the measured differential cross section; however, as already seen for the integrated cross section, the normalisation of this prediction is much lower than that of the data. A similar picture holds for the transverse momentum of the sub-leading photon, p_{T,γ_2}, with the only notable difference being the shape of the Diphox prediction, which adequately describes the shape of the measured cross section for $p_{\mathrm{T},\gamma_2} \geq 40$ GeV, but considerably underestimates the rate of photons at lower p_{T,γ_2} values.

Stark features of the theory predictions can be seen in the $m_{\gamma\gamma}$ spectrum. The shape of this distribution is governed by the transverse-momentum requirements placed on the individual photons, with the region $m_{\gamma\gamma} < p_{\mathrm{T},\gamma_1} + p_{\mathrm{T},\gamma_2}$ being suppressed and only populated through $\gamma\gamma$+multi-jet configurations. Such configurations are not modelled well at NLO accuracy in Diphox, but benefit significantly from the higher-order contributions included in the Nnlojet and Sherpa predictions. The predictions from Nnlojet and Sherpa agree with the data within uncertainties, while the uncertainties in the Diphox prediction are severely underestimated judging from the higher-order predictions. At high $m_{\gamma\gamma}$, the Sherpa predictions are compatible with the data, while Nnlojet underestimates the rate slightly.

For high $p_{\mathrm{T},\gamma\gamma}$, Sherpa and Nnlojet agree well with the data, while for intermediate values the Nnlojet prediction is slightly too low to cover the data within uncertainties, and Sherpa is slightly high but still compatible. As expected, the fixed-order predictions fail at low $p_{\mathrm{T},\gamma\gamma} < 10$ GeV, where soft QCD emissions are relevant, while Sherpa is in good agreement with the data also in this region of phase space.

The three observables $\pi - \Delta\phi_{\gamma\gamma}$, $a_{\mathrm{T},\gamma\gamma}$, and ϕ^*_η are closely related and reveal very similar features in the comparison between the data and the theory predictions. The almost back-to-back configuration of the two photons ($\pi - \Delta\phi_{\gamma\gamma} < 0.1$, $a_{\mathrm{T},\gamma\gamma} < 10$ GeV, or $\phi^*_\eta < 0.1$) is difficult to model correctly with fixed-order predictions, because even almost collinear or low-energy parton emissions can decorrelate the two photons. Only the parton-shower-based Sherpa prediction includes a resummation of these effects and is able to model the back-to-back region reliably, agreeing well with the data over the full measured range in these three observables. In the region of intermediate azimuthal separation of the photons ($\pi - \Delta\phi_{\gamma\gamma} \approx 1$, $a_{\mathrm{T},\gamma\gamma} \approx 40$ GeV, or $\phi^*_\eta \approx 0.5$), Nnlojet underestimates the data, while for a large decorrelation they agree

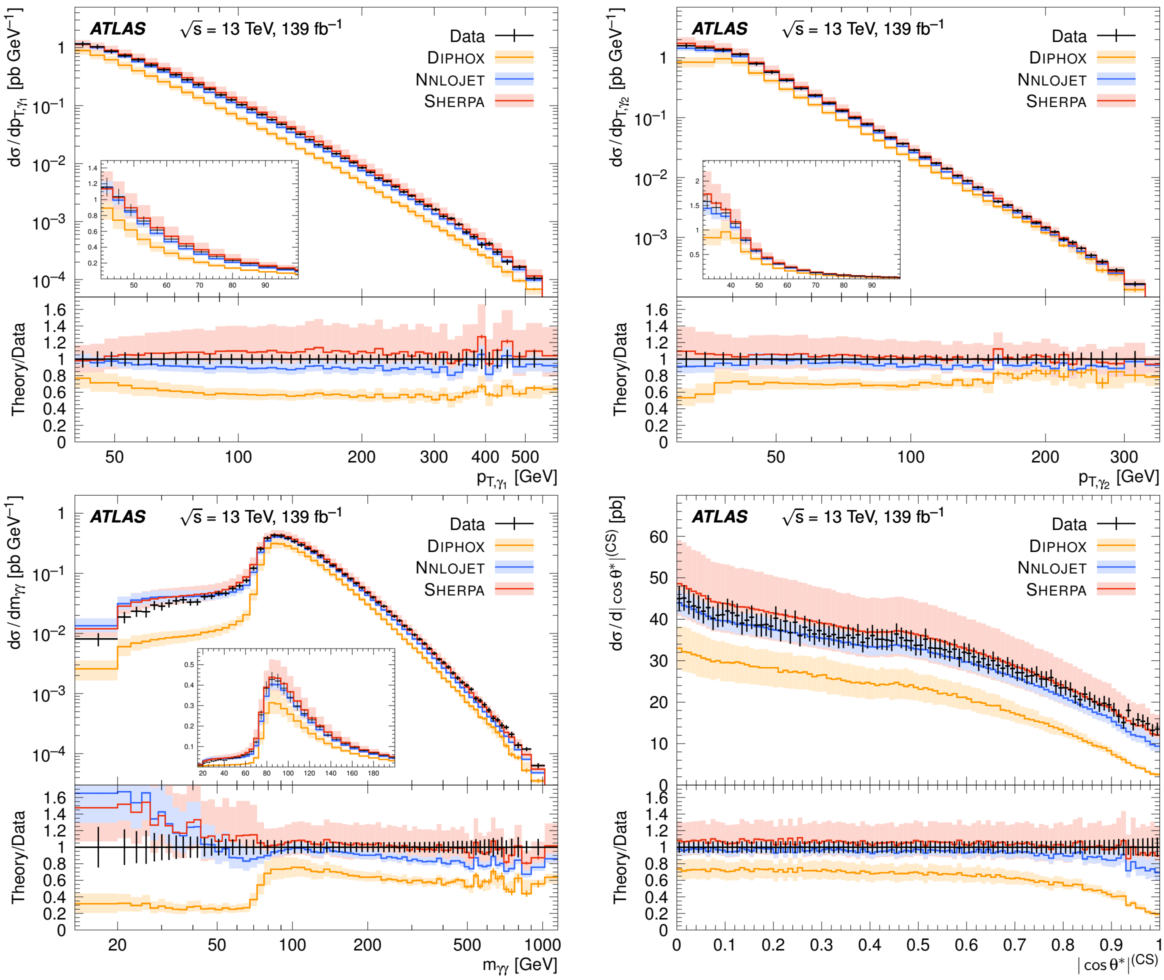

Figure 11: Differential cross sections measured as functions of p_{T,γ_1}, p_{T,γ_2}, $m_{\gamma\gamma}$ and $|\cos\theta^*|^{(\mathrm{CS})}$ (black error bars) compared with the predictions from DIPHOX NLO, NNLOJET NNLO and SHERPA MEPS@NLO (lines with coloured bands). At the bottom of each plot, the ratio of the prediction to the data is shown. Uncertainty bars on the data represent the total uncertainty, while uncertainty bands (bars) on the predictions represent perturbative scale (statistical) uncertainties. Inset plots show the core of each distribution on a linear scale. For p_{T,γ_1}, p_{T,γ_2} and $m_{\gamma\gamma}$ the last bin is only visible in the ratio inset and includes the overflow events.

well, in contrast to the NLO predictions from DIPHOX, which fail to accurately model the shape of these distributions over the full measured range.

For scattering angles close to the limit $|\cos\theta^*|^{(\mathrm{CS})} \to 1$, the fixed-order predictions underestimate the measured rate. This region is sensitive to uncorrelated photons, which can occur as a consequence of the associated production of multiple jets. The NNLO prediction is affected by larger perturbative uncertainties in this region; this is an indication of the (N)LO-accurate associated production of two jets (one jet) becoming relevant. The multi-leg merged prediction from SHERPA provides a better description of the measured cross section in this region.

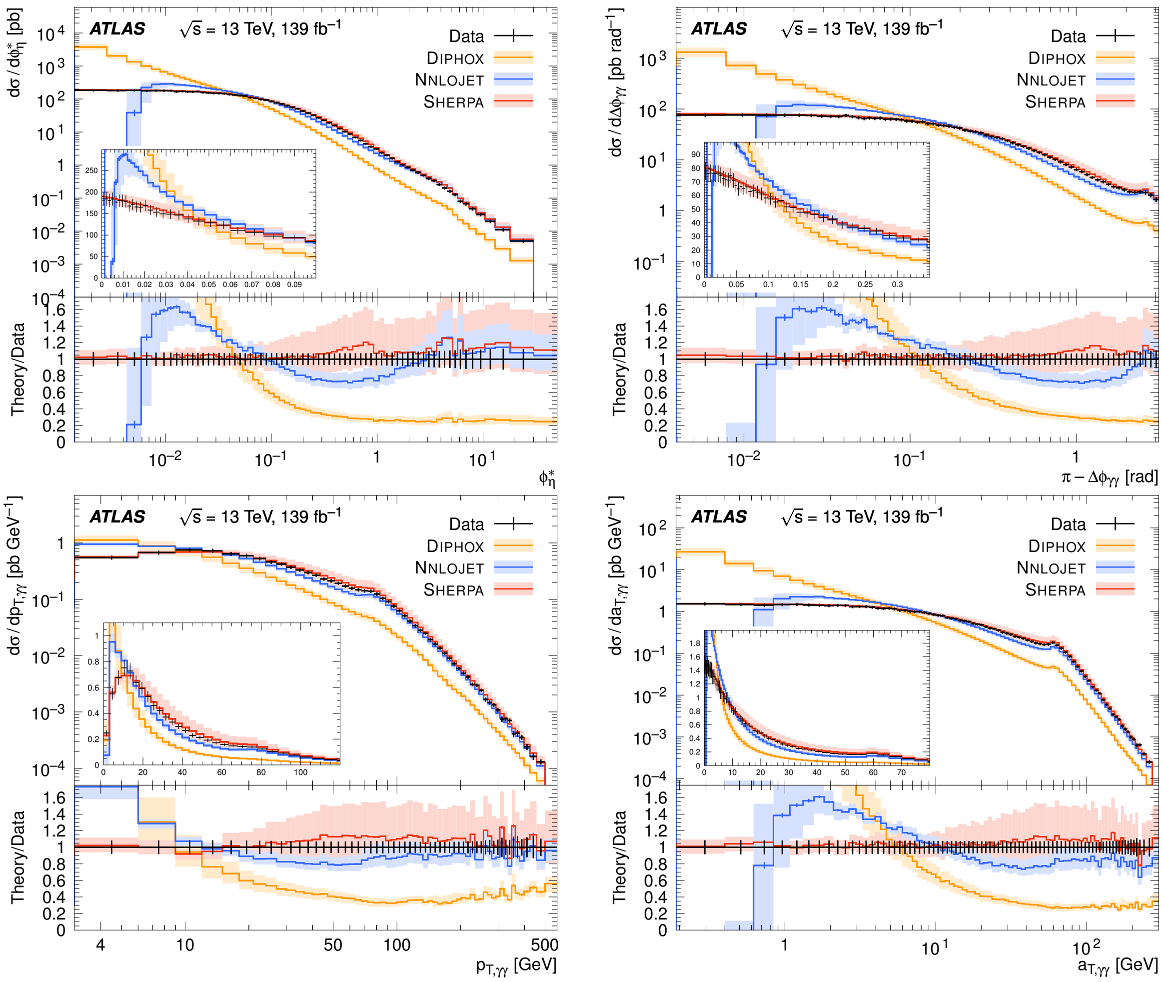

Figure 12: Differential cross sections measured as functions of ϕ^*_η, $\pi - \Delta\phi_{\gamma\gamma}$, $p_{\mathrm{T},\gamma\gamma}$, and $a_{\mathrm{T},\gamma\gamma}$ (black error bars) compared with the predictions from DIPHOX NLO, NNLOJET NNLO and SHERPA MEPS@NLO (lines with coloured bands). At the bottom of each plot, the ratio of the prediction to the data is shown. Uncertainty bars on the data represent the total uncertainty, while uncertainty bands (bars) on the predictions represent perturbative scale (statistical) uncertainties. Inset plots show the core of each distribution on a linear scale. For ϕ^*_η, $p_{\mathrm{T},\gamma\gamma}$ and $a_{\mathrm{T},\gamma\gamma}$ the last bin is only visible in the ratio inset and includes the overflow events.

10 Conclusion

A measurement of prompt photon pair production in proton–proton collisions at $\sqrt{s} = 13$ TeV is presented. The data were recorded by the ATLAS detector at the LHC with an integrated luminosity of 139 fb^{-1}.

Events with two photons in the well-instrumented region of the detector are selected, and the photons are required to be isolated and have $p_{\mathrm{T},\gamma_{1(2)}} > 40$ (30) GeV for the leading (sub-leading) photon ordered in transverse momentum. The dominant background stems from non-prompt photons from hadron decays, which is very challenging to estimate using simulation. A sophisticated data-driven method is used to estimate this background using background-rich control regions based on inverted photon identification and isolation requirements. Using a data-driven technique, the small background from two photons being produced in separate proton–proton collisions in the same bunch crossing is also taken into account, which will become even more relevant for future LHC runs.

The background-subtracted signal yields are corrected for detector efficiencies and migrations, and converted into fiducial cross sections. The measured integrated fiducial cross section is 31.4 ± 2.4 pb. Differential cross sections as functions of several observables of the diphoton system are presented, including the transverse momenta of the leading (sub-leading) photon up to 550 (330) GeV, the invariant mass of the diphoton system from 15 GeV to 1 TeV, and the transverse momentum of the diphoton system up to 500 GeV. Specifically, diphoton variables sensitive to different aspects of higher-order corrections in perturbative QCD are studied and compared with theory predictions from state-of-the-art MC and fixed-order calculations.

Good agreement is generally found with the predictions at the highest theoretical precision. An impressive improvement is observed when taking into account higher-order terms in perturbative QCD. Only the merged approach with multi-leg matrix elements at NLO, as implemented by Sherpa, and a fixed-order NNLO calculation, as implemented by Nnlojet, give a satisfactory description of the data. The fixed-order NNLO calculation has a higher formal precision than Sherpa and thus lower theoretical uncertainties in the regions governed by perturbative QCD. The multi-leg merged prediction yields larger uncertainties, but is in better agreement with the data in all regions. Sherpa includes QCD resummation through the parton shower, and thus provides a more reliable prediction in regions sensitive to collinear or low-energy parton emissions. The shape of the measured cross section as a function of $m_{\gamma\gamma}$ is best described by the Sherpa predictions. The region of low $m_{\gamma\gamma}$ is sensitive to multi-jet configurations, which are only modelled with low precision in all predictions.

Acknowledgements

We thank CERN for the very successful operation of the LHC, as well as the support staff from our institutions without whom ATLAS could not be operated efficiently.

We acknowledge the support of ANPCyT, Argentina; YerPhI, Armenia; ARC, Australia; BMWFW and FWF, Austria; ANAS, Azerbaijan; SSTC, Belarus; CNPq and FAPESP, Brazil; NSERC, NRC and CFI, Canada; CERN; ANID, Chile; CAS, MOST and NSFC, China; Minciencias, Colombia; MSMT CR, MPO CR and VSC CR, Czech Republic; DNRF and DNSRC, Denmark; IN2P3-CNRS and CEA-DRF/IRFU, France; SRNSFG, Georgia; BMBF, HGF and MPG, Germany; GSRT, Greece; RGC and Hong Kong SAR, China; ISF and Benoziyo Center, Israel; INFN, Italy; MEXT and JSPS, Japan; CNRST, Morocco; NWO, Netherlands; RCN, Norway; MNiSW and NCN, Poland; FCT, Portugal; MNE/IFA, Romania; JINR; MES of Russia and NRC KI, Russian Federation; MESTD, Serbia; MSSR, Slovakia; ARRS and MIZŠ, Slovenia; DST/NRF, South Africa; MICINN, Spain; SRC and Wallenberg Foundation, Sweden; SERI, SNSF and Cantons of Bern and Geneva, Switzerland; MOST, Taiwan; TAEK, Turkey; STFC, United Kingdom; DOE and NSF, United States of America. In addition, individual groups and members have received support from BCKDF, CANARIE, Compute Canada, CRC and IVADO, Canada; Beijing Municipal Science & Technology Commission, China; COST, ERC, ERDF, Horizon 2020 and Marie Skłodowska-Curie Actions, European Union; Investissements d'Avenir Labex, Investissements d'Avenir Idex and ANR, France; DFG and AvH Foundation, Germany; Herakleitos, Thales and Aristeia programmes co-financed by EU-ESF and the Greek NSRF, Greece; BSF-NSF and GIF, Israel; La Caixa Banking Foundation, CERCA Programme Generalitat de Catalunya and PROMETEO and GenT Programmes Generalitat Valenciana, Spain; Göran Gustafssons Stiftelse, Sweden; The Royal Society and Leverhulme Trust, United Kingdom.

The crucial computing support from all WLCG partners is acknowledged gratefully, in particular from CERN, the ATLAS Tier-1 facilities at TRIUMF (Canada), NDGF (Denmark, Norway, Sweden), CC-IN2P3 (France), KIT/GridKA (Germany), INFN-CNAF (Italy), NL-T1 (Netherlands), PIC (Spain), ASGC (Taiwan), RAL (UK) and BNL (USA), the Tier-2 facilities worldwide and large non-WLCG resource providers. Major contributors of computing resources are listed in Ref. [68].

References

[1] CDF Collaboration, *Measurement of the Cross Section for Prompt Isolated Diphoton Production Using the Full CDF Run II Data Sample*, Phys. Rev. Lett. **110** (2013) 101801, arXiv: 1212.4204 [hep-ex].

[2] D0 Collaboration, *Measurement of the differential cross sections for isolated direct photon pair production in $p\bar{p}$ collisions at $\sqrt{s} = 1.96$ TeV*, Phys. Lett. B **725** (2013) 6, arXiv: 1301.4536 [hep-ex].

[3] CMS Collaboration, *Measurement of the production cross section for pairs of isolated photons in pp collisions at $\sqrt{s} = 7$ TeV*, JHEP **01** (2012) 133, arXiv: 1110.6461 [hep-ex].

[4] CMS Collaboration, *Measurement of differential cross sections for the production of a pair of isolated photons in pp collisions at $\sqrt{s} = 7$ TeV*, Eur. Phys. J. C **74** (2014) 3129, arXiv: 1405.7225 [hep-ex].

[5] ATLAS Collaboration, *Measurement of the isolated diphoton cross section in pp collisions at $\sqrt{s} = 7$ TeV with the ATLAS detector*, Phys. Rev. D **85** (2012) 012003, arXiv: 1107.0581 [hep-ex].

[6] ATLAS Collaboration, *Measurement of isolated-photon pair production in pp collisions at $\sqrt{s} = 7$ TeV with the ATLAS detector*, JHEP **01** (2013) 086, arXiv: 1211.1913 [hep-ex].

[7] ATLAS Collaboration, *Measurements of integrated and differential cross sections for isolated photon pair production in pp collisions at $\sqrt{s} = 8$ TeV with the ATLAS detector*, Phys. Rev. D **95** (2017) 112005, arXiv: 1704.03839 [hep-ex].

[8] CMS Collaboration, *Measurement of differential cross sections for inclusive isolated-photon and photon+jet production in proton–proton collisions at $\sqrt{s} = 13$ TeV*, Eur. Phys. J. C **79** (2019) 20, arXiv: 1807.00782 [hep-ex].

[9] ATLAS Collaboration, *Measurement of the cross section for inclusive isolated-photon production in pp collisions at $\sqrt{s} = 13$ TeV using the ATLAS detector*, Phys. Lett. B **770** (2017) 473, arXiv: 1701.06882 [hep-ex].

[10] ATLAS Collaboration, *Measurement of the cross section for isolated-photon plus jet production in pp collisions at $\sqrt{s} = 13$ TeV using the ATLAS detector*, Phys. Lett. B **780** (2018) 578, arXiv: 1801.00112 [hep-ex].

[11] ATLAS Collaboration, *Measurement of the ratio of cross sections for inclusive isolated-photon production in pp collisions at $\sqrt{s} = 13$ and 8 TeV with the ATLAS detector*, JHEP **04** (2019) 093, arXiv: 1901.10075 [hep-ex].

[12] ATLAS Collaboration, *Measurement of the inclusive isolated-photon cross section in pp collisions at $\sqrt{s} = 13$ TeV using 36 fb^{-1} of ATLAS data*, JHEP **10** (2019) 203, arXiv: 1908.02746 [hep-ex].

[13] ATLAS Collaboration, *Measurement of isolated-photon plus two-jet production in pp collisions at $\sqrt{s} = 13$ TeV with the ATLAS detector*, JHEP **03** (2020) 179, arXiv: 1912.09866 [hep-ex].

[14] ATLAS Collaboration, *The ATLAS Experiment at the CERN Large Hadron Collider*, JINST **3** (2008) S08003.

[15] ATLAS Collaboration, *Performance of the ATLAS trigger system in 2015*, Eur. Phys. J. C **77** (2017) 317, arXiv: 1611.09661 [hep-ex].

[16] ATLAS Collaboration, *The ATLAS Collaboration Software and Firmware*, ATL-SOFT-PUB-2021-001, 2021, URL: https://cds.cern.ch/record/2767187.

[17] ATLAS Collaboration, *ATLAS data quality operations and performance for 2015–2018 data-taking*, JINST **15** (2020) P04003, arXiv: 1911.04632 [physics.ins-det].

[18] ATLAS Collaboration, *Performance of electron and photon triggers in ATLAS during LHC Run 2*, Eur. Phys. J. C **80** (2020) 47, arXiv: 1909.00761 [hep-ex].

[19] ATLAS Collaboration, *The ATLAS Simulation Infrastructure*, Eur. Phys. J. C **70** (2010) 823, arXiv: 1005.4568 [physics.ins-det].

[20] GEANT4 Collaboration, S. Agostinelli et al., *Geant4 – a simulation toolkit*, Nucl. Instrum. Meth. A **506** (2003) 250.

[21] E. Bothmann et al., *Event generation with Sherpa 2.2*, SciPost Phys. **7** (2019) 034, arXiv: 1905.09127 [hep-ph].

[22] T. Sjöstrand, S. Mrenna and P. Skands, *A brief introduction to PYTHIA 8.1*, Comput. Phys. Commun. **178** (2008) 852, arXiv: 0710.3820 [hep-ph].

[23] T. Gleisberg and S. Höche, *Comix, a new matrix element generator*, JHEP **12** (2008) 039, arXiv: 0808.3674 [hep-ph].

[24] S. Schumann and F. Krauss, *A parton shower algorithm based on Catani–Seymour dipole factorisation*, JHEP **03** (2008) 038, arXiv: 0709.1027 [hep-ph].

[25] S. Höche, F. Krauss, M. Schönherr and F. Siegert, *A critical appraisal of NLO+PS matching methods*, JHEP **09** (2012) 049, arXiv: 1111.1220 [hep-ph].

[26] S. Höche, F. Krauss, M. Schönherr and F. Siegert, *QCD matrix elements + parton showers. The NLO case*, JHEP **04** (2013) 027, arXiv: 1207.5030 [hep-ph].

[27] F. Cascioli, P. Maierhöfer and S. Pozzorini, *Scattering Amplitudes with Open Loops*, Phys. Rev. Lett. **108** (2012) 111601, arXiv: 1111.5206 [hep-ph].

[28] A. Denner, S. Dittmaier and L. Hofer, *Collier: A fortran-based complex one-loop library in extended regularizations*, Comput. Phys. Commun. **212** (2017) 220, arXiv: 1604.06792 [hep-ph].

[29] R. D. Ball et al., *Parton distributions for the LHC run II*, JHEP **04** (2015) 040, arXiv: 1410.8849 [hep-ph].

[30] F. Siegert, *A practical guide to event generation for prompt photon production with Sherpa*, J. Phys. G **44** (2017) 044007, arXiv: 1611.07226 [hep-ph].

[31] S. Frixione, *Isolated photons in perturbative QCD*, Phys. Lett. B **429** (1998) 369, arXiv: hep-ph/9801442.

[32] R. D. Ball et al., *Parton distributions with LHC data*, Nucl. Phys. B **867** (2013) 244, arXiv: 1207.1303 [hep-ph].

[33] ATLAS Collaboration, *ATLAS Pythia 8 tunes to* 7 *TeV data*, ATL-PHYS-PUB-2014-021, 2014, URL: https://cds.cern.ch/record/1966419.

[34] S. Alioli, P. Nason, C. Oleari and E. Re, *A general framework for implementing NLO calculations in shower Monte Carlo programs: the POWHEG BOX*, JHEP **06** (2010) 043, arXiv: 1002.2581 [hep-ph].

[35] P. Nason, *A new method for combining NLO QCD with shower Monte Carlo algorithms*, JHEP **11** (2004) 040, arXiv: hep-ph/0409146.

[36] ATLAS Collaboration, *Measurement of the Z/γ^* boson transverse momentum distribution in pp collisions at $\sqrt{s} = 7$ TeV with the ATLAS detector*, JHEP **09** (2014) 145, arXiv: 1406.3660 [hep-ex].

[37] N. Davidson, T. Przedzinski and Z. Was, *PHOTOS Interface in C++: Technical and physics documentation*, Comput. Phys. Commun. **199** (2016) 86, arXiv: 1011.0937 [hep-ph].

[38] C. Anastasiou, L. J. Dixon, K. Melnikov and F. Petriello, *High precision QCD at hadron colliders: Electroweak gauge boson rapidity distributions at next-to-next-to leading order*, Phys. Rev. D **69** (2004) 094008, arXiv: hep-ph/0312266.

[39] ATLAS Collaboration, *Measurement of the transverse momentum distribution of Drell–Yan lepton pairs in proton–proton collisions at $\sqrt{s} = 13$ TeV with the ATLAS detector*, Eur. Phys. J. C **80** (2020) 616, arXiv: 1912.02844 [hep-ex].

[40] ATLAS Collaboration, *Electron and photon performance measurements with the ATLAS detector using the 2015–2017 LHC proton–proton collision data*, JINST **14** (2019) P12006, arXiv: 1908.00005 [hep-ex].

[41] ATLAS Collaboration, *Topological cell clustering in the ATLAS calorimeters and its performance in LHC Run 1*, Eur. Phys. J. C **77** (2017) 490, arXiv: 1603.02934 [hep-ex].

[42] ATLAS Collaboration, *Electron and photon energy calibration with the ATLAS detector using LHC Run 1 data*, Eur. Phys. J. C **74** (2014) 3071, arXiv: 1407.5063 [hep-ex].

[43] ATLAS Collaboration, *Electron and photon energy calibration with the ATLAS detector using 2015–2016 LHC proton–proton collision data*, JINST **14** (2019) P03017, arXiv: 1812.03848 [hep-ex].

[44] ATLAS Collaboration, *Measurement of Higgs boson production in the diphoton decay channel in pp collisions at center-of-mass energies of* 7 *and* 8 *TeV with the ATLAS detector*, Phys. Rev. D **90** (2014) 112015, arXiv: 1408.7084 [hep-ex].

[45] M. Cacciari, G. P. Salam and G. Soyez, *The catchment area of jets*, JHEP **04** (2008) 005, arXiv: 0802.1188 [hep-ph].

[46] S. D. Ellis and D. E. Soper, *Successive combination jet algorithm for hadron collisions*, Phys. Rev. D **48** (1993) 3160, arXiv: hep-ph/9305266.

[47] J. C. Collins and D. E. Soper, *Angular distribution of dileptons in high-energy hadron collisions*, Phys. Rev. D **16** (1977) 2219.

[48] A. Banfi, S. Redford, M. Vesterinen, P. Waller and T. R. Wyatt, *Optimisation of variables for studying dilepton transverse momentum distributions at hadron colliders*, Eur. Phys. J. C **71** (2011) 1600, arXiv: 1009.1580 [hep-ex].

[49] ATLAS Collaboration, *Measurement of the inclusive isolated prompt photon cross section in pp collisions at* $\sqrt{s} = 7$ *TeV with the ATLAS detector*, Phys. Rev. D **83** (2011) 052005, arXiv: 1012.4389 [hep-ex].

[50] ATLAS Collaboration, *Measurement of the inclusive isolated prompt photon cross-section in pp collisions at* $\sqrt{s} = 7$ *TeV using* 35 pb^{-1} *of ATLAS data*, Phys. Lett. B **706** (2011) 150, arXiv: 1108.0253 [hep-ex].

[51] ATLAS Collaboration, *Measurement of the production cross section of an isolated photon associated with jets in proton–proton collisions at* $\sqrt{s} = 7$ *TeV with the ATLAS detector*, Phys. Rev. D **85** (2012) 092014, arXiv: 1203.3161 [hep-ex].

[52] ATLAS Collaboration, *Dynamics of isolated-photon plus jet production in pp collisions at* $\sqrt{s} = 7$ *TeV with the ATLAS detector*, Nucl. Phys. B **875** (2013) 483, arXiv: 1307.6795 [hep-ex].

[53] ATLAS Collaboration, *Measurement of the inclusive isolated prompt photons cross section in pp collisions at* $\sqrt{s} = 7$ *TeV with the ATLAS detector using* 4.6 fb^{-1}, Phys. Rev. D **89** (2014) 052004, arXiv: 1311.1440 [hep-ex].

[54] ATLAS Collaboration, *Measurement of the inclusive isolated prompt photon cross section in pp collisions at* $\sqrt{s} = 8$ *TeV with the ATLAS detector*, JHEP **08** (2016) 005, arXiv: 1605.03495 [hep-ex].

[55] ATLAS Collaboration, *High-*E_T *isolated-photon plus jets production in pp collisions at* $\sqrt{s} = 8$ *TeV with the ATLAS detector*, Nucl. Phys. B **918** (2017) 257, arXiv: 1611.06586 [hep-ex].

[56] G. D'Agostini, *A multidimensional unfolding method based on Bayes' theorem*, Nucl. Instrum. Meth. A **362** (1995) 487.

[57] ATLAS Collaboration, *Luminosity determination in pp collisions at* $\sqrt{s} = 13$ *TeV using the ATLAS detector at the LHC*, ATLAS-CONF-2019-021, 2019, URL: https://cds.cern.ch/record/2677054.

[58] G. Avoni et al., *The new LUCID-2 detector for luminosity measurement and monitoring in ATLAS*, JINST **13** (2018) P07017.

[59] T. Gehrmann et al., *Jet cross sections and transverse momentum distributions with NNLOJET*, PoS **RADCOR2017** (2018) 074, ed. by A. Hoang and C. Schneider, arXiv: 1801.06415 [hep-ph].

[60] A. Gehrmann-De Ridder, T. Gehrmann and E. W. N. Glover, *Antenna subtraction at NNLO*, JHEP **09** (2005) 056, arXiv: hep-ph/0505111.

[61] J. Currie, E. W. N. Glover and S. Wells, *Infrared structure at NNLO using antenna subtraction*, JHEP **04** (2013) 066, arXiv: 1301.4693 [hep-ph].

[62] X. Chen, T. Gehrmann, N. Glover, M. Höfer and A. Huss, *Isolated photon and photon+jet production at NNLO QCD accuracy*, JHEP **04** (2020) 166, arXiv: 1904.01044 [hep-ph].

[63] S. Amoroso et al., 'Les Houches 2019: Physics at TeV Colliders: Standard Model Working Group Report', 2020, arXiv: 2003.01700 [hep-ph].

[64] T. Binoth, J. P. Guillet, E. Pilon and M. Werlen, *A full next-to-leading order study of direct photon pair production in hadronic collisions*, Eur. Phys. J. C **16** (2000) 311, arXiv: hep-ph/9911340 [hep-ph].

[65] H.-L. Lai et al., *New parton distributions for collider physics*, Phys. Rev. D **82** (2010) 074024, arXiv: 1007.2241 [hep-ph].

[66] A. D. Martin, W. J. Stirling, R. S. Thorne and G. Watt, *Parton distributions for the LHC*, Eur. Phys. J. C **63** (2009) 189, arXiv: 0901.0002 [hep-ph].

[67] E. Bothmann, M. Schönherr and S. Schumann, *Reweighting QCD matrix-element and parton-shower calculations*, Eur. Phys. J. C **76** (2016) 590, arXiv: 1606.08753 [hep-ph].

[68] ATLAS Collaboration, *ATLAS Computing Acknowledgements*, ATL-SOFT-PUB-2020-001, URL: https://cds.cern.ch/record/2717821.

The ATLAS Collaboration

G. Aad[99], B. Abbott[125], D.C. Abbott[100], A. Abed Abud[34], K. Abeling[51], D.K. Abhayasinghe[91], S.H. Abidi[27], H. Abramowicz[158], H. Abreu[157], Y. Abulaiti[5], A.C. Abusleme Hoffman[143a], B.S. Acharya[64a,64b,p], B. Achkar[51], L. Adam[97], C. Adam Bourdarios[4], L. Adamczyk[81a], L. Adamek[163], S.V. Addepalli[24], J. Adelman[117], A. Adiguzel[11c,ad], S. Adorni[52], T. Adye[140], A.A. Affolder[142], Y. Afik[157], C. Agapopoulou[62], M.N. Agaras[12], J. Agarwala[68a,68b], A. Aggarwal[115], C. Agheorghiesei[25c], J.A. Aguilar-Saavedra[136f,136a,ac], A. Ahmad[34], F. Ahmadov[77], W.S. Ahmed[101], X. Ai[44], G. Aielli[71a,71b], I. Aizenberg[176], S. Akatsuka[83], M. Akbiyik[97], T.P.A. Åkesson[94], A.V. Akimov[108], K. Al Khoury[37], G.L. Alberghi[21b,21a], J. Albert[172], M.J. Alconada Verzini[86], S. Alderweireldt[48], M. Aleksa[34], I.N. Aleksandrov[77], C. Alexa[25b], T. Alexopoulos[9], A. Alfonsi[116], F. Alfonsi[21b,21a], M. Alhroob[125], B. Ali[138], S. Ali[155], M. Aliev[162], G. Alimonti[66a], C. Allaire[34], B.M.M. Allbrooke[153], P.P. Allport[19], A. Aloisio[67a,67b], F. Alonso[86], C. Alpigiani[145], E. Alunno Camelia[71a,71b], M. Alvarez Estevez[96], M.G. Alviggi[67a,67b], Y. Amaral Coutinho[78b], A. Ambler[101], L. Ambroz[131], C. Amelung[34], D. Amidei[103], S.P. Amor Dos Santos[136a], S. Amoroso[44], C.S. Amrouche[52], C. Anastopoulos[146], N. Andari[141], T. Andeen[10], J.K. Anders[18], S.Y. Andrean[43a,43b], A. Andreazza[66a,66b], S. Angelidakis[8], A. Angerami[37], A.V. Anisenkov[118b,118a], A. Annovi[69a], C. Antel[52], M.T. Anthony[146], E. Antipov[126], M. Antonelli[49], D.J.A. Antrim[16], F. Anulli[70a], M. Aoki[79], J.A. Aparisi Pozo[170], M.A. Aparo[153], L. Aperio Bella[44], N. Aranzabal[34], V. Araujo Ferraz[78a], C. Arcangeletti[49], A.T.H. Arce[47], E. Arena[88], J-F. Arguin[107], S. Argyropoulos[50], J.-H. Arling[44], A.J. Armbruster[34], A. Armstrong[167], O. Arnaez[163], H. Arnold[34], Z.P. Arrubarrena Tame[111], G. Artoni[131], H. Asada[113], K. Asai[123], S. Asai[160], N.A. Asbah[57], E.M. Asimakopoulou[168], L. Asquith[153], J. Assahsah[33d], K. Assamagan[27], R. Astalos[26a], R.J. Atkin[31a], M. Atkinson[169], N.B. Atlay[17], H. Atmani[58b], P.A. Atmasiddha[103], K. Augsten[138], S. Auricchio[67a,67b], V.A. Austrup[178], G. Avner[157], G. Avolio[34], M.K. Ayoub[13c], G. Azuelos[107,aj], D. Babal[26a], H. Bachacou[141], K. Bachas[159], A. Bachiu[32], F. Backman[43a,43b], A. Badea[57], P. Bagnaia[70a,70b], H. Bahrasemani[149], A.J. Bailey[170], V.R. Bailey[169], J.T. Baines[140], C. Bakalis[9], O.K. Baker[179], P.J. Bakker[116], E. Bakos[14], D. Bakshi Gupta[7], S. Balaji[154], R. Balasubramanian[116], E.M. Baldin[118b,118a], P. Balek[139], E. Ballabene[66a,66b], F. Balli[141], W.K. Balunas[131], J. Balz[97], E. Banas[82], M. Bandieramonte[135], A. Bandyopadhyay[17], S. Bansal[22], L. Barak[158], E.L. Barberio[102], D. Barberis[53b,53a], M. Barbero[99], G. Barbour[92], K.N. Barends[31a], T. Barillari[112], M-S. Barisits[34], J. Barkeloo[128], T. Barklow[150], B.M. Barnett[140], R.M. Barnett[16], A. Baroncelli[58a], G. Barone[27], A.J. Barr[131], L. Barranco Navarro[43a,43b], F. Barreiro[96], J. Barreiro Guimarães da Costa[13a], U. Barron[158], S. Barsov[134], F. Bartels[59a], R. Bartoldus[150], G. Bartolini[99], A.E. Barton[87], P. Bartos[26a], A. Basalaev[44], A. Basan[97], I. Bashta[72a,72b], A. Bassalat[62], M.J. Basso[163], C.R. Basson[98], R.L. Bates[55], S. Batlamous[33e], J.R. Batley[30], B. Batool[148], M. Battaglia[142], M. Bauce[70a,70b], F. Bauer[141,*], P. Bauer[22], H.S. Bawa[29], A. Bayirli[11c], J.B. Beacham[47], T. Beau[132], P.H. Beauchemin[166], F. Becherer[50], P. Bechtle[22], H.P. Beck[18,r], K. Becker[174], C. Becot[44], A.J. Beddall[11a], V.A. Bednyakov[77], C.P. Bee[152], T.A. Beermann[178], M. Begalli[78b], M. Begel[27], A. Behera[152], J.K. Behr[44], C. Beirao Da Cruz E Silva[34], J.F. Beirer[51,34], F. Beisiegel[22], M. Belfkir[4], G. Bella[158], L. Bellagamba[21b], A. Bellerive[32], P. Bellos[19], K. Beloborodov[118b,118a], K. Belotskiy[109], N.L. Belyaev[109], D. Benchekroun[33a], Y. Benhammou[158], D.P. Benjamin[27], M. Benoit[27], J.R. Bensinger[24], S. Bentvelsen[116], L. Beresford[34], M. Beretta[49], D. Berge[17], E. Bergeaas Kuutmann[168], N. Berger[4], B. Bergmann[138], L.J. Bergsten[24], J. Beringer[16], S. Berlendis[6], G. Bernardi[132], C. Bernius[150], F.U. Bernlochner[22], T. Berry[91], P. Berta[139], A. Berthold[46], I.A. Bertram[87], O. Bessidskaia Bylund[178], S. Bethke[112], A. Betti[40], A.J. Bevan[90], S. Bhatta[152], D.S. Bhattacharya[173], P. Bhattarai[24], V.S. Bhopatkar[5], R. Bi[135], R.M. Bianchi[135], O. Biebel[111], R. Bielski[128], N.V. Biesuz[69a,69b], M. Biglietti[72a], T.R.V. Billoud[138], M. Bindi[51], A. Bingul[11d], C. Bini[70a,70b], S. Biondi[21b,21a], A. Biondini[88], C.J. Birch-sykes[98], G.A. Bird[19,140], M. Birman[176],

T. Bisanz[34], J.P. Biswal[2], D. Biswas[177,k], A. Bitadze[98], C. Bittrich[46], K. Bjørke[130], I. Bloch[44], C. Blocker[24], A. Blue[55], U. Blumenschein[90], G.J. Bobbink[116], V.S. Bobrovnikov[118b,118a], D. Bogavac[12], A.G. Bogdanchikov[118b,118a], C. Bohm[43a], V. Boisvert[91], P. Bokan[44], T. Bold[81a], M. Bomben[132], M. Bona[90], M. Boonekamp[141], C.D. Booth[91], A.G. Borbély[55], H.M. Borecka-Bielska[107], L.S. Borgna[92], G. Borissov[87], D. Bortoletto[131], D. Boscherini[21b], M. Bosman[12], J.D. Bossio Sola[34], K. Bouaouda[33a], J. Boudreau[135], E.V. Bouhova-Thacker[87], D. Boumediene[36], R. Bouquet[132], A. Boveia[124], J. Boyd[34], D. Boye[27], I.R. Boyko[77], A.J. Bozson[91], J. Bracinik[19], N. Brahimi[58d,58c], G. Brandt[178], O. Brandt[30], F. Braren[44], B. Brau[100], J.E. Brau[128], W.D. Breaden Madden[55], K. Brendlinger[44], R. Brener[176], L. Brenner[34], R. Brenner[168], S. Bressler[176], B. Brickwedde[97], D.L. Briglin[19], D. Britton[55], D. Britzger[112], I. Brock[22], R. Brock[104], G. Brooijmans[37], W.K. Brooks[143e], E. Brost[27], P.A. Bruckman de Renstrom[82], B. Brüers[44], D. Bruncko[26b], A. Bruni[21b], G. Bruni[21b], M. Bruschi[21b], N. Bruscino[70a,70b], L. Bryngemark[150], T. Buanes[15], Q. Buat[152], P. Buchholz[148], A.G. Buckley[55], I.A. Budagov[77], M.K. Bugge[130], O. Bulekov[109], B.A. Bullard[57], T.J. Burch[117], S. Burdin[88], C.D. Burgard[44], A.M. Burger[126], B. Burghgrave[7], J.T.P. Burr[44], C.D. Burton[10], J.C. Burzynski[100], V. Büscher[97], P.J. Bussey[55], J.M. Butler[23], C.M. Buttar[55], J.M. Butterworth[92], W. Buttinger[140], C.J. Buxo Vazquez[104], A.R. Buzykaev[118b,118a], G. Cabras[21b,21a], S. Cabrera Urbán[170], D. Caforio[54], H. Cai[135], V.M.M. Cairo[150], O. Cakir[3a], N. Calace[34], P. Calafiura[16], G. Calderini[132], P. Calfayan[63], G. Callea[55], L.P. Caloba[78b], S. Calvente Lopez[96], D. Calvet[36], S. Calvet[36], T.P. Calvet[99], M. Calvetti[69a,69b], R. Camacho Toro[132], S. Camarda[34], D. Camarero Munoz[96], P. Camarri[71a,71b], M.T. Camerlingo[72a,72b], D. Cameron[130], C. Camincher[172], M. Campanelli[92], A. Camplani[38], V. Canale[67a,67b], A. Canesse[101], M. Cano Bret[75], J. Cantero[126], Y. Cao[169], F. Capocasa[24], M. Capua[39b,39a], A. Carbone[66a,66b], R. Cardarelli[71a], F. Cardillo[170], G. Carducci[39b,39a], T. Carli[34], G. Carlino[67a], B.T. Carlson[135], E.M. Carlson[172,164a], L. Carminati[66a,66b], M. Carnesale[70a,70b], R.M.D. Carney[150], S. Caron[115], E. Carquin[143e], S. Carrá[44], G. Carratta[21b,21a], J.W.S. Carter[163], T.M. Carter[48], D. Casadei[31c], M.P. Casado[12,h], A.F. Casha[163], E.G. Castiglia[179], F.L. Castillo[59a], L. Castillo Garcia[12], V. Castillo Gimenez[170], N.F. Castro[136a,136e], A. Catinaccio[34], J.R. Catmore[130], A. Cattai[34], V. Cavaliere[27], N. Cavalli[21b,21a], V. Cavasinni[69a,69b], E. Celebi[11b], F. Celli[131], M.S. Centonze[65a,65b], K. Cerny[127], A.S. Cerqueira[78a], A. Cerri[153], L. Cerrito[71a,71b], F. Cerutti[16], A. Cervelli[21b,21a], S.A. Cetin[11b], Z. Chadi[33a], D. Chakraborty[117], M. Chala[136f], J. Chan[177], W.S. Chan[116], W.Y. Chan[88], J.D. Chapman[30], B. Chargeishvili[156b], D.G. Charlton[19], T.P. Charman[90], M. Chatterjee[18], S. Chekanov[5], S.V. Chekulaev[164a], G.A. Chelkov[77,af], A. Chen[103], B. Chen[158], C. Chen[58a], C.H. Chen[76], H. Chen[13c], H. Chen[27], J. Chen[58c], J. Chen[37], J. Chen[24], S. Chen[133], S.J. Chen[13c], X. Chen[58c], X. Chen[13b], Y. Chen[58a], Y-H. Chen[44], C.L. Cheng[177], H.C. Cheng[60a], H.J. Cheng[13a], A. Cheplakov[77], E. Cheremushkina[44], E. Cherepanova[77], R. Cherkaoui El Moursli[33e], E. Cheu[6], K. Cheung[61], L. Chevalier[141], V. Chiarella[49], G. Chiarelli[69a], G. Chiodini[65a], A.S. Chisholm[19], A. Chitan[25b], Y.H. Chiu[172], M.V. Chizhov[77,t], K. Choi[10], A.R. Chomont[70a,70b], Y. Chou[100], Y.S. Chow[116], L.D. Christopher[31f], M.C. Chu[60a], X. Chu[13a,13d], J. Chudoba[137], J.J. Chwastowski[82], D. Cieri[112], K.M. Ciesla[82], V. Cindro[89], I.A. Cioară[25b], A. Ciocio[16], F. Cirotto[67a,67b], Z.H. Citron[176,l], M. Citterio[66a], D.A. Ciubotaru[25b], B.M. Ciungu[163], A. Clark[52], P.J. Clark[48], J.M. Clavijo Columbie[44], S.E. Clawson[98], C. Clement[43a,43b], L. Clissa[21b,21a], Y. Coadou[99], M. Cobal[64a,64c], A. Coccaro[53b], J. Cochran[76], R.F. Coelho Barrue[136a], R. Coelho Lopes De Sa[100], S. Coelli[66a], H. Cohen[158], A.E.C. Coimbra[34], B. Cole[37], J. Collot[56], P. Conde Muiño[136a,136h], S.H. Connell[31c], I.A. Connelly[55], E.I. Conroy[131], F. Conventi[67a,ak], H.G. Cooke[19], A.M. Cooper-Sarkar[131], F. Cormier[171], L.D. Corpe[34], M. Corradi[70a,70b], E.E. Corrigan[94], F. Corriveau[101,aa], M.J. Costa[170], F. Costanza[4], D. Costanzo[146], B.M. Cote[124], G. Cowan[91], J.W. Cowley[30], K. Cranmer[122], S. Crépé-Renaudin[56], F. Crescioli[132], M. Cristinziani[148], M. Cristoforetti[73a,73b,b], V. Croft[166], G. Crosetti[39b,39a], A. Cueto[34], T. Cuhadar Donszelmann[167], H. Cui[13a,13d], A.R. Cukierman[150], W.R. Cunningham[55], P. Czodrowski[34], M.M. Czurylo[59b], M.J. Da Cunha Sargedas De Sousa[58a], J.V. Da Fonseca Pinto[78b], C. Da Via[98], W. Dabrowski[81a], T. Dado[45],

S. Dahbi[31f], T. Dai[103], C. Dallapiccola[100], M. Dam[38], G. D'amen[27], V. D'Amico[72a,72b], J. Damp[97], J.R. Dandoy[133], M.F. Daneri[28], M. Danninger[149], V. Dao[34], G. Darbo[53b], S. Darmora[5], A. Dattagupta[128], S. D'Auria[66a,66b], C. David[164b], T. Davidek[139], D.R. Davis[47], B. Davis-Purcell[32], I. Dawson[90], K. De[7], R. De Asmundis[67a], M. De Beurs[116], S. De Castro[21b,21a], N. De Groot[115], P. de Jong[116], H. De la Torre[104], A. De Maria[13c], D. De Pedis[70a], A. De Salvo[70a], U. De Sanctis[71a,71b], M. De Santis[71a,71b], A. De Santo[153], J.B. De Vivie De Regie[56], D.V. Dedovich[77], J. Degens[116], A.M. Deiana[40], J. Del Peso[96], Y. Delabat Diaz[44], F. Deliot[141], C.M. Delitzsch[6], M. Della Pietra[67a,67b], D. Della Volpe[52], A. Dell'Acqua[34], L. Dell'Asta[66a,66b], M. Delmastro[4], P.A. Delsart[56], S. Demers[179], M. Demichev[77], S.P. Denisov[119], L. D'Eramo[117], D. Derendarz[82], J.E. Derkaoui[33d], F. Derue[132], P. Dervan[88], K. Desch[22], K. Dette[163], C. Deutsch[22], P.O. Deviveiros[34], F.A. Di Bello[70a,70b], A. Di Ciaccio[71a,71b], L. Di Ciaccio[4], C. Di Donato[67a,67b], A. Di Girolamo[34], G. Di Gregorio[69a,69b], A. Di Luca[73a,73b], B. Di Micco[72a,72b], R. Di Nardo[72a,72b], C. Diaconu[99], F.A. Dias[116], T. Dias Do Vale[136a], M.A. Diaz[143a], F.G. Diaz Capriles[22], J. Dickinson[16], M. Didenko[170], E.B. Diehl[103], J. Dietrich[17], S. Díez Cornell[44], C. Diez Pardos[148], A. Dimitrievska[16], W. Ding[13b], J. Dingfelder[22], I-M. Dinu[25b], S.J. Dittmeier[59b], F. Dittus[34], F. Djama[99], T. Djobava[156b], J.I. Djuvsland[15], M.A.B. Do Vale[144], D. Dodsworth[24], C. Doglioni[94], J. Dolejsi[139], Z. Dolezal[139], M. Donadelli[78c], B. Dong[58c], J. Donini[36], A. D'onofrio[13c], M. D'Onofrio[88], J. Dopke[140], A. Doria[67a], M.T. Dova[86], A.T. Doyle[55], E. Drechsler[149], E. Dreyer[149], T. Dreyer[51], A.S. Drobac[166], D. Du[58b], T.A. du Pree[116], F. Dubinin[108], M. Dubovsky[26a], A. Dubreuil[52], E. Duchovni[176], G. Duckeck[111], O.A. Ducu[34,25b], D. Duda[112], A. Dudarev[34], M. D'uffizi[98], L. Duflot[62], M. Dührssen[34], C. Dülsen[178], A.E. Dumitriu[25b], M. Dunford[59a], S. Dungs[45], K. Dunne[43a,43b], A. Duperrin[99], H. Duran Yildiz[3a], M. Düren[54], A. Durglishvili[156b], B. Dutta[44], G.I. Dyckes[133], M. Dyndal[81a], S. Dysch[98], B.S. Dziedzic[82], B. Eckerova[26a], M.G. Eggleston[47], E. Egidio Purcino De Souza[78b], L.F. Ehrke[52], T. Eifert[7], G. Eigen[15], K. Einsweiler[16], T. Ekelof[168], Y. El Ghazali[33b], H. El Jarrari[33e], A. El Moussaouy[33a], V. Ellajosyula[168], M. Ellert[168], F. Ellinghaus[178], A.A. Elliot[90], N. Ellis[34], J. Elmsheuser[27], M. Elsing[34], D. Emeliyanov[140], A. Emerman[37], Y. Enari[160], J. Erdmann[45], A. Ereditato[18], P.A. Erland[82], M. Errenst[178], M. Escalier[62], C. Escobar[170], O. Estrada Pastor[170], E. Etzion[158], G. Evans[136a], H. Evans[63], M.O. Evans[153], A. Ezhilov[134], F. Fabbri[55], L. Fabbri[21b,21a], V. Fabiani[115], G. Facini[174], V. Fadeyev[142], R.M. Fakhrutdinov[119], S. Falciano[70a], P.J. Falke[22], S. Falke[34], J. Faltova[139], Y. Fan[13a], Y. Fang[13a], Y. Fang[13a], G. Fanourakis[42], M. Fanti[66a,66b], M. Faraj[58c], A. Farbin[7], A. Farilla[72a], E.M. Farina[68a,68b], T. Farooque[104], S.M. Farrington[48], P. Farthouat[34], F. Fassi[33e], D. Fassouliotis[8], M. Faucci Giannelli[71a,71b], W.J. Fawcett[30], L. Fayard[62], O.L. Fedin[134,q], A. Fehr[18], M. Feickert[169], L. Feligioni[99], A. Fell[146], C. Feng[58b], M. Feng[13b], M.J. Fenton[167], A.B. Fenyuk[119], S.W. Ferguson[41], J. Ferrando[44], A. Ferrari[168], P. Ferrari[116], R. Ferrari[68a], D. Ferrere[52], C. Ferretti[103], F. Fiedler[97], A. Filipčič[89], F. Filthaut[115], M.C.N. Fiolhais[136a,136c,a], L. Fiorini[170], F. Fischer[148], J. Fischer[97], W.C. Fisher[104], T. Fitschen[19], I. Fleck[148], P. Fleischmann[103], T. Flick[178], B.M. Flierl[111], L. Flores[133], L.R. Flores Castillo[60a], F.M. Follega[73a,73b], N. Fomin[15], J.H. Foo[163], G.T. Forcolin[73a,73b], B.C. Forland[63], A. Formica[141], F.A. Förster[12], A.C. Forti[98], E. Fortin[99], M.G. Foti[131], D. Fournier[62], H. Fox[87], P. Francavilla[69a,69b], S. Francescato[70a,70b], M. Franchini[21b,21a], S. Franchino[59a], D. Francis[34], L. Franco[4], L. Franconi[18], M. Franklin[57], G. Frattari[70a,70b], A.C. Freegard[90], P.M. Freeman[19], B. Freund[107], W.S. Freund[78b], E.M. Freundlich[45], D. Froidevaux[34], J.A. Frost[131], Y. Fu[58a], M. Fujimoto[123], E. Fullana Torregrosa[170], J. Fuster[170], A. Gabrielli[21b,21a], A. Gabrielli[34], P. Gadow[44], G. Gagliardi[53b,53a], L.G. Gagnon[16], G.E. Gallardo[131], E.J. Gallas[131], B.J. Gallop[140], R. Gamboa Goni[90], K.K. Gan[124], S. Ganguly[176], J. Gao[58a], Y. Gao[48], Y.S. Gao[29,n], F.M. Garay Walls[143a], C. García[170], J.E. García Navarro[170], J.A. García Pascual[13a], M. Garcia-Sciveres[16], R.W. Gardner[35], D. Garg[75], S. Gargiulo[50], C.A. Garner[163], V. Garonne[130], S.J. Gasiorowski[145], P. Gaspar[78b], G. Gaudio[68a], P. Gauzzi[70a,70b], I.L. Gavrilenko[108], A. Gavrilyuk[120], C. Gay[171], G. Gaycken[44], E.N. Gazis[9], A.A. Geanta[25b], C.M. Gee[142], C.N.P. Gee[140], J. Geisen[94], M. Geisen[97], C. Gemme[53b], M.H. Genest[56], S. Gentile[70a,70b], S. George[91], W.F. George[19], T. Geralis[42], L.O. Gerlach[51], P. Gessinger-Befurt[34],

M. Ghasemi Bostanabad[172], M. Ghneimat[148], A. Ghosh[167], A. Ghosh[75], B. Giacobbe[21b], S. Giagu[70a,70b], N. Giangiacomi[163], P. Giannetti[69a], A. Giannini[67a,67b], S.M. Gibson[91], M. Gignac[142], D.T. Gil[81b], B.J. Gilbert[37], D. Gillberg[32], G. Gilles[116], N.E.K. Gillwald[44], D.M. Gingrich[2,aj], M.P. Giordani[64a,64c], P.F. Giraud[141], G. Giugliarelli[64a,64c], D. Giugni[66a], F. Giuli[71a,71b], I. Gkialas[8,i], P. Gkountoumis[9], L.K. Gladilin[110], C. Glasman[96], G.R. Gledhill[128], M. Glisic[128], I. Gnesi[39b,d], M. Goblirsch-Kolb[24], D. Godin[107], S. Goldfarb[102], T. Golling[52], D. Golubkov[119], J.P. Gombas[104], A. Gomes[136a,136b], R. Goncalves Gama[51], R. Gonçalo[136a,136c], G. Gonella[128], L. Gonella[19], A. Gongadze[77], F. Gonnella[19], J.L. Gonski[37], S. González de la Hoz[170], S. Gonzalez Fernandez[12], R. Gonzalez Lopez[88], C. Gonzalez Renteria[16], R. Gonzalez Suarez[168], S. Gonzalez-Sevilla[52], G.R. Gonzalvo Rodriguez[170], R.Y. González Andana[143a], L. Goossens[34], N.A. Gorasia[19], P.A. Gorbounov[120], H.A. Gordon[27], B. Gorini[34], E. Gorini[65a,65b], A. Gorišek[89], A.T. Goshaw[47], M.I. Gostkin[77], C.A. Gottardo[115], M. Gouighri[33b], V. Goumarre[44], A.G. Goussiou[145], N. Govender[31c], C. Goy[4], I. Grabowska-Bold[81a], K. Graham[32], E. Gramstad[130], S. Grancagnolo[17], M. Grandi[153], V. Gratchev[134], P.M. Gravila[25f], F.G. Gravili[65a,65b], H.M. Gray[16], C. Grefe[22], I.M. Gregor[44], P. Grenier[150], K. Grevtsov[44], C. Grieco[12], N.A. Grieser[125], A.A. Grillo[142], K. Grimm[29,m], S. Grinstein[12,x], J.-F. Grivaz[62], S. Groh[97], E. Gross[176], J. Grosse-Knetter[51], Z.J. Grout[92], C. Grud[103], A. Grummer[114], J.C. Grundy[131], L. Guan[103], W. Guan[177], C. Gubbels[171], J. Guenther[34], J.G.R. Guerrero Rojas[170], F. Guescini[112], D. Guest[17], R. Gugel[97], A. Guida[44], T. Guillemin[4], S. Guindon[34], J. Guo[58c], L. Guo[62], Y. Guo[103], R. Gupta[44], S. Gurbuz[22], G. Gustavino[125], M. Guth[52], P. Gutierrez[125], L.F. Gutierrez Zagazeta[133], C. Gutschow[92], C. Guyot[141], C. Gwenlan[131], C.B. Gwilliam[88], E.S. Haaland[130], A. Haas[122], M. Habedank[17], C. Haber[16], H.K. Hadavand[7], A. Hadef[97], M. Haleem[173], J. Haley[126], J.J. Hall[146], G. Halladjian[104], G.D. Hallewell[99], L. Halser[18], K. Hamano[172], H. Hamdaoui[33e], M. Hamer[22], G.N. Hamity[48], K. Han[58a], L. Han[13c], L. Han[58a], S. Han[16], Y.F. Han[163], K. Hanagaki[79,v], M. Hance[142], M.D. Hank[35], R. Hankache[98], E. Hansen[94], J.B. Hansen[38], J.D. Hansen[38], M.C. Hansen[22], P.H. Hansen[38], K. Hara[165], T. Harenberg[178], S. Harkusha[105], Y.T. Harris[131], P.F. Harrison[174], N.M. Hartman[150], N.M. Hartmann[111], Y. Hasegawa[147], A. Hasib[48], S. Hassani[141], S. Haug[18], R. Hauser[104], M. Havranek[138], C.M. Hawkes[19], R.J. Hawkings[34], S. Hayashida[113], D. Hayden[104], C. Hayes[103], R.L. Hayes[171], C.P. Hays[131], J.M. Hays[90], H.S. Hayward[88], S.J. Haywood[140], F. He[58a], Y. He[161], Y. He[132], M.P. Heath[48], V. Hedberg[94], A.L. Heggelund[130], N.D. Hehir[90], C. Heidegger[50], K.K. Heidegger[50], W.D. Heidorn[76], J. Heilman[32], S. Heim[44], T. Heim[16], B. Heinemann[44,ah], J.G. Heinlein[133], J.J. Heinrich[128], L. Heinrich[34], J. Hejbal[137], L. Helary[44], A. Held[122], S. Hellesund[130], C.M. Helling[142], S. Hellman[43a,43b], C. Helsens[34], R.C.W. Henderson[87], L. Henkelmann[30], A.M. Henriques Correia[34], H. Herde[150], Y. Hernández Jiménez[152], H. Herr[97], M.G. Herrmann[111], T. Herrmann[46], G. Herten[50], R. Hertenberger[111], L. Hervas[34], N.P. Hessey[164a], H. Hibi[80], S. Higashino[79], E. Higón-Rodriguez[170], K.K. Hill[27], K.H. Hiller[44], S.J. Hillier[19], M. Hils[46], I. Hinchliffe[16], F. Hinterkeuser[22], M. Hirose[129], S. Hirose[165], D. Hirschbuehl[178], B. Hiti[89], O. Hladik[137], J. Hobbs[152], R. Hobincu[25e], N. Hod[176], M.C. Hodgkinson[146], B.H. Hodkinson[30], A. Hoecker[34], J. Hofer[44], D. Hohn[50], T. Holm[22], T.R. Holmes[35], M. Holzbock[112], L.B.A.H. Hommels[30], B.P. Honan[98], J. Hong[58c], T.M. Hong[135], J.C. Honig[50], A. Hönle[112], B.H. Hooberman[169], W.H. Hopkins[5], Y. Horii[113], P. Horn[46], L.A. Horyn[35], S. Hou[155], J. Howarth[55], J. Hoya[86], M. Hrabovsky[127], A. Hrynevich[106], T. Hryn'ova[4], P.J. Hsu[61], S.-C. Hsu[145], Q. Hu[37], S. Hu[58c], Y.F. Hu[13a,13d,al], D.P. Huang[92], X. Huang[13c], Y. Huang[58a], Y. Huang[13a], Z. Hubacek[138], F. Hubaut[99], M. Huebner[22], F. Huegging[22], T.B. Huffman[131], M. Huhtinen[34], R. Hulsken[56], N. Huseynov[77,ab], J. Huston[104], J. Huth[57], R. Hyneman[150], S. Hyrych[26a], G. Iacobucci[52], G. Iakovidis[27], I. Ibragimov[148], L. Iconomidou-Fayard[62], P. Iengo[34], R. Iguchi[160], T. Iizawa[52], Y. Ikegami[79], N. Ilic[163], H. Imam[33a], T. Ingebretsen Carlson[43a,43b], G. Introzzi[68a,68b], M. Iodice[72a], V. Ippolito[70a,70b], M. Ishino[160], W. Islam[126], C. Issever[17,44], S. Istin[11c,am], J.M. Iturbe Ponce[60a], R. Iuppa[73a,73b], A. Ivina[176], J.M. Izen[41], V. Izzo[67a], P. Jacka[137], P. Jackson[1], R.M. Jacobs[44], B.P. Jaeger[149], C.S. Jagfeld[111], G. Jäkel[178], K. Jakobs[50], T. Jakoubek[176], J. Jamieson[55], K.W. Janas[81a], G. Jarlskog[94], A.E. Jaspan[88], N. Javadov[77,ab], T. Javůrek[34], M. Javurkova[100], F. Jeanneau[141], L. Jeanty[128], J. Jejelava[156a], P. Jenni[50,e], S. Jézéquel[4], J. Jia[152], Z. Jia[13c], Y. Jiang[58a], S. Jiggins[50], J. Jimenez Pena[112], S. Jin[13c], A. Jinaru[25b], O. Jinnouchi[161], H. Jivan[31f], P. Johansson[146], K.A. Johns[6], C.A. Johnson[63], D.M. Jones[30], E. Jones[174], R.W.L. Jones[87], T.J. Jones[88], J. Jovicevic[51], X. Ju[16], J.J. Junggeburth[34], A. Juste Rozas[12,x], S. Kabana[143d], A. Kaczmarska[82], M. Kado[70a,70b], H. Kagan[124], M. Kagan[150], A. Kahn[37], C. Kahra[97], T. Kaji[175], E. Kajomovitz[157], C.W. Kalderon[27], A. Kamenshchikov[119], M. Kaneda[160], N.J. Kang[142], S. Kang[76], Y. Kano[113], J. Kanzaki[79], D. Kar[31f], K. Karava[131], M.J. Kareem[164b], I. Karkanias[159], S.N. Karpov[77], Z.M. Karpova[77], V. Kartvelishvili[87], A.N. Karyukhin[119], E. Kasimi[159], C. Kato[58d], J. Katzy[44], K. Kawade[147], K. Kawagoe[85], T. Kawaguchi[113], T. Kawamoto[141], G. Kawamura[51], E.F. Kay[172], F.I. Kaya[166], S. Kazakos[12], V.F. Kazanin[118b,118a], Y. Ke[152], J.M. Keaveney[31a], R. Keeler[172], J.S. Keller[32], D. Kelsey[153], J.J. Kempster[19], J. Kendrick[19], K.E. Kennedy[37], O. Kepka[137], S. Kersten[178], B.P. Kerševan[89], S. Ketabchi Haghighat[163], M. Khandoga[132], A. Khanov[126], A.G. Kharlamov[118b,118a], T. Kharlamova[118b,118a], E.E. Khoda[145], T.J. Khoo[17], G. Khoriauli[173], E. Khramov[77], J. Khubua[156b], S. Kido[80], M. Kiehn[34], A. Kilgallon[128], E. Kim[161], Y.K. Kim[35], N. Kimura[92], A. Kirchhoff[51], D. Kirchmeier[46], C. Kirfel[22], J. Kirk[140], A.E. Kiryunin[112], T. Kishimoto[160], D.P. Kisliuk[163], V. Kitali[44], C. Kitsaki[9], O. Kivernyk[22], T. Klapdor-Kleingrothaus[50], M. Klassen[59a], C. Klein[32], L. Klein[173], M.H. Klein[103], M. Klein[88], U. Klein[88], P. Klimek[34], A. Klimentov[27], F. Klimpel[34], T. Klingl[22], T. Klioutchnikova[34], F.F. Klitzner[111], P. Kluit[116], S. Kluth[112], E. Kneringer[74], T.M. Knight[163], A. Knue[50], D. Kobayashi[85], M. Kobel[46], M. Kocian[150], T. Kodama[160], P. Kodys[139], D.M. Koeck[153], P.T. Koenig[22], T. Koffas[32], N.M. Köhler[34], M. Kolb[141], I. Koletsou[4], T. Komarek[127], K. Köneke[50], A.X.Y. Kong[1], T. Kono[123], V. Konstantinides[92], N. Konstantinidis[92], B. Konya[94], R. Kopeliansky[63], S. Koperny[81a], K. Korcyl[82], K. Kordas[159], G. Koren[158], A. Korn[92], S. Korn[51], I. Korolkov[12], E.V. Korolkova[146], N. Korotkova[110], B. Kortman[116], O. Kortner[112], S. Kortner[112], V.V. Kostyukhin[146,162], A. Kotsokechagia[62], A. Kotwal[47], A. Koulouris[34], A. Kourkoumeli-Charalampidi[68a,68b], C. Kourkoumelis[8], E. Kourlitis[5], O. Kovanda[153], R. Kowalewski[172], W. Kozanecki[141], A.S. Kozhin[119], V.A. Kramarenko[110], G. Kramberger[89], D. Krasnopevtsev[58a], M.W. Krasny[132], A. Krasznahorkay[34], J.A. Kremer[97], J. Kretzschmar[88], K. Kreul[17], P. Krieger[163], F. Krieter[111], S. Krishnamurthy[100], A. Krishnan[59b], M. Krivos[139], K. Krizka[16], K. Kroeninger[45], H. Kroha[112], J. Kroll[137], J. Kroll[133], K.S. Krowpman[104], U. Kruchonak[77], H. Krüger[22], N. Krumnack[76], M.C. Kruse[47], J.A. Krzysiak[82], A. Kubota[161], O. Kuchinskaia[162], S. Kuday[3b], D. Kuechler[44], J.T. Kuechler[44], S. Kuehn[34], T. Kuhl[44], V. Kukhtin[77], Y. Kulchitsky[105,ae], S. Kuleshov[143c], M. Kumar[31f], N. Kumari[99], M. Kuna[56], A. Kupco[137], T. Kupfer[45], O. Kuprash[50], H. Kurashige[80], L.L. Kurchaninov[164a], Y.A. Kurochkin[105], A. Kurova[109], M.G. Kurth[13a,13d], E.S. Kuwertz[34], M. Kuze[161], A.K. Kvam[145], J. Kvita[127], T. Kwan[101], K.W. Kwok[60a], C. Lacasta[170], F. Lacava[70a,70b], H. Lacker[17], D. Lacour[132], N.N. Lad[92], E. Ladygin[77], R. Lafaye[4], B. Laforge[132], T. Lagouri[143d], S. Lai[51], I.K. Lakomiec[81a], N. Lalloue[56], J.E. Lambert[125], S. Lammers[63], W. Lampl[6], C. Lampoudis[159], E. Lançon[27], U. Landgraf[50], M.P.J. Landon[90], V.S. Lang[50], J.C. Lange[51], R.J. Langenberg[100], A.J. Lankford[167], F. Lanni[27], K. Lantzsch[22], A. Lanza[68a], A. Lapertosa[53b,53a], J.F. Laporte[141], T. Lari[66a], F. Lasagni Manghi[21b,21a], M. Lassnig[34], V. Latonova[137], T.S. Lau[60a], A. Laudrain[97], A. Laurier[32], M. Lavorgna[67a,67b], S.D. Lawlor[91], Z. Lawrence[98], M. Lazzaroni[66a,66b], B. Le[98], B. Leban[89], A. Lebedev[76], M. LeBlanc[34], T. LeCompte[5], F. Ledroit-Guillon[56], A.C.A. Lee[92], G.R. Lee[15], L. Lee[57], S.C. Lee[155], S. Lee[76], L.L. Leeuw[31c], B. Lefebvre[164a], H.P. Lefebvre[91], M. Lefebvre[172], C. Leggett[16], K. Lehmann[149], N. Lehmann[18], G. Lehmann Miotto[34], W.A. Leight[44], A. Leisos[159,w], M.A.L. Leite[78c], C.E. Leitgeb[44], R. Leitner[139], K.J.C. Leney[40], T. Lenz[22], S. Leone[69a], C. Leonidopoulos[48], A. Leopold[132], C. Leroy[107], R. Les[104], C.G. Lester[30], M. Levchenko[134], J. Levêque[4], D. Levin[103], L.J. Levinson[176], D.J. Lewis[19], B. Li[13b], B. Li[58b], C. Li[58a], C-Q. Li[58c,58d], H. Li[58a], H. Li[58b], J. Li[58c], K. Li[145], L. Li[58c], M. Li[13a,13d], Q.Y. Li[58a], S. Li[58d,c], X. Li[44], Y. Li[44], Z. Li[58b], Z. Li[131], Z. Li[101], Z. Li[88], Z. Liang[13a], M. Liberatore[44], B. Liberti[71a], K. Lie[60c], K. Lin[104], R.A. Linck[63], R.E. Lindley[6], J.H. Lindon[2], A. Linss[44], E. Lipeles[133], A. Lipniacka[15], T.M. Liss[169,ai], A. Lister[171], J.D. Little[7], B. Liu[13a], B.X. Liu[149], J.B. Liu[58a], J.K.K. Liu[35], K. Liu[58d,58c], M. Liu[58a], M.Y. Liu[58a], P. Liu[13a], X. Liu[58a], Y. Liu[44], Y. Liu[13c,13d], Y.L. Liu[103], Y.W. Liu[58a], M. Livan[68a,68b], A. Lleres[56], J. Llorente Merino[149], S.L. Lloyd[90], E.M. Lobodzinska[44], P. Loch[6], S. Loffredo[71a,71b], T. Lohse[17], K. Lohwasser[146], M. Lokajicek[137], J.D. Long[169], I. Longarini[70a,70b], L. Longo[34], R. Longo[169], I. Lopez Paz[12], A. Lopez Solis[44], J. Lorenz[111], N. Lorenzo Martinez[4], A.M. Lory[111], A. Lösle[50], X. Lou[43a,43b], X. Lou[13a], A. Lounis[62], J. Love[5], P.A. Love[87], J.J. Lozano Bahilo[170], G. Lu[13a], M. Lu[58a], S. Lu[133], Y.J. Lu[61], H.J. Lubatti[145], C. Luci[70a,70b], F.L. Lucio Alves[13c], A. Lucotte[56], F. Luehring[63], I. Luise[152], L. Luminari[70a], O. Lundberg[151], B. Lund-Jensen[151], N.A. Luongo[128], M.S. Lutz[158], D. Lynn[27], H. Lyons[88], R. Lysak[137], E. Lytken[94], F. Lyu[13a], V. Lyubushkin[77], T. Lyubushkina[77], H. Ma[27], L.L. Ma[58b], Y. Ma[92], D.M. Mac Donell[172], G. Maccarrone[49], C.M. Macdonald[146], J.C. MacDonald[146], R. Madar[36], W.F. Mader[46], M. Madugoda Ralalage Don[126], N. Madysa[46], J. Maeda[80], T. Maeno[27], M. Maerker[46], V. Magerl[50], J. Magro[64a,64c], D.J. Mahon[37], C. Maidantchik[78b], A. Maio[136a,136b,136d], K. Maj[81a], O. Majersky[26a], S. Majewski[128], N. Makovec[62], B. Malaescu[132], Pa. Malecki[82], V.P. Maleev[134], F. Malek[56], D. Malito[39b,39a], U. Mallik[75], C. Malone[30], S. Maltezos[9], S. Malyukov[77], J. Mamuzic[170], G. Mancini[49], J.P. Mandalia[90], I. Mandić[89], L. Manhaes de Andrade Filho[78a], I.M. Maniatis[159], M. Manisha[141], J. Manjarres Ramos[46], K.H. Mankinen[94], A. Mann[111], A. Manousos[74], B. Mansoulie[141], I. Manthos[159], S. Manzoni[116], A. Marantis[159,w], L. Marchese[131], G. Marchiori[132], M. Marcisovsky[137], L. Marcoccia[71a,71b], C. Marcon[94], M. Marjanovic[125], Z. Marshall[16], S. Marti-Garcia[170], T.A. Martin[174], V.J. Martin[48], B. Martin dit Latour[15], L. Martinelli[70a,70b], M. Martinez[12,x], P. Martinez Agullo[170], V.I. Martinez Outschoorn[100], S. Martin-Haugh[140], V.S. Martoiu[25b], A.C. Martyniuk[92], A. Marzin[34], S.R. Maschek[112], L. Masetti[97], T. Mashimo[160], J. Masik[98], A.L. Maslennikov[118b,118a], L. Massa[21b,21a], P. Massarotti[67a,67b], P. Mastrandrea[69a,69b], A. Mastroberardino[39b,39a], T. Masubuchi[160], D. Matakias[27], T. Mathisen[168], A. Matic[111], N. Matsuzawa[160], J. Maurer[25b], B. Maček[89], D.A. Maximov[118b,118a], R. Mazini[155], I. Maznas[159], S.M. Mazza[142], C. Mc Ginn[27], J.P. Mc Gowan[101], S.P. Mc Kee[103], T.G. McCarthy[112], W.P. McCormack[16], E.F. McDonald[102], A.E. McDougall[116], J.A. Mcfayden[153], G. Mchedlidze[156b], M.A. McKay[40], K.D. McLean[172], S.J. McMahon[140], P.C. McNamara[102], R.A. McPherson[172,aa], J.E. Mdhluli[31f], Z.A. Meadows[100], S. Meehan[34], T. Megy[36], S. Mehlhase[111], A. Mehta[88], B. Meirose[41], D. Melini[157], B.R. Mellado Garcia[31f], F. Meloni[44], A. Melzer[22], E.D. Mendes Gouveia[136a], A.M. Mendes Jacques Da Costa[19], H.Y. Meng[163], L. Meng[34], S. Menke[112], M. Mentink[34], E. Meoni[39b,39a], S.A.M. Merkt[135], C. Merlassino[131], P. Mermod[52,*], L. Merola[67a,67b], C. Meroni[66a], G. Merz[103], O. Meshkov[110,108], J.K.R. Meshreki[148], J. Metcalfe[5], A.S. Mete[5], C. Meyer[63], J-P. Meyer[141], M. Michetti[17], R.P. Middleton[140], L. Mijović[48], G. Mikenberg[176], M. Mikestikova[137], M. Mikuž[89], H. Mildner[146], A. Milic[163], C.D. Milke[40], D.W. Miller[35], L.S. Miller[32], A. Milov[176], D.A. Milstead[43a,43b], A.A. Minaenko[119], I.A. Minashvili[156b], L. Mince[55], A.I. Mincer[122], B. Mindur[81a], M. Mineev[77], Y. Minegishi[160], Y. Mino[83], L.M. Mir[12], M. Miralles Lopez[170], M. Mironova[131], T. Mitani[175], V.A. Mitsou[170], M. Mittal[58c], O. Miu[163], P.S. Miyagawa[90], Y. Miyazaki[85], A. Mizukami[79], J.U. Mjörnmark[94], T. Mkrtchyan[59a], M. Mlynarikova[117], T. Moa[43a,43b], S. Mobius[51], K. Mochizuki[107], P. Moder[44], P. Mogg[111], A.F. Mohammed[13a], S. Mohapatra[37], G. Mokgatitswane[31f], B. Mondal[148], S. Mondal[138], K. Mönig[44], E. Monnier[99], A. Montalbano[149], J. Montejo Berlingen[34], M. Montella[124], F. Monticelli[86], N. Morange[62], A.L. Moreira De Carvalho[136a], M. Moreno Llácer[170], C. Moreno Martinez[12], P. Morettini[53b], M. Morgenstern[157], S. Morgenstern[174], D. Mori[149], M. Morii[57], M. Morinaga[160], V. Morisbak[130], A.K. Morley[34], A.P. Morris[92], L. Morvaj[34], P. Moschovakos[34], B. Moser[116], M. Mosidze[156b], T. Moskalets[50], P. Moskvitina[115], J. Moss[29,o], E.J.W. Moyse[100], S. Muanza[99], J. Mueller[135], R. Mueller[18], D. Muenstermann[87], G.A. Mullier[94], J.J. Mullin[133], D.P. Mungo[66a,66b], J.L. Munoz Martinez[12], F.J. Munoz Sanchez[98], M. Murin[98], P. Murin[26b], W.J. Murray[174,140], A. Murrone[66a,66b], J.M. Muse[125], M. Muškinja[16], C. Mwewa[27], A.G. Myagkov[119,af], A.A. Myers[135], G. Myers[63], M. Myska[138], B.P. Nachman[16], O. Nackenhorst[45], A.Nag Nag[46], K. Nagai[131], K. Nagano[79], J.L. Nagle[27], E. Nagy[99], A.M. Nairz[34], Y. Nakahama[113], K. Nakamura[79], H. Nanjo[129], F. Napolitano[59a], R. Narayan[40], I. Naryshkin[134], M. Naseri[32], C. Nass[22], T. Naumann[44], G. Navarro[20a], J. Navarro-Gonzalez[170], R. Nayak[158], P.Y. Nechaeva[108], F. Nechansky[44], T.J. Neep[19], A. Negri[68a,68b], M. Negrini[21b], C. Nellist[115], C. Nelson[101], K. Nelson[103], M.E. Nelson[43a,43b], S. Nemecek[137], M. Nessi[34,g], M.S. Neubauer[169], F. Neuhaus[97], J. Neundorf[44], R. Newhouse[171], P.R. Newman[19], C.W. Ng[135], Y.S. Ng[17], Y.W.Y. Ng[167], B. Ngair[33e], H.D.N. Nguyen[99], R.B. Nickerson[131], R. Nicolaidou[141], D.S. Nielsen[38], J. Nielsen[142], M. Niemeyer[51], N. Nikiforou[10], V. Nikolaenko[119,af], I. Nikolic-Audit[132], K. Nikolopoulos[19], P. Nilsson[27], H.R. Nindhito[52], A. Nisati[70a], N. Nishu[2], R. Nisius[112], T. Nitta[175], T. Nobe[160], D.L. Noel[30], Y. Noguchi[83], I. Nomidis[132], M.A. Nomura[27], M.B. Norfolk[146], R.R.B. Norisam[92], J. Novak[89], T. Novak[44], O. Novgorodova[46], L. Novotny[138], R. Novotny[114], L. Nozka[127], K. Ntekas[167], E. Nurse[92], F.G. Oakham[32,aj], J. Ocariz[132], A. Ochi[80], I. Ochoa[136a], J.P. Ochoa-Ricoux[143a], S. Oda[85], S. Odaka[79], S. Oerdek[168], A. Ogrodnik[81a], A. Oh[98], C.C. Ohm[151], H. Oide[161], R. Oishi[160], M.L. Ojeda[163], Y. Okazaki[83], M.W. O'Keefe[88], Y. Okumura[160], A. Olariu[25b], L.F. Oleiro Seabra[136a], S.A. Olivares Pino[143d], D. Oliveira Damazio[27], D. Oliveira Goncalves[78a], J.L. Oliver[167], M.J.R. Olsson[167], A. Olszewski[82], J. Olszowska[82], Ö.O. Öncel[22], D.C. O'Neil[149], A.P. O'neill[131], A. Onofre[136a,136e], P.U.E. Onyisi[10], R.G. Oreamuno Madriz[117], M.J. Oreglia[35], G.E. Orellana[86], D. Orestano[72a,72b], N. Orlando[12], R.S. Orr[163], V. O'Shea[55], R. Ospanov[58a], G. Otero y Garzon[28], H. Otono[85], P.S. Ott[59a], G.J. Ottino[16], M. Ouchrif[33d], J. Ouellette[27], F. Ould-Saada[130], A. Ouraou[141,*], Q. Ouyang[13a], M. Owen[55], R.E. Owen[140], K.Y. Oyulmaz[11c], V.E. Ozcan[11c], N. Ozturk[7], S. Ozturk[11c], J. Pacalt[127], H.A. Pacey[30], K. Pachal[47], A. Pacheco Pages[12], C. Padilla Aranda[12], S. Pagan Griso[16], G. Palacino[63], S. Palazzo[48], S. Palestini[34], M. Palka[81b], P. Palni[81a], D.K. Panchal[10], C.E. Pandini[52], J.G. Panduro Vazquez[91], P. Pani[44], G. Panizzo[64a,64c], L. Paolozzi[52], C. Papadatos[107], S. Parajuli[40], A. Paramonov[5], C. Paraskevopoulos[9], D. Paredes Hernandez[60b], S.R. Paredes Saenz[131], B. Parida[176], T.H. Park[163], A.J. Parker[29], M.A. Parker[30], F. Parodi[53b,53a], E.W. Parrish[117], J.A. Parsons[37], U. Parzefall[50], L. Pascual Dominguez[158], V.R. Pascuzzi[16], F. Pasquali[116], E. Pasqualucci[70a], S. Passaggio[53b], F. Pastore[91], P. Pasuwan[43a,43b], J.R. Pater[98], A. Pathak[177], J. Patton[88], T. Pauly[34], J. Pearkes[150], M. Pedersen[130], L. Pedraza Diaz[115], R. Pedro[136a], T. Peiffer[51], S.V. Peleganchuk[118b,118a], O. Penc[137], C. Peng[60b], H. Peng[58a], M. Penzin[162], B.S. Peralva[78a], M.M. Perego[62], A.P. Pereira Peixoto[136a], L. Pereira Sanchez[43a,43b], D.V. Perepelitsa[27], E. Perez Codina[164a], M. Perganti[9], L. Perini[66a,66b], H. Pernegger[34], S. Perrella[34], A. Perrevoort[116], K. Peters[44], R.F.Y. Peters[98], B.A. Petersen[34], T.C. Petersen[38], E. Petit[99], V. Petousis[138], C. Petridou[159], P. Petroff[62], F. Petrucci[72a,72b], M. Pettee[179], N.E. Pettersson[34], K. Petukhova[139], A. Peyaud[141], R. Pezoa[143e], L. Pezzotti[68a,68b], G. Pezzullo[179], T. Pham[102], P.W. Phillips[140], M.W. Phipps[169], G. Piacquadio[152], E. Pianori[16], F. Piazza[66a,66b], A. Picazio[100], R. Piegaia[28], D. Pietreanu[25b], J.E. Pilcher[35], A.D. Pilkington[98], M. Pinamonti[64a,64c], J.L. Pinfold[2], C. Pitman Donaldson[92], D.A. Pizzi[32], L. Pizzimento[71a,71b], A. Pizzini[116], M.-A. Pleier[27], V. Plesanovs[50], V. Pleskot[139], E. Plotnikova[77], P. Podberezko[118b,118a], R. Poettgen[94], R. Poggi[52], L. Poggioli[132], I. Pogrebnyak[104], D. Pohl[22], I. Pokharel[51], G. Polesello[68a], A. Poley[149,164a], A. Policicchio[70a,70b], R. Polifka[139], A. Polini[21b], C.S. Pollard[131], Z.B. Pollock[124], V. Polychronakos[27], D. Ponomarenko[109], L. Pontecorvo[34], S. Popa[25a], G.A. Popeneciu[25d], L. Portales[4], D.M. Portillo Quintero[164a], S. Pospisil[138], P. Postolache[25c], K. Potamianos[131], I.N. Potrap[77], C.J. Potter[30], H. Potti[1], T. Poulsen[44], J. Poveda[170], T.D. Powell[146], G. Pownall[44], M.E. Pozo Astigarraga[34], A. Prades Ibanez[170], P. Pralavorio[99], M.M. Prapa[42], S. Prell[76], D. Price[98], M. Primavera[65a], M.A. Principe Martin[96], M.L. Proffitt[145], N. Proklova[109], K. Prokofiev[60c], F. Prokoshin[77], S. Protopopescu[27], J. Proudfoot[5], M. Przybycien[81a], D. Pudzha[134], P. Puzo[62], D. Pyatiizbyantseva[109], J. Qian[103], Y. Qin[98], A. Quadt[51], M. Queitsch-Maitland[34], G. Rabanal Bolanos[57], F. Ragusa[66a,66b], G. Rahal[95], J.A. Raine[52], S. Rajagopalan[27], K. Ran[13a,13d], D.F. Rassloff[59a], D.M. Rauch[44], S. Rave[97], B. Ravina[55], I. Ravinovich[176], M. Raymond[34], A.L. Read[130], N.P. Readioff[146], D.M. Rebuzzi[68a,68b],

G. Redlinger[27], K. Reeves[41], D. Reikher[158], A. Reiss[97], A. Rej[148], C. Rembser[34], A. Renardi[44], M. Renda[25b], M.B. Rendel[112], A.G. Rennie[55], S. Resconi[66a], E.D. Resseguie[16], S. Rettie[92], B. Reynolds[124], E. Reynolds[19], M. Rezaei Estabragh[178], O.L. Rezanova[118b,118a], P. Reznicek[139], E. Ricci[73a,73b], R. Richter[112], S. Richter[44], E. Richter-Was[81b], M. Ridel[132], P. Rieck[112], P. Riedler[34], O. Rifki[44], M. Rijssenbeek[152], A. Rimoldi[68a,68b], M. Rimoldi[44], L. Rinaldi[21b], T.T. Rinn[169], M.P. Rinnagel[111], G. Ripellino[151], I. Riu[12], P. Rivadeneira[44], J.C. Rivera Vergara[172], F. Rizatdinova[126], E. Rizvi[90], C. Rizzi[52], B.A. Roberts[174], S.H. Robertson[101,aa], M. Robin[44], D. Robinson[30], C.M. Robles Gajardo[143e], M. Robles Manzano[97], A. Robson[55], A. Rocchi[71a,71b], C. Roda[69a,69b], S. Rodriguez Bosca[59a], A. Rodriguez Rodriguez[50], A.M. Rodríguez Vera[164b], S. Roe[34], A.R. Roepe[125], J. Roggel[178], O. Røhne[130], R.A. Rojas[143e], B. Roland[50], C.P.A. Roland[63], J. Roloff[27], A. Romaniouk[109], M. Romano[21b,21a], A.C. Romero Hernandez[169], N. Rompotis[88], M. Ronzani[122], L. Roos[132], S. Rosati[70a], G. Rosin[100], B.J. Rosser[133], E. Rossi[163], E. Rossi[4], E. Rossi[67a,67b], L.P. Rossi[53b], L. Rossini[44], R. Rosten[124], M. Rotaru[25b], B. Rottler[50], D. Rousseau[62], D. Rousso[30], G. Rovelli[68a,68b], A. Roy[10], A. Rozanov[99], Y. Rozen[157], X. Ruan[31f], A.J. Ruby[88], T.A. Ruggeri[1], F. Rühr[50], A. Ruiz-Martinez[170], A. Rummler[34], Z. Rurikova[50], N.A. Rusakovich[77], H.L. Russell[34], L. Rustige[36], J.P. Rutherfoord[6], E.M. Rüttinger[146], M. Rybar[139], E.B. Rye[130], A. Ryzhov[119], J.A. Sabater Iglesias[44], P. Sabatini[170], L. Sabetta[70a,70b], H.F-W. Sadrozinski[142], R. Sadykov[77], F. Safai Tehrani[70a], B. Safarzadeh Samani[153], M. Safdari[150], P. Saha[117], S. Saha[101], M. Sahinsoy[112], A. Sahu[178], M. Saimpert[141], M. Saito[160], T. Saito[160], D. Salamani[34], G. Salamanna[72a,72b], A. Salnikov[150], J. Salt[170], A. Salvador Salas[12], D. Salvatore[39b,39a], F. Salvatore[153], A. Salzburger[34], D. Sammel[50], D. Sampsonidis[159], D. Sampsonidou[58d,58c], J. Sánchez[170], A. Sanchez Pineda[4], V. Sanchez Sebastian[170], H. Sandaker[130], C.O. Sander[44], I.G. Sanderswood[87], J.A. Sandesara[100], M. Sandhoff[178], C. Sandoval[20b], D.P.C. Sankey[140], M. Sannino[53b,53a], Y. Sano[113], A. Sansoni[49], C. Santoni[36], H. Santos[136a,136b], S.N. Santpur[16], A. Santra[176], K.A. Saoucha[146], A. Sapronov[77], J.G. Saraiva[136a,136d], O. Sasaki[79], K. Sato[165], C. Sauer[59b], F. Sauerburger[50], E. Sauvan[4], P. Savard[163,aj], R. Sawada[160], C. Sawyer[140], L. Sawyer[93], I. Sayago Galvan[170], C. Sbarra[21b], A. Sbrizzi[64a,64c], T. Scanlon[92], J. Schaarschmidt[145], P. Schacht[112], D. Schaefer[35], L. Schaefer[133], U. Schäfer[97], A.C. Schaffer[62], D. Schaile[111], R.D. Schamberger[152], E. Schanet[111], C. Scharf[17], N. Scharmberg[98], V.A. Schegelsky[134], D. Scheirich[139], F. Schenck[17], M. Schernau[167], C. Schiavi[53b,53a], L.K. Schildgen[22], Z.M. Schillaci[24], E.J. Schioppa[65a,65b], M. Schioppa[39b,39a], B. Schlag[97], K.E. Schleicher[50], S. Schlenker[34], K. Schmieden[97], C. Schmitt[97], S. Schmitt[44], L. Schoeffel[141], A. Schoening[59b], P.G. Scholer[50], E. Schopf[131], M. Schott[97], J. Schovancova[34], S. Schramm[52], F. Schroeder[178], H-C. Schultz-Coulon[59a], M. Schumacher[50], B.A. Schumm[142], Ph. Schune[141], A. Schwartzman[150], T.A. Schwarz[103], Ph. Schwemling[141], R. Schwienhorst[104], A. Sciandra[142], G. Sciolla[24], F. Scuri[69a], F. Scutti[102], C.D. Sebastiani[88], K. Sedlaczek[45], P. Seema[17], S.C. Seidel[114], A. Seiden[142], B.D. Seidlitz[27], T. Seiss[35], C. Seitz[44], J.M. Seixas[78b], G. Sekhniaidze[67a], S.J. Sekula[40], L.P. Selem[4], N. Semprini-Cesari[21b,21a], S. Sen[47], C. Serfon[27], L. Serin[62], L. Serkin[64a,64b], M. Sessa[58a], H. Severini[125], S. Sevova[150], F. Sforza[53b,53a], A. Sfyrla[52], E. Shabalina[51], R. Shaheen[151], J.D. Shahinian[133], N.W. Shaikh[43a,43b], D. Shaked Renous[176], L.Y. Shan[13a], M. Shapiro[16], A. Sharma[34], A.S. Sharma[1], S. Sharma[44], P.B. Shatalov[120], K. Shaw[153], S.M. Shaw[98], P. Sherwood[92], L. Shi[92], C.O. Shimmin[179], Y. Shimogama[175], J.D. Shinner[91], I.P.J. Shipsey[131], S. Shirabe[52], M. Shiyakova[77], J. Shlomi[176], M.J. Shochet[35], J. Shojaii[102], D.R. Shope[151], S. Shrestha[124], E.M. Shrif[31f], M.J. Shroff[172], E. Shulga[176], P. Sicho[137], A.M. Sickles[169], E. Sideras Haddad[31f], O. Sidiropoulou[34], A. Sidoti[21b,21a], F. Siegert[46], Dj. Sijacki[14], M.V. Silva Oliveira[34], S.B. Silverstein[43a], S. Simion[62], R. Simoniello[34], S. Simsek[11b], P. Sinervo[163], V. Sinetckii[110], S. Singh[149], S. Sinha[44], S. Sinha[31f], M. Sioli[21b,21a], I. Siral[128], S.Yu. Sivoklokov[110], J. Sjölin[43a,43b], A. Skaf[51], E. Skorda[94], P. Skubic[125], M. Slawinska[82], K. Sliwa[166], V. Smakhtin[176], B.H. Smart[140], J. Smiesko[139], S.Yu. Smirnov[109], Y. Smirnov[109], L.N. Smirnova[110,s], O. Smirnova[94], E.A. Smith[35], H.A. Smith[131], M. Smizanska[87], K. Smolek[138], A. Smykiewicz[82], A.A. Snesarev[108], H.L. Snoek[116], S. Snyder[27], R. Sobie[172,aa], A. Soffer[158], F. Sohns[51], C.A. Solans Sanchez[34], E.Yu. Soldatov[109], U. Soldevila[170], A.A. Solodkov[119], S. Solomon[50], A. Soloshenko[77], O.V. Solovyanov[119], V. Solovyev[134], P. Sommer[146], H. Son[166], A. Sonay[12], W.Y. Song[164b], A. Sopczak[138], A.L. Sopio[92], F. Sopkova[26b], S. Sottocornola[68a,68b], R. Soualah[64a,64c], A.M. Soukharev[118b,118a], Z. Soumaimi[33e], D. South[44], S. Spagnolo[65a,65b], M. Spalla[112], M. Spangenberg[174], F. Spanò[91], D. Sperlich[50], T.M. Spieker[59a], G. Spigo[34], M. Spina[153], D.P. Spiteri[55], M. Spousta[139], A. Stabile[66a,66b], B.L. Stamas[117], R. Stamen[59a], M. Stamenkovic[116], A. Stampekis[19], M. Standke[22], E. Stanecka[82], B. Stanislaus[34], M.M. Stanitzki[44], M. Stankaityte[131], B. Stapf[44], E.A. Starchenko[119], G.H. Stark[142], J. Stark[99], D.M. Starko[164b], P. Staroba[137], P. Starovoitov[59a], S. Stärz[101], R. Staszewski[82], G. Stavropoulos[42], P. Steinberg[27], A.L. Steinhebel[128], B. Stelzer[149,164a], H.J. Stelzer[135], O. Stelzer-Chilton[164a], H. Stenzel[54], T.J. Stevenson[153], G.A. Stewart[34], M.C. Stockton[34], G. Stoicea[25b], M. Stolarski[136a], S. Stonjek[112], A. Straessner[46], J. Strandberg[151], S. Strandberg[43a,43b], M. Strauss[125], T. Strebler[99], P. Strizenec[26b], R. Ströhmer[173], D.M. Strom[128], L.R. Strom[44], R. Stroynowski[40], A. Strubig[43a,43b], S.A. Stucci[27], B. Stugu[15], J. Stupak[125], N.A. Styles[44], D. Su[150], S. Su[58a], W. Su[58d,145,58c], X. Su[58a], N.B. Suarez[135], K. Sugizaki[160], V.V. Sulin[108], M.J. Sullivan[88], D.M.S. Sultan[52], S. Sultansoy[3c], T. Sumida[83], S. Sun[103], S. Sun[177], X. Sun[98], O. Sunneborn Gudnadottir[168], C.J.E. Suster[154], M.R. Sutton[153], M. Svatos[137], M. Swiatlowski[164a], T. Swirski[173], I. Sykora[26a], M. Sykora[139], T. Sykora[139], D. Ta[97], K. Tackmann[44,y], A. Taffard[167], R. Tafirout[164a], E. Tagiev[119], R.H.M. Taibah[132], R. Takashima[84], K. Takeda[80], T. Takeshita[147], E.P. Takeva[48], Y. Takubo[79], M. Talby[99], A.A. Talyshev[118b,118a], K.C. Tam[60b], N.M. Tamir[158], A. Tanaka[160], J. Tanaka[160], R. Tanaka[62], Z. Tao[171], S. Tapia Araya[76], S. Tapprogge[97], A. Tarek Abouelfadl Mohamed[104], S. Tarem[157], K. Tariq[58b], G. Tarna[25b,f], G.F. Tartarelli[66a], P. Tas[139], M. Tasevsky[137], E. Tassi[39b,39a], G. Tateno[160], Y. Tayalati[33e], G.N. Taylor[102], W. Taylor[164b], H. Teagle[88], A.S. Tee[177], R. Teixeira De Lima[150], P. Teixeira-Dias[91], H. Ten Kate[34], J.J. Teoh[116], K. Terashi[160], J. Terron[96], S. Terzo[12], M. Testa[49], R.J. Teuscher[163,aa], N. Themistokleous[48], T. Theveneaux-Pelzer[17], O. Thielmann[178], D.W. Thomas[91], J.P. Thomas[19], E.A. Thompson[44], P.D. Thompson[19], E. Thomson[133], E.J. Thorpe[90], Y. Tian[51], V.O. Tikhomirov[108,ag], Yu.A. Tikhonov[118b,118a], S. Timoshenko[109], P. Tipton[179], S. Tisserant[99], S.H. Tlou[31f], A. Tnourji[36], K. Todome[21b,21a], S. Todorova-Nova[139], S. Todt[46], M. Togawa[79], J. Tojo[85], S. Tokár[26a], K. Tokushuku[79], E. Tolley[124], R. Tombs[30], M. Tomoto[79,113], L. Tompkins[150], P. Tornambe[100], E. Torrence[128], H. Torres[46], E. Torró Pastor[170], M. Toscani[28], C. Tosciri[35], J. Toth[99,z], D.R. Tovey[146], A. Traeet[15], C.J. Treado[122], T. Trefzger[173], A. Tricoli[27], I.M. Trigger[164a], S. Trincaz-Duvoid[132], D.A. Trischuk[171], W. Trischuk[163], B. Trocmé[56], A. Trofymov[62], C. Troncon[66a], F. Trovato[153], L. Truong[31c], M. Trzebinski[82], A. Trzupek[82], F. Tsai[152], A. Tsiamis[159], P.V. Tsiareshka[105,ae], A. Tsirigotis[159,w], V. Tsiskaridze[152], E.G. Tskhadadze[156a], M. Tsopoulou[159], I.I. Tsukerman[120], V. Tsulaia[16], S. Tsuno[79], O. Tsur[157], D. Tsybychev[152], Y. Tu[60b], A. Tudorache[25b], V. Tudorache[25b], A.N. Tuna[34], S. Turchikhin[77], I. Turk Cakir[3b,u], R.J. Turner[19], R. Turra[66a], P.M. Tuts[37], S. Tzamarias[159], P. Tzanis[9], E. Tzovara[97], K. Uchida[160], F. Ukegawa[165], G. Unal[34], M. Unal[10], A. Undrus[27], G. Unel[167], F.C. Ungaro[102], K. Uno[160], J. Urban[26b], P. Urquijo[102], G. Usai[7], R. Ushioda[161], M. Usman[107], Z. Uysal[11d], V. Vacek[138], B. Vachon[101], K.O.H. Vadla[130], T. Vafeiadis[34], C. Valderanis[111], E. Valdes Santurio[43a,43b], M. Valente[164a], S. Valentinetti[21b,21a], A. Valero[170], L. Valéry[44], R.A. Vallance[19], A. Vallier[99], J.A. Valls Ferrer[170], T.R. Van Daalen[12], P. Van Gemmeren[5], S. Van Stroud[92], I. Van Vulpen[116], M. Vanadia[71a,71b], W. Vandelli[34], M. Vandenbroucke[141], E.R. Vandewall[126], D. Vannicola[70a,70b], L. Vannoli[53b,53a], R. Vari[70a], E.W. Varnes[6], C. Varni[16], T. Varol[155], D. Varouchas[62], K.E. Varvell[154], M.E. Vasile[25b], L. Vaslin[36], G.A. Vasquez[172], F. Vazeille[36], D. Vazquez Furelos[12], T. Vazquez Schroeder[34], J. Veatch[51], V. Vecchio[98], M.J. Veen[116], I. Veliscek[131], L.M. Veloce[163], F. Veloso[136a,136c], S. Veneziano[70a], A. Ventura[65a,65b], A. Verbytskyi[112], M. Verducci[69a,69b], C. Vergis[22], M. Verissimo De Araujo[78b], W. Verkerke[116], A.T. Vermeulen[116], J.C. Vermeulen[116], C. Vernieri[150], P.J. Verschuuren[91], M.L. Vesterbacka[122], M.C. Vetterli[149,aj], A. Vgenopoulos[159], N. Viaux Maira[143e], T. Vickey[146], O.E. Vickey Boeriu[146], G.H.A. Viehhauser[131], L. Vigani[59b], M. Villa[21b,21a], M. Villaplana Perez[170], E.M. Villhauer[48], E. Vilucchi[49], M.G. Vincter[32], G.S. Virdee[19], A. Vishwakarma[48], C. Vittori[21b,21a], I. Vivarelli[153], V. Vladimirov[174], E. Voevodina[112], M. Vogel[178], P. Vokac[138], J. Von Ahnen[44], S.E. von Buddenbrock[31f], E. Von Toerne[22], V. Vorobel[139], K. Vorobev[109], M. Vos[170], J.H. Vossebeld[88], M. Vozak[98], L. Vozdecky[90], N. Vranjes[14], M. Vranjes Milosavljevic[14], V. Vrba[138,*], M. Vreeswijk[116], N.K. Vu[99], R. Vuillermet[34], I. Vukotic[35], S. Wada[165], C. Wagner[100], P. Wagner[22], W. Wagner[178], S. Wahdan[178], H. Wahlberg[86], R. Wakasa[165], M. Wakida[113], V.M. Walbrecht[112], J. Walder[140], R. Walker[111], S.D. Walker[91], W. Walkowiak[148], A.M. Wang[57], A.Z. Wang[177], C. Wang[58a], C. Wang[58c], H. Wang[16], J. Wang[60a], P. Wang[40], R.-J. Wang[97], R. Wang[57], R. Wang[117], S.M. Wang[155], S. Wang[58b], T. Wang[58a], W.T. Wang[58a], W.X. Wang[58a], X. Wang[13c], X. Wang[169], Y. Wang[58a], Z. Wang[103], C. Wanotayaroj[34], A. Warburton[101], C.P. Ward[30], R.J. Ward[19], N. Warrack[55], A.T. Watson[19], M.F. Watson[19], G. Watts[145], B.M. Waugh[92], A.F. Webb[10], C. Weber[27], M.S. Weber[18], S.A. Weber[32], S.M. Weber[59a], C. Wei[58a], Y. Wei[131], A.R. Weidberg[131], J. Weingarten[45], M. Weirich[97], C. Weiser[50], P.S. Wells[34], T. Wenaus[27], B. Wendland[45], T. Wengler[34], S. Wenig[34], N. Wermes[22], M. Wessels[59a], K. Whalen[128], A.M. Wharton[87], A.S. White[57], A. White[7], M.J. White[1], D. Whiteson[167], L. Wickremasinghe[129], W. Wiedenmann[177], C. Wiel[46], M. Wielers[140], N. Wieseotte[97], C. Wiglesworth[38], L.A.M. Wiik-Fuchs[50], D.J. Wilbern[125], H.G. Wilkens[34], L.J. Wilkins[91], D.M. Williams[37], H.H. Williams[133], S. Williams[30], S. Willocq[100], P.J. Windischhofer[131], I. Wingerter-Seez[4], F. Winklmeier[128], B.T. Winter[50], M. Wittgen[150], M. Wobisch[93], A. Wolf[97], R. Wölker[131], J. Wollrath[167], M.W. Wolter[82], H. Wolters[136a,136c], V.W.S. Wong[171], A.F. Wongel[44], S.D. Worm[44], B.K. Wosiek[82], K.W. Woźniak[82], K. Wraight[55], J. Wu[13a,13d], S.L. Wu[177], X. Wu[52], Y. Wu[58a], Z. Wu[141,58a], J. Wuerzinger[131], T.R. Wyatt[98], B.M. Wynne[48], S. Xella[38], J. Xiang[60c], X. Xiao[103], M. Xie[58a], X. Xie[58a], I. Xiotidis[153], D. Xu[13a], H. Xu[58a], H. Xu[58a], L. Xu[58a], R. Xu[133], W. Xu[103], Y. Xu[13b], Z. Xu[58b], Z. Xu[150], B. Yabsley[154], S. Yacoob[31a], N. Yamaguchi[85], Y. Yamaguchi[161], M. Yamatani[160], H. Yamauchi[165], T. Yamazaki[16], Y. Yamazaki[80], J. Yan[58c], S. Yan[131], Z. Yan[23], H.J. Yang[58c,58d], H.T. Yang[16], S. Yang[58a], T. Yang[60c], X. Yang[58a], X. Yang[13a], Y. Yang[160], Z. Yang[103,58a], W-M. Yao[16], Y.C. Yap[44], H. Ye[13c], J. Ye[40], S. Ye[27], I. Yeletskikh[77], M.R. Yexley[87], P. Yin[37], K. Yorita[175], K. Yoshihara[76], C.J.S. Young[50], C. Young[150], R. Yuan[58b,j], X. Yue[59a], M. Zaazoua[33e], B. Zabinski[82], G. Zacharis[9], E. Zaffaroni[52], J. Zahreddine[99], E. Zaid[48], A.M. Zaitsev[119,af], T. Zakareishvili[156b], N. Zakharchuk[32], S. Zambito[34], D. Zanzi[50], S.V. Zeißner[45], C. Zeitnitz[178], G. Zemaityte[131], J.C. Zeng[169], O. Zenin[119], T. Ženiš[26a], S. Zenz[90], S. Zerradi[33a], D. Zerwas[62], M. Zgubič[131], B. Zhang[13c], D.F. Zhang[13b], G. Zhang[13b], J. Zhang[5], K. Zhang[13a], L. Zhang[13c], M. Zhang[169], R. Zhang[177], S. Zhang[103], X. Zhang[58c], X. Zhang[58b], Z. Zhang[62], P. Zhao[47], Y. Zhao[142], Z. Zhao[58a], A. Zhemchugov[77], Z. Zheng[150], D. Zhong[169], B. Zhou[103], C. Zhou[177], H. Zhou[6], N. Zhou[58c], Y. Zhou[6], C.G. Zhu[58b], C. Zhu[13a,13d], H.L. Zhu[58a], H. Zhu[13a], J. Zhu[103], Y. Zhu[58a], X. Zhuang[13a], K. Zhukov[108], V. Zhulanov[118b,118a], D. Zieminska[63], N.I. Zimine[77], S. Zimmermann[50,*], M. Ziolkowski[148], L. Živković[14], A. Zoccoli[21b,21a], K. Zoch[52], T.G. Zorbas[146], O. Zormpa[42], W. Zou[37], L. Zwalinski[34].

[1]Department of Physics, University of Adelaide, Adelaide; Australia.
[2]Department of Physics, University of Alberta, Edmonton AB; Canada.
[3](a)Department of Physics, Ankara University, Ankara;(b)Istanbul Aydin University, Application and Research Center for Advanced Studies, Istanbul;(c)Division of Physics, TOBB University of Economics and Technology, Ankara; Turkey.
[4]LAPP, Univ. Savoie Mont Blanc, CNRS/IN2P3, Annecy ; France.
[5]High Energy Physics Division, Argonne National Laboratory, Argonne IL; United States of America.
[6]Department of Physics, University of Arizona, Tucson AZ; United States of America.
[7]Department of Physics, University of Texas at Arlington, Arlington TX; United States of America.
[8]Physics Department, National and Kapodistrian University of Athens, Athens; Greece.

[9]Physics Department, National Technical University of Athens, Zografou; Greece.
[10]Department of Physics, University of Texas at Austin, Austin TX; United States of America.
[11(a)]Bahcesehir University, Faculty of Engineering and Natural Sciences, Istanbul;[(b)]Istanbul Bilgi University, Faculty of Engineering and Natural Sciences, Istanbul;[(c)]Department of Physics, Bogazici University, Istanbul;[(d)]Department of Physics Engineering, Gaziantep University, Gaziantep; Turkey.
[12]Institut de Física d'Altes Energies (IFAE), Barcelona Institute of Science and Technology, Barcelona; Spain.
[13(a)]Institute of High Energy Physics, Chinese Academy of Sciences, Beijing;[(b)]Physics Department, Tsinghua University, Beijing;[(c)]Department of Physics, Nanjing University, Nanjing;[(d)]University of Chinese Academy of Science (UCAS), Beijing; China.
[14]Institute of Physics, University of Belgrade, Belgrade; Serbia.
[15]Department for Physics and Technology, University of Bergen, Bergen; Norway.
[16]Physics Division, Lawrence Berkeley National Laboratory and University of California, Berkeley CA; United States of America.
[17]Institut für Physik, Humboldt Universität zu Berlin, Berlin; Germany.
[18]Albert Einstein Center for Fundamental Physics and Laboratory for High Energy Physics, University of Bern, Bern; Switzerland.
[19]School of Physics and Astronomy, University of Birmingham, Birmingham; United Kingdom.
[20(a)]Facultad de Ciencias y Centro de Investigaciónes, Universidad Antonio Nariño, Bogotá;[(b)]Departamento de Física, Universidad Nacional de Colombia, Bogotá, Colombia; Colombia.
[21(a)]INFN Bologna and Universita' di Bologna, Dipartimento di Fisica;[(b)]INFN Sezione di Bologna; Italy.
[22]Physikalisches Institut, Universität Bonn, Bonn; Germany.
[23]Department of Physics, Boston University, Boston MA; United States of America.
[24]Department of Physics, Brandeis University, Waltham MA; United States of America.
[25(a)]Transilvania University of Brasov, Brasov;[(b)]Horia Hulubei National Institute of Physics and Nuclear Engineering, Bucharest;[(c)]Department of Physics, Alexandru Ioan Cuza University of Iasi, Iasi;[(d)]National Institute for Research and Development of Isotopic and Molecular Technologies, Physics Department, Cluj-Napoca;[(e)]University Politehnica Bucharest, Bucharest;[(f)]West University in Timisoara, Timisoara; Romania.
[26(a)]Faculty of Mathematics, Physics and Informatics, Comenius University, Bratislava;[(b)]Department of Subnuclear Physics, Institute of Experimental Physics of the Slovak Academy of Sciences, Kosice; Slovak Republic.
[27]Physics Department, Brookhaven National Laboratory, Upton NY; United States of America.
[28]Departamento de Física, Universidad de Buenos Aires, Buenos Aires; Argentina.
[29]California State University, CA; United States of America.
[30]Cavendish Laboratory, University of Cambridge, Cambridge; United Kingdom.
[31(a)]Department of Physics, University of Cape Town, Cape Town;[(b)]iThemba Labs, Western Cape;[(c)]Department of Mechanical Engineering Science, University of Johannesburg, Johannesburg;[(d)]National Institute of Physics, University of the Philippines Diliman;[(e)]University of South Africa, Department of Physics, Pretoria;[(f)]School of Physics, University of the Witwatersrand, Johannesburg; South Africa.
[32]Department of Physics, Carleton University, Ottawa ON; Canada.
[33(a)]Faculté des Sciences Ain Chock, Réseau Universitaire de Physique des Hautes Energies - Université Hassan II, Casablanca;[(b)]Faculté des Sciences, Université Ibn-Tofail, Kénitra;[(c)]Faculté des Sciences Semlalia, Université Cadi Ayyad, LPHEA-Marrakech;[(d)]LPMR, Faculté des Sciences, Université Mohamed Premier, Oujda;[(e)]Faculté des sciences, Université Mohammed V, Rabat;[(f)]Mohammed VI Polytechnic University, Ben Guerir; Morocco.

[34]CERN, Geneva; Switzerland.
[35]Enrico Fermi Institute, University of Chicago, Chicago IL; United States of America.
[36]LPC, Université Clermont Auvergne, CNRS/IN2P3, Clermont-Ferrand; France.
[37]Nevis Laboratory, Columbia University, Irvington NY; United States of America.
[38]Niels Bohr Institute, University of Copenhagen, Copenhagen; Denmark.
[39(a)]Dipartimento di Fisica, Università della Calabria, Rende;[(b)]INFN Gruppo Collegato di Cosenza, Laboratori Nazionali di Frascati; Italy.
[40]Physics Department, Southern Methodist University, Dallas TX; United States of America.
[41]Physics Department, University of Texas at Dallas, Richardson TX; United States of America.
[42]National Centre for Scientific Research "Demokritos", Agia Paraskevi; Greece.
[43(a)]Department of Physics, Stockholm University;[(b)]Oskar Klein Centre, Stockholm; Sweden.
[44]Deutsches Elektronen-Synchrotron DESY, Hamburg and Zeuthen; Germany.
[45]Lehrstuhl für Experimentelle Physik IV, Technische Universität Dortmund, Dortmund; Germany.
[46]Institut für Kern- und Teilchenphysik, Technische Universität Dresden, Dresden; Germany.
[47]Department of Physics, Duke University, Durham NC; United States of America.
[48]SUPA - School of Physics and Astronomy, University of Edinburgh, Edinburgh; United Kingdom.
[49]INFN e Laboratori Nazionali di Frascati, Frascati; Italy.
[50]Physikalisches Institut, Albert-Ludwigs-Universität Freiburg, Freiburg; Germany.
[51]II. Physikalisches Institut, Georg-August-Universität Göttingen, Göttingen; Germany.
[52]Département de Physique Nucléaire et Corpusculaire, Université de Genève, Genève; Switzerland.
[53(a)]Dipartimento di Fisica, Università di Genova, Genova;[(b)]INFN Sezione di Genova; Italy.
[54]II. Physikalisches Institut, Justus-Liebig-Universität Giessen, Giessen; Germany.
[55]SUPA - School of Physics and Astronomy, University of Glasgow, Glasgow; United Kingdom.
[56]LPSC, Université Grenoble Alpes, CNRS/IN2P3, Grenoble INP, Grenoble; France.
[57]Laboratory for Particle Physics and Cosmology, Harvard University, Cambridge MA; United States of America.
[58(a)]Department of Modern Physics and State Key Laboratory of Particle Detection and Electronics, University of Science and Technology of China, Hefei;[(b)]Institute of Frontier and Interdisciplinary Science and Key Laboratory of Particle Physics and Particle Irradiation (MOE), Shandong University, Qingdao;[(c)]School of Physics and Astronomy, Shanghai Jiao Tong University, Key Laboratory for Particle Astrophysics and Cosmology (MOE), SKLPPC, Shanghai;[(d)]Tsung-Dao Lee Institute, Shanghai; China.
[59(a)]Kirchhoff-Institut für Physik, Ruprecht-Karls-Universität Heidelberg, Heidelberg;[(b)]Physikalisches Institut, Ruprecht-Karls-Universität Heidelberg, Heidelberg; Germany.
[60(a)]Department of Physics, Chinese University of Hong Kong, Shatin, N.T., Hong Kong;[(b)]Department of Physics, University of Hong Kong, Hong Kong;[(c)]Department of Physics and Institute for Advanced Study, Hong Kong University of Science and Technology, Clear Water Bay, Kowloon, Hong Kong; China.
[61]Department of Physics, National Tsing Hua University, Hsinchu; Taiwan.
[62]IJCLab, Université Paris-Saclay, CNRS/IN2P3, 91405, Orsay; France.
[63]Department of Physics, Indiana University, Bloomington IN; United States of America.
[64(a)]INFN Gruppo Collegato di Udine, Sezione di Trieste, Udine;[(b)]ICTP, Trieste;[(c)]Dipartimento Politecnico di Ingegneria e Architettura, Università di Udine, Udine; Italy.
[65(a)]INFN Sezione di Lecce;[(b)]Dipartimento di Matematica e Fisica, Università del Salento, Lecce; Italy.
[66(a)]INFN Sezione di Milano;[(b)]Dipartimento di Fisica, Università di Milano, Milano; Italy.
[67(a)]INFN Sezione di Napoli;[(b)]Dipartimento di Fisica, Università di Napoli, Napoli; Italy.
[68(a)]INFN Sezione di Pavia;[(b)]Dipartimento di Fisica, Università di Pavia, Pavia; Italy.
[69(a)]INFN Sezione di Pisa;[(b)]Dipartimento di Fisica E. Fermi, Università di Pisa, Pisa; Italy.
[70(a)]INFN Sezione di Roma;[(b)]Dipartimento di Fisica, Sapienza Università di Roma, Roma; Italy.

[71] [(a)] INFN Sezione di Roma Tor Vergata; [(b)] Dipartimento di Fisica, Università di Roma Tor Vergata, Roma; Italy.
[72] [(a)] INFN Sezione di Roma Tre; [(b)] Dipartimento di Matematica e Fisica, Università Roma Tre, Roma; Italy.
[73] [(a)] INFN-TIFPA; [(b)] Università degli Studi di Trento, Trento; Italy.
[74] Institut für Astro- und Teilchenphysik, Leopold-Franzens-Universität, Innsbruck; Austria.
[75] University of Iowa, Iowa City IA; United States of America.
[76] Department of Physics and Astronomy, Iowa State University, Ames IA; United States of America.
[77] Joint Institute for Nuclear Research, Dubna; Russia.
[78] [(a)] Departamento de Engenharia Elétrica, Universidade Federal de Juiz de Fora (UFJF), Juiz de Fora; [(b)] Universidade Federal do Rio De Janeiro COPPE/EE/IF, Rio de Janeiro; [(c)] Instituto de Física, Universidade de São Paulo, São Paulo; Brazil.
[79] KEK, High Energy Accelerator Research Organization, Tsukuba; Japan.
[80] Graduate School of Science, Kobe University, Kobe; Japan.
[81] [(a)] AGH University of Science and Technology, Faculty of Physics and Applied Computer Science, Krakow; [(b)] Marian Smoluchowski Institute of Physics, Jagiellonian University, Krakow; Poland.
[82] Institute of Nuclear Physics Polish Academy of Sciences, Krakow; Poland.
[83] Faculty of Science, Kyoto University, Kyoto; Japan.
[84] Kyoto University of Education, Kyoto; Japan.
[85] Research Center for Advanced Particle Physics and Department of Physics, Kyushu University, Fukuoka ; Japan.
[86] Instituto de Física La Plata, Universidad Nacional de La Plata and CONICET, La Plata; Argentina.
[87] Physics Department, Lancaster University, Lancaster; United Kingdom.
[88] Oliver Lodge Laboratory, University of Liverpool, Liverpool; United Kingdom.
[89] Department of Experimental Particle Physics, Jožef Stefan Institute and Department of Physics, University of Ljubljana, Ljubljana; Slovenia.
[90] School of Physics and Astronomy, Queen Mary University of London, London; United Kingdom.
[91] Department of Physics, Royal Holloway University of London, Egham; United Kingdom.
[92] Department of Physics and Astronomy, University College London, London; United Kingdom.
[93] Louisiana Tech University, Ruston LA; United States of America.
[94] Fysiska institutionen, Lunds universitet, Lund; Sweden.
[95] Centre de Calcul de l'Institut National de Physique Nucléaire et de Physique des Particules (IN2P3), Villeurbanne; France.
[96] Departamento de Física Teorica C-15 and CIAFF, Universidad Autónoma de Madrid, Madrid; Spain.
[97] Institut für Physik, Universität Mainz, Mainz; Germany.
[98] School of Physics and Astronomy, University of Manchester, Manchester; United Kingdom.
[99] CPPM, Aix-Marseille Université, CNRS/IN2P3, Marseille; France.
[100] Department of Physics, University of Massachusetts, Amherst MA; United States of America.
[101] Department of Physics, McGill University, Montreal QC; Canada.
[102] School of Physics, University of Melbourne, Victoria; Australia.
[103] Department of Physics, University of Michigan, Ann Arbor MI; United States of America.
[104] Department of Physics and Astronomy, Michigan State University, East Lansing MI; United States of America.
[105] B.I. Stepanov Institute of Physics, National Academy of Sciences of Belarus, Minsk; Belarus.
[106] Research Institute for Nuclear Problems of Byelorussian State University, Minsk; Belarus.
[107] Group of Particle Physics, University of Montreal, Montreal QC; Canada.
[108] P.N. Lebedev Physical Institute of the Russian Academy of Sciences, Moscow; Russia.
[109] National Research Nuclear University MEPhI, Moscow; Russia.

[110]D.V. Skobeltsyn Institute of Nuclear Physics, M.V. Lomonosov Moscow State University, Moscow; Russia.
[111]Fakultät für Physik, Ludwig-Maximilians-Universität München, München; Germany.
[112]Max-Planck-Institut für Physik (Werner-Heisenberg-Institut), München; Germany.
[113]Graduate School of Science and Kobayashi-Maskawa Institute, Nagoya University, Nagoya; Japan.
[114]Department of Physics and Astronomy, University of New Mexico, Albuquerque NM; United States of America.
[115]Institute for Mathematics, Astrophysics and Particle Physics, Radboud University/Nikhef, Nijmegen; Netherlands.
[116]Nikhef National Institute for Subatomic Physics and University of Amsterdam, Amsterdam; Netherlands.
[117]Department of Physics, Northern Illinois University, DeKalb IL; United States of America.
[118][(a)]Budker Institute of Nuclear Physics and NSU, SB RAS, Novosibirsk;[(b)]Novosibirsk State University Novosibirsk; Russia.
[119]Institute for High Energy Physics of the National Research Centre Kurchatov Institute, Protvino; Russia.
[120]Institute for Theoretical and Experimental Physics named by A.I. Alikhanov of National Research Centre "Kurchatov Institute", Moscow; Russia.
[121][(a)]New York University Abu Dhabi, Abu Dhabi;[(b)]United Arab Emirates University, Al Ain;[(c)]University of Sharjah, Sharjah; United Arab Emirates.
[122]Department of Physics, New York University, New York NY; United States of America.
[123]Ochanomizu University, Otsuka, Bunkyo-ku, Tokyo; Japan.
[124]Ohio State University, Columbus OH; United States of America.
[125]Homer L. Dodge Department of Physics and Astronomy, University of Oklahoma, Norman OK; United States of America.
[126]Department of Physics, Oklahoma State University, Stillwater OK; United States of America.
[127]Palacký University, Joint Laboratory of Optics, Olomouc; Czech Republic.
[128]Institute for Fundamental Science, University of Oregon, Eugene, OR; United States of America.
[129]Graduate School of Science, Osaka University, Osaka; Japan.
[130]Department of Physics, University of Oslo, Oslo; Norway.
[131]Department of Physics, Oxford University, Oxford; United Kingdom.
[132]LPNHE, Sorbonne Université, Université de Paris, CNRS/IN2P3, Paris; France.
[133]Department of Physics, University of Pennsylvania, Philadelphia PA; United States of America.
[134]Konstantinov Nuclear Physics Institute of National Research Centre "Kurchatov Institute", PNPI, St. Petersburg; Russia.
[135]Department of Physics and Astronomy, University of Pittsburgh, Pittsburgh PA; United States of America.
[136][(a)]Laboratório de Instrumentação e Física Experimental de Partículas - LIP, Lisboa;[(b)]Departamento de Física, Faculdade de Ciências, Universidade de Lisboa, Lisboa;[(c)]Departamento de Física, Universidade de Coimbra, Coimbra;[(d)]Centro de Física Nuclear da Universidade de Lisboa, Lisboa;[(e)]Departamento de Física, Universidade do Minho, Braga;[(f)]Departamento de Física Teórica y del Cosmos, Universidad de Granada, Granada (Spain);[(g)]Dep Física and CEFITEC of Faculdade de Ciências e Tecnologia, Universidade Nova de Lisboa, Caparica;[(h)]Instituto Superior Técnico, Universidade de Lisboa, Lisboa; Portugal.
[137]Institute of Physics of the Czech Academy of Sciences, Prague; Czech Republic.
[138]Czech Technical University in Prague, Prague; Czech Republic.
[139]Charles University, Faculty of Mathematics and Physics, Prague; Czech Republic.
[140]Particle Physics Department, Rutherford Appleton Laboratory, Didcot; United Kingdom.

[141]IRFU, CEA, Université Paris-Saclay, Gif-sur-Yvette; France.
[142]Santa Cruz Institute for Particle Physics, University of California Santa Cruz, Santa Cruz CA; United States of America.
[143][(a)]Departamento de Física, Pontificia Universidad Católica de Chile, Santiago;[(b)]Universidad de la Serena, La Serena;[(c)]Universidad Andres Bello, Department of Physics, Santiago;[(d)]Instituto de Alta Investigación, Universidad de Tarapacá, Arica;[(e)]Departamento de Física, Universidad Técnica Federico Santa María, Valparaíso; Chile.
[144]Universidade Federal de São João del Rei (UFSJ), São João del Rei; Brazil.
[145]Department of Physics, University of Washington, Seattle WA; United States of America.
[146]Department of Physics and Astronomy, University of Sheffield, Sheffield; United Kingdom.
[147]Department of Physics, Shinshu University, Nagano; Japan.
[148]Department Physik, Universität Siegen, Siegen; Germany.
[149]Department of Physics, Simon Fraser University, Burnaby BC; Canada.
[150]SLAC National Accelerator Laboratory, Stanford CA; United States of America.
[151]Department of Physics, Royal Institute of Technology, Stockholm; Sweden.
[152]Departments of Physics and Astronomy, Stony Brook University, Stony Brook NY; United States of America.
[153]Department of Physics and Astronomy, University of Sussex, Brighton; United Kingdom.
[154]School of Physics, University of Sydney, Sydney; Australia.
[155]Institute of Physics, Academia Sinica, Taipei; Taiwan.
[156][(a)]E. Andronikashvili Institute of Physics, Iv. Javakhishvili Tbilisi State University, Tbilisi;[(b)]High Energy Physics Institute, Tbilisi State University, Tbilisi; Georgia.
[157]Department of Physics, Technion, Israel Institute of Technology, Haifa; Israel.
[158]Raymond and Beverly Sackler School of Physics and Astronomy, Tel Aviv University, Tel Aviv; Israel.
[159]Department of Physics, Aristotle University of Thessaloniki, Thessaloniki; Greece.
[160]International Center for Elementary Particle Physics and Department of Physics, University of Tokyo, Tokyo; Japan.
[161]Department of Physics, Tokyo Institute of Technology, Tokyo; Japan.
[162]Tomsk State University, Tomsk; Russia.
[163]Department of Physics, University of Toronto, Toronto ON; Canada.
[164][(a)]TRIUMF, Vancouver BC;[(b)]Department of Physics and Astronomy, York University, Toronto ON; Canada.
[165]Division of Physics and Tomonaga Center for the History of the Universe, Faculty of Pure and Applied Sciences, University of Tsukuba, Tsukuba; Japan.
[166]Department of Physics and Astronomy, Tufts University, Medford MA; United States of America.
[167]Department of Physics and Astronomy, University of California Irvine, Irvine CA; United States of America.
[168]Department of Physics and Astronomy, University of Uppsala, Uppsala; Sweden.
[169]Department of Physics, University of Illinois, Urbana IL; United States of America.
[170]Instituto de Física Corpuscular (IFIC), Centro Mixto Universidad de Valencia - CSIC, Valencia; Spain.
[171]Department of Physics, University of British Columbia, Vancouver BC; Canada.
[172]Department of Physics and Astronomy, University of Victoria, Victoria BC; Canada.
[173]Fakultät für Physik und Astronomie, Julius-Maximilians-Universität Würzburg, Würzburg; Germany.
[174]Department of Physics, University of Warwick, Coventry; United Kingdom.
[175]Waseda University, Tokyo; Japan.
[176]Department of Particle Physics and Astrophysics, Weizmann Institute of Science, Rehovot; Israel.
[177]Department of Physics, University of Wisconsin, Madison WI; United States of America.

[178]Fakultät für Mathematik und Naturwissenschaften, Fachgruppe Physik, Bergische Universität Wuppertal, Wuppertal; Germany.
[179]Department of Physics, Yale University, New Haven CT; United States of America.
[a] Also at Borough of Manhattan Community College, City University of New York, New York NY; United States of America.
[b] Also at Bruno Kessler Foundation, Trento; Italy.
[c] Also at Center for High Energy Physics, Peking University; China.
[d] Also at Centro Studi e Ricerche Enrico Fermi; Italy.
[e] Also at CERN, Geneva; Switzerland.
[f] Also at CPPM, Aix-Marseille Université, CNRS/IN2P3, Marseille; France.
[g] Also at Département de Physique Nucléaire et Corpusculaire, Université de Genève, Genève; Switzerland.
[h] Also at Departament de Fisica de la Universitat Autonoma de Barcelona, Barcelona; Spain.
[i] Also at Department of Financial and Management Engineering, University of the Aegean, Chios; Greece.
[j] Also at Department of Physics and Astronomy, Michigan State University, East Lansing MI; United States of America.
[k] Also at Department of Physics and Astronomy, University of Louisville, Louisville, KY; United States of America.
[l] Also at Department of Physics, Ben Gurion University of the Negev, Beer Sheva; Israel.
[m] Also at Department of Physics, California State University, East Bay; United States of America.
[n] Also at Department of Physics, California State University, Fresno; United States of America.
[o] Also at Department of Physics, California State University, Sacramento; United States of America.
[p] Also at Department of Physics, King's College London, London; United Kingdom.
[q] Also at Department of Physics, St. Petersburg State Polytechnical University, St. Petersburg; Russia.
[r] Also at Department of Physics, University of Fribourg, Fribourg; Switzerland.
[s] Also at Faculty of Physics, M.V. Lomonosov Moscow State University, Moscow; Russia.
[t] Also at Faculty of Physics, Sofia University, 'St. Kliment Ohridski', Sofia; Bulgaria.
[u] Also at Giresun University, Faculty of Engineering, Giresun; Turkey.
[v] Also at Graduate School of Science, Osaka University, Osaka; Japan.
[w] Also at Hellenic Open University, Patras; Greece.
[x] Also at Institucio Catalana de Recerca i Estudis Avancats, ICREA, Barcelona; Spain.
[y] Also at Institut für Experimentalphysik, Universität Hamburg, Hamburg; Germany.
[z] Also at Institute for Particle and Nuclear Physics, Wigner Research Centre for Physics, Budapest; Hungary.
[aa] Also at Institute of Particle Physics (IPP); Canada.
[ab] Also at Institute of Physics, Azerbaijan Academy of Sciences, Baku; Azerbaijan.
[ac] Also at Instituto de Fisica Teorica, IFT-UAM/CSIC, Madrid; Spain.
[ad] Also at Istanbul University, Dept. of Physics, Istanbul; Turkey.
[ae] Also at Joint Institute for Nuclear Research, Dubna; Russia.
[af] Also at Moscow Institute of Physics and Technology State University, Dolgoprudny; Russia.
[ag] Also at National Research Nuclear University MEPhI, Moscow; Russia.
[ah] Also at Physikalisches Institut, Albert-Ludwigs-Universität Freiburg, Freiburg; Germany.
[ai] Also at The City College of New York, New York NY; United States of America.
[aj] Also at TRIUMF, Vancouver BC; Canada.
[ak] Also at Universita di Napoli Parthenope, Napoli; Italy.
[al] Also at University of Chinese Academy of Sciences (UCAS), Beijing; China.
[am] Also at Yeditepe University, Physics Department, Istanbul; Turkey.

* Deceased